# Journal Pre-proof

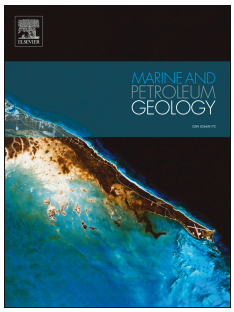


Hydrate occurrence in Europe: A review of available evidence

Timothy A. Minshull, Hector Marín-Moreno, Peter Betlem, Joerg Bialas, Stefan Buenz, Ewa Burwicz, Alejandra L. Cameselle, Gunay Cifci, Michela Giustiniani, Jess I.T. Hillman, Sebastian Hölz, John R. Hopper, Gabriel Ion, Ricardo León, Vitor Magalhaes, Yizhaq Makovsky, Maria-Pilar Mata, Michael D. Max, Tove Nielsen, Seda Okay, Ilia Ostrovsky, Nick O'Neill, Luis M. Pinheiro, Andreia A. Plaza-Faverola, Daniel Rey, Srikumar Roy, Katrin Schwalenberg, Kim Senger, Sunil Vadakkepuliyambatta, Atanas Vasilev, Juan-Tomás Vázquez

PII: S0264-8172(19)30386-1

DOI: https://doi.org/10.1016/j.marpetgeo.2019.08.014

Reference: JMPG 3986

To appear in: *Marine and Petroleum Geology*

Received Date: 19 March 2019

Revised Date: 30 July 2019

Accepted Date: 9 August 2019

Please cite this article as: Minshull, T.A., Marín-Moreno, H., Betlem, P., Bialas, J., Buenz, S., Burwicz, E., Cameselle, A.L., Cifci, G., Giustiniani, M., Hillman, J.I.T., Hölz, S., Hopper, J.R., Ion, G., León, R., Magalhaes, V., Makovsky, Y., Mata, M.-P., Max, M.D., Nielsen, T., Okay, S., Ostrovsky, I., O'Neill, N., Pinheiro, L.M., Plaza-Faverola, A.A., Rey, D., Roy, S., Schwalenberg, K., Senger, K., Vadakkepuliyambatta, S., Vasilev, A., Vázquez, Juan.-Tomá., Hydrate occurrence in Europe: A review of available evidence, *Marine and Petroleum Geology* (2019), doi: https://doi.org/10.1016/j.marpetgeo.2019.08.014.

# Hydrate occurrence in Europe: a review of available evidence

Timothy A. Minshull[a]* Hector Marín-Moreno[b], Peter Betlem[c], Joerg Bialas[d], Stefan Buenz[e], Ewa Burwicz[d], Alejandra L. Cameselle[f, r], Gunay Cifci[g], Michela Giustiniani[h], Jess I. T. Hillman[i], Sebastian Hölz[d], John R. Hopper[j], Gabriel Ion[k], Ricardo León[l], Vitor Magalhaes[m], Yizhaq Makovsky[n], Maria-Pilar Mata[l], Michael D. Max[o], Tove Nielsen[j], Seda Okay[g], Ilia Ostrovsky[p], Nick O'Neill[q], Luis M. Pinheiro[f], Andreia A. Plaza-Faverola[e], Daniel Rey[r], Srikumar Roy[s], Katrin Schwalenberg[t], Kim Senger[c], Sunil Vadakkepuliyambatta[e], Atanas Vasilev[u] and Juan-Tomás Vázquez[v]

a School of Ocean and Earth Science, National Oceanography Centre Southampton, University of Southampton, European Way, Southampton SO14 3ZH, UK; tmin@noc.soton.ac.uk
b National Oceanography Centre, European Way, Southampton SO14 3ZH, UK; hector.marin.moreno@noc.ac.uk
c Department of Arctic Geology, The University Centre in Svalbard, P.O. Box 156, 9171 Longyearbyen, Norway; Peter.Betlem@unis.no; Kim.Senger@unis.no
d Geomar Helmholtz Centre for Ocean Research Kiel, Marine Geodynamics, 24148 Kiel, Germany; jbialas@geomar.de; eburwicz@geomar.de; shoelz@geomar.de
e CAGE-Center for Arctic Gas Hydrate, Environment and Climate, Department of Geosciences, UiT-The Arctic University of Norway, 9037 Tromsø, Norway; stefan.buenz@uit.no; andreia.a.faverola@uit.no; sunil.vadakkepuliyambatta@uit.no
f University of Aveiro, Geosciences Department and CESAM, Campus Santiago, 3810-193 Aveiro, Portugal; lmp@ua.pt
g Institute of Marine Sciences and Technology, Dokuz Eylul University, Inciralti, Izmir, Turkey; Gunay.cifci@deu.edu.tr
h National Institute of Oceanography and Applied Geophysics, 1-34010 Sgonico, Italy; mgiustiniani@inogs.it
i GNS Science, 1, Fairway Drive, Avalon 5010, New Zealand; j.hillman@gns.cri.nz
j Geological Survey of Denmark and Greenland, Department of Geophysics, DK-1350 Copenhagen, Denmark; jrh@geus.dk; tni@geus.dk;
k National Institute of Marine Geology and Geoecology, RO-024053 Bucharest, Romania; gion@geoecomar.ro
l Geological Survey of Spain, C/Rios Rosas 23, Madrid 28003, Spain; r.leon@igme.es; p.mata@igme.es
m Portuguese Institute for Sea and Atmosphere, Marine Geology and Georesources Division, Rua C Aeroporto, P-1749077 Lisbon, Portugal; vitor.magalhaes@ipma.pt
n Dr Moses Strauss Department of Marine Geosciences, Leon H. Charney School of Marine Sciences, University of Haifa, Haifa, Israel; yizhaq@univ.haifa.ac.il
o MaxSystems LLC, Washington D.C., USA; michael.max@icrag-centre.org
p Israel Oceanographic and Limnological Research, Kinneret Limnological Laboratory, P. O. Box 447, Migdal 1495001, Israel; ostrovsky@ocean.org.il
q Irish Shelf Petroleum Studies Group (ISPSG), PIP Secretariat, 7 Dundrum Business Park, Windy Arbour, Dublin 14 N2Y7, Ireland; noneill@pip.ie
r Department of Marine Geosciences and Territorial Planning, University of Vigo, CP.36.310 Vigo (Pontevedra), Spain; danirey@uvigo.es; acamaselle@uvigo.es
s Irish Centre for Research in Applied Geosciences, School of Earth Sciences, University College Dublin, Belfield, Dublin 4, Ireland; srikumar.roy@icrag-centre.org

t Federal Institute for Geosciences and Natural Resources, Hannover, Germany;
katrin.schwalenberg@bgr.de
u Institute of Oceanology, Varna, Bulgaria; gasberg@mail.bg
v Spanish Institute of Oceanography, Spain; juantomas.vazquez@ieo.es

* Corresponding author

Declarations of interest: none

**Abstract**

Large national programs in the United States and several Asian countries have defined and characterised their marine methane hydrate occurrences in some detail, but European hydrate occurrence has received less attention. The European Union-funded project "Marine gas hydrate – an indigenous resource of natural gas for Europe" (MIGRATE) aimed to determine the European potential inventory of exploitable gas hydrate, to assess current technologies for their production, and to evaluate the associated risks. We present a synthesis of results from a MIGRATE working group that focused on the definition and assessment of hydrate in Europe. Our review includes the western and eastern margins of Greenland, the Barents Sea and onshore and offshore Svalbard, the Atlantic margin of Europe, extending south to the northwestern margin of Morocco, the Mediterranean Sea, the Sea of Marmara, and the western and southern margins of the Black Sea. We have not attempted to cover the high Arctic, the Russian, Ukrainian and Georgian sectors of the Black Sea, or overseas territories of European nations. Following a formalised process, we defined a range of indicators of hydrate presence based on geophysical, geochemical and geological data. Our study was framed by the constraint of the hydrate stability field in European seas. Direct hydrate indicators included sampling of hydrate; the presence of bottom simulating reflectors in seismic reflection profiles; gas seepage into the ocean; and chlorinity anomalies in sediment cores. Indirect indicators included geophysical survey evidence for seismic velocity and/or resistivity anomalies, seismic reflectivity anomalies or subsurface gas escape structures; various seabed features associated with gas escape, and the presence of an underlying conventional petroleum system. We used these indicators to develop a database of hydrate occurrence across Europe. We identified a series of regions where there is substantial evidence for hydrate occurrence (some areas offshore Greenland, offshore west Svalbard, the Barents Sea, the mid-Norwegian margin, the Gulf of Cadiz, parts of the eastern Mediterranean, the Sea of Marmara and the Black Sea) and regions where the evidence is more tenuous (other areas offshore Greenland and of the eastern Mediterranean, onshore Svalbard, offshore Ireland and offshore northwest Iberia). We provide an overview of the evidence for hydrate occurrence in each of these regions. We conclude that around Europe, areas with strong evidence for the presence of hydrate commonly coincide with conventional thermogenic hydrocarbon provinces.

*Keywords:* methane hydrate; Europe

## 1. Introduction

Gas hydrate is an ice-like, crystalline solid comprising a hydrogen-bonded water lattice with trapped gas molecules that is stable at high pressures and low temperatures (e.g., Sloan and Koh, 2008). In nature the most common hydrate-forming gas is methane. Methane hydrate is widespread in seafloor sediments and as such may provide a useful energy resource. Because, for equivalent energy production, burning methane generates significantly less greenhouse gases than burning coal, the

energy mix required to satisfy the target of keeping the average global temperature rise below 2ºC during the 21st century may involve substantial gas production, including from undiscovered sources (e.g., McGlade and Ekins, 2015). Methane hydrate could be one such source, providing a transition fuel to a low-carbon energy system that compliments intermittent renewable energy generation and supports energy security. Hydrate-bearing sands have been identified as a key target for production (Boswell and Collett, 2011). Hydrate is also of interest because hydrate dissociation might be triggered by global ocean warming, potentially leading to further greenhouse warming (e.g., Archer et al., 2009; Ruppel and Kessler, 2017), and because of their role as a potential geohazard for offshore operations and infrastructure.

Driven by high demand for energy and limited conventional hydrocarbon resources, several nations, including the USA, Japan, China, Korea and India, have developed large national hydrate research and exploration programmes (e.g., Gabitto, 2010; Oyama and Masutani, 2017; Song et al., 2014). In Europe, however, there has been less investment in hydrate research. Gas demand declined in Europe during the first half of this decade, but is likely to show a modest increase in the next decade, despite increasing development of renewables (Honoré, 2014). Thus there is a continuing need to better understand hydrate potential in Europe, and the original motivation for this study was to provide a foundation for future hydrate exploration in Europe. However, for many European nations, imported shale gas is now seen as a more cost-efficient route to supplement conventional gas supplies, and hydrate exploration is not seen as a priority. Therefore our study has expanded beyond a focus on hydrate in sands, to cover all forms of hydrate occurrence around Europe and some adjacent areas. Our goal is to review the current state of knowledge of hydrate occurrence within this area.

Our study is framed by the offshore stability field for pure methane hydrate in seawater around Europe, estimated from global databases (Fig. 1). The region of stability is most poorly constrained offshore Greenland, where few constraints are available on the geothermal gradient, but is likely to include many of the deeper fjords. The limit of stability lies at varying distances from the coast on the northwest European margin, and hydrate is stable in parts of the Barents Sea and a small part of the Skagerrak. Hydrate is stable in large areas of the western and eastern Mediterranean basins, the Tyrrhenian Sea and the Black Sea, and in small areas of the Adriatic and Aegean Seas and the Sea of Marmara. Hydrate also can be stable beneath permafrost and beneath ice sheets. These settings require more complex hydrate stability calculations that depend on often poorly known parameters. Therefore we have not attempted to carry out such calculations for the whole of our study area. However, in section 4 below we discuss the possibility of hydrate stability beneath permafrost and ice caps onshore Svalbard.

We first describe the methods that we used to identify areas where the presence of hydrate was indicated. Then we describe in a series of sections the evidence for hydrate occurrence within these areas. Finally we synthesise the available evidence on hydrate occurrence in Europe.

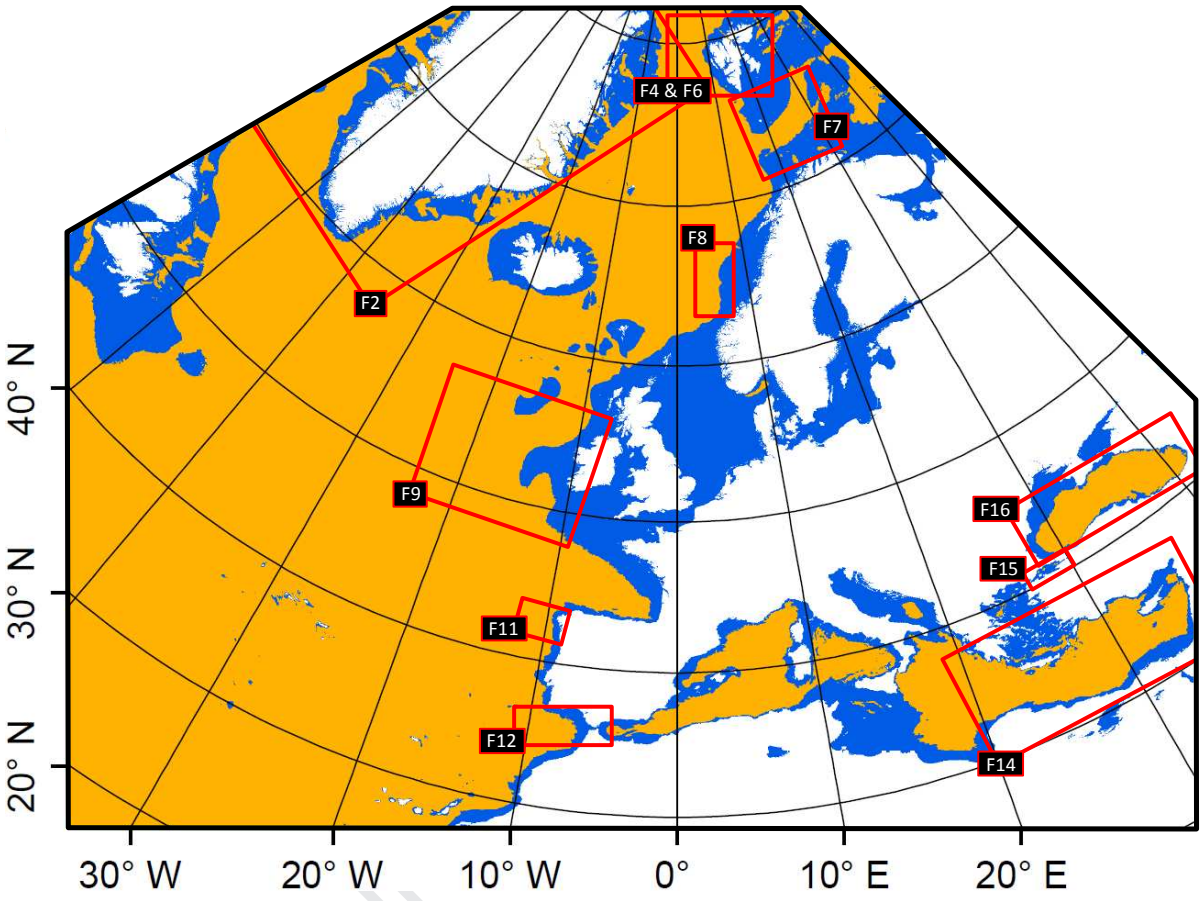


Figure 1: Pure methane hydrate stability zone around Europe (orange area). Blue marks offshore areas where pure methane hydrate is not stable, but other forms of hydrate may be stable. The limit of stability is estimated using the 30 arc-second bathymetry grid from the General Bathymetric Chart of the Oceans, GEBCO (https://www.gebco.net/data_and_products/gridded_bathymetry_data/), the 0.25° seabed temperature grid from the National Oceanic and Atmospheric Administration, NOOA (https://www.nodc.noaa.gov/cgi-bin/OC5/SELECT/woaselect.pl), a salinity of 3.5% wt, and the Moridis (2003) phase boundary for Structure I hydrate. Seabed temperature data were interpolated to match the resolution of the bathymetric grid. Red boxes mark the areas shown in other figures.

## 2. Methods

To frame our study, we developed a list of hydrate indicators and a workflow for scientific exploration of marine hydrate; our workflow is adapted from the hydrate petroleum system approach of Max and Johnson (2014). For a detailed hydrate assessment from an energy resource perspective, readers are referred to Boswell et al. (2016), and for a complete review on the hydrate systems concept we refer to Collett et al. (2009).

### 2.1 Hydrate indicators

We define hydrate indicators as geological, geophysical and geochemical observations that either provide strong evidence to confirm the current presence of hydrate, or simply suggest that hydrate might be present. We considered two categories of hydrate indicators, based on their confidence in confirming the hydrate presence: (i) direct indicators and (ii) indirect indicators. Direct indicators include sampling of hydrate, and observations of hydrate bottom simulating reflectors (BSRs), gas seepage and pore water chlorinity anomalies. Indirect indicators include gas chimneys, anomalies in seismic velocity and electrical resistivity, zones of anomalous reflectivity, the presence of a conventional petroleum province, and various seabed features (cold seeps without gas, backscatter anomalies, mud volcanoes, pockmarks and pingos). Except for the sampling of hydrate, all the other indicators are not only found in hydrate systems and should be considered as hydrate indicators only if they are inferred within or close to the hydrate stability zone (HSZ). In marine settings, the HSZ is the region with appropriate sub-seafloor pressure and temperature conditions to form hydrate. Its thickness is given by the distance between the seabed and the intersection of the thermal structure (obtained using the seabed temperature and geothermal gradient) with a hydrate phase boundary (e.g., Marín-Moreno et al., 2016).

A hydrate BSR is a seismic reflector with opposite polarity to the seafloor that generally mimics the seafloor at a depth consistent with the expected base of the HSZ. The presence of a continuous BSR may be an indication of dispersed gas being present in pore water below it rather than being an indicator of the presence of significant hydrate above (e.g., Max and Johnson, 2014). Also, other geological phenomena can create BSRs at different depths (e.g., Berndt et al., 2004). Nevertheless, the presence of a hydrate BSR allows us to constrain the extent of the HSZ (Boswell et al., 2016) and likely requires the presence of at least some hydrate, so we consider it as a direct indicator for hydrate. Hydrate accumulations often have been identified without associated BSRs, for example in the Gulf of Mexico (Majumdar et al., 2016).

Pore water chlorinity anomalies can arise from dissociation of hydrate during the ascent of a core from the seabed to the surface vessel. Gas seeps from the seabed within the HSZ indicate that pore waters are saturated with gas and therefore hydrate is very likely to be present. Gas escape structures such as pipes and chimneys may be imaged in seismic reflection data and may indicate the presence of hydrate-forming gas within the HSZ. The presence of hydrate increases seismic velocities and electrical resistivities, while the presence of gas decreases seismic velocities but also increases electrical resistivities. High seismic reflectivity (“bright spots”) can result from the presence of subsurface gas, while seismic “blanking”, involving loss of coherent reflectivity, can result from the presence of gas or of chaotic fluid escape structures. Conventional petroleum provinces can provide a source of thermogenic gas entering the HSZ, while the various seabed features listed above provide possible evidence for past or present gas escape through the seabed.

187

188 2.2 Hydrate exploration workflow

189 We developed a hydrate scientific exploration workflow consisting of four clearly defined steps:

190 1. Determining the likelihood of hydrate stability.
191 2. Imposing better constraints on the likelihood of hydrate presence considering relevant recent
192 geological, physical and chemical changes.
193 3. Hydrate petroleum system analysis.
194 4. Prospect identification and scientific drilling.

195 The first step is to determine the likelihood of hydrate thermodynamic stability under steady state
196 conditions, i.e., to calculate the HSZ. For this calculation, the bathymetry, seabed temperature, pore
197 water salinity, hydrate forming gases, and geothermal gradient or heat flow need to be known or
198 assumed. In general, sufficient bathymetric data exist or can be easily acquired, but seabed
199 temperature and/or geothermal gradient/heat flow data are generally sparse, and sometimes non-
200 existent. Therefore interpolation/extrapolation techniques need to be employed, with caution to avoid
201 creation of artefacts. In marine environments, the first estimate of the HSZ is commonly made by
202 assuming a salinity of 3.5% and that the hydrate-forming gas is 100% methane.

203

204 The second step involves constraining the likelihood of hydrate presence by assessing existing
205 geological, geophysical and geochemical data. This step also considers the temporal variability of the
206 system and includes: (i) the identification of BSR(s) and their character (continuous or discontinuous)
207 in existing seismic data; (ii) assessment of the sediment thickness that may contain hydrate, based on
208 the identification of source beds and quantification of total organic carbon; (iii) re-assessment of the
209 hydrate-forming gas and its saturation based on possible thermogenic sources; (iv) re-calculation of
210 the HSZ using better constraints on the hydrate-forming gas and any time-dependent parameters
211 affecting the volume of the HSZ, including the influence of geologically recent oceanographic, seabed
212 and tectonic changes on seabed pressure and temperature, geothermal gradient and salinity.

213

214 The third step involves developing a hydrate system analysis, beginning with identifying what
215 additional data need to be acquired. This step might involve the following surveys: (i) a regional 2D
216 seismic survey to study the large scale structure of the geological system and identify BSRs (e.g., Lee
217 et al., 2005); (ii) an ocean bottom seismometer (OBS) survey and/or a 2D long streamer seismic
218 survey to derive information on seismic-wave velocity, porosity, and hydrate and gas saturation (e.g.,
219 Westbrook et al., 2008); (iii) a high resolution local 2D/3D seismic survey to clearly identify direct
220 indicators of hydrate and/or potential clues (e.g., Riedel et al., 2002); (iv) a controlled source
221 electromagnetic survey (CSEM) to impose better constraints in porosity contrasts and pore phase
222 saturations (e.g., Weitemeyer et al., 2006); (v) less well established exploration techniques such as
223 heat flow-based methods for additional information and/or for independent validation of the seismic

and electromagnetic observations. Such surveys might lead to a more formal analysis for gas hydrate identification and saturation estimation (e.g., Dai et al., 2008). A joint interpretation approach can be applied to the different geophysical datasets (e.g., Goswami et al., 2015), and focus the interpretation on identifying the depositional environments within and immediately beneath the HSZ, gas sources, and depocentres for sand, turbidite and mass transport deposits, and on assessing the morphology of the sand deposits. At this stage, there are enough data to estimate the approximate volume of methane that might be recoverable from hydrate using average hydrate saturations, and the dominant hydrate distribution and morphology.

The fourth step, prospect identification, brings the detailed information needed to make an informed decision about scientific drilling targets. This step includes a detailed analysis of seismic and CSEM data to identify features such as sweet spots or structures with enhanced fluid flow, or elevated resistivities or seismic velocities. Such analysis may be followed by rock physics and geotechnical laboratory experiments to determine the elastic (e.g., Priest et al., 2005), electrical (e.g., Spangenberg and Kulenkampff, 2006) and thermo-hydro-mechanical (e.g., Santamarina et al., 2015) properties of hydrate-bearing samples. These properties are then used to calibrate rock physics and geotechnical models (e.g., Marín-Moreno et al., 2017; Uchida et al., 2012) that provide a quantitative understanding of the above properties, of the likely response of the target natural hydrate bearing deposits to natural and/or anthropogenic perturbations, and of local relationships between relevant properties such as porosity and permeability. Then potential drilling targets can be chosen and a geohazard assessment performed for each target to help to decide which, if any, should be prioritized. Finally, scientific drilling should take place to evaluate more fully the prospectivity of the area.

Below we cover in a series of regional sections the areas where there is evidence for the presence of hydrate. Some large sections of the eastern Atlantic margin have been extensively sampled using both seismic and acoustic techniques, as well as direct sampling. However, to date there are no published reports of hydrate BSRs, gas seeps, chlorinity anomalies or other significant hydrate indicators within or in close proximity to the HSZ. Examples include the northwest margin of the UK and the Bay of Biscay; in both areas, gas seeps have been detected at shelf depths (e.g., Judd et al., 1997; Ruffine et al., 2017) but not in regions of hydrate stability. In most of the areas described below, only the first step and some aspects of the second step have been conducted (Table 1). To date, scientific drilling for hydrate in Europe has been limited to the west Svalbard margin and the western Black Sea, though hydrate has been encountered several times during drilling for other purposes.

Table 1: Summary of the most relevant hydrate-related information for all the regions described in the text. ODP = Ocean Drilling Program; MV = mud volcano; see text for definitions of indicators.

| Region | Location | Data | Direct hydrate indicator | Indirect hydrate indicator | Occurrence and host sediment | Gas source and migration path | Hydrate extent and amount |
|---|---|---|---|---|---|---|---|
| Offshore Greenland | Northeast | ODP 909; 2D seismic; heat flow; seabed temperature | Possible BSR | Gassy sediment sampling; bright spots; chimneys | No hydrate recovered | No information available | Not estimated |
| | West | Gravity core; 2D & 3D seismic; heat flow; seabed temperature | BSRs | Seismic blanking; oil and gas shows; Ikaite crystals; fluid/gas escape structures; pockmarks | No hydrate recovered | Thermogenic gas; migration through faults and fractures | Not estimated |
| Offshore Svalbard | Vestnesa Ridge and slope | 2D & 3D seismic; OBS; CSEM; cores; MeBo drilling; seafloor imaging; HSZ modelling | Hydrate sampled; gas seeps; BSR | Chimneys; pockmarks; seismic blanking | Topographically & structurally controlled; Small, thin chips, in veins or as chunks in the upper 2-4 m of fine-grained hemipelagic sediments | Dominant thermogenic; thermogenic input increases with depth; thermogenic gas migration through faults | 700 $km^3$ extent of HSZ at ~800-2000 mbsl; saturation from Vp 6-18%; from CSEM 20-30% and 40-68% in chimneys |
| | Prinz Karl Forland | 2D seismic; OBS; CSEM; cores; MeBo drilling; seafloor imaging; HSZ modeling | Hydrate sampled; gas seeps; patchy BSR | Chimneys; bright spots | Hydrate recovered from one pockmark | Microbial with significant thermogenic contribution | Not estimated |
| | Elsewhere West | 2D & 3D seismic; cores; HSZ modelling | Gas seeps; BSRs | Bright spots; gas chimneys | No hydrate recovered | Abiotic gas inferred in the South Molloy Transform Fault & West Knipovich Ridge region | Not estimated |
| Onshore Svalbard | | HSZ modelling; scientific and industry drilling; 2D seismic | None | Hydrate stability; hydrate found offshore; fluid escape structures; gas seeps | Fractured sandstones and shales; coal beds | Partly thermogenic; migration via fractures and seeps | Not estimated |
| Norwegian Margin | Barents Sea | 2D seismic; cores; HSZ modelling | Hydrate sampled; gas seeps; BSRs | Bright spots; chimneys; pockmarks | Structurally controlled; BSRs in consolidated low-porosity sediments and glacial sediments | Mostly thermogenic gas; migration through faults and fractures | Volume 0.19 $GSm^3$ in Bjornoya Basin; 93-650 $GSm^3$ in SW Barents Sea or 470-3320 $GSm^3$ if higher hydrocarbons |
| | Mid-Norwegian Margin | Core sampling; 2D seismic; OBS; Multi-component seismic; CSEM; HSZ modelling | Hydrate sampled; BSRs | Fluid escape structures; pockmarks | Finely bedded contourite and hemipelagic deposits – mainly silty clays | Microbial with thermogenic component | 4000 $km^2$ BSR along N flank of Storegga Slide; saturation 2-10%; volume of 625 $GSm^3$ |

260 Table 1: Continuation

| Region | Location | Data | Direct hydrate indicator | Indirect hydrate indicator | Occurrence and host sediment | Gas source and migration path | Hydrate extent and amount |
|---|---|---|---|---|---|---|---|
| Offshore Ireland | Rockall and Porcupine Basins | Scientific & industry drilling; 2D & 3D seismic; HSZ modelling | Possible BSRs | Hydrocarbon seeps; fluid escape structures; bright spots | No hydrate recovered | Thermogenic gas migration through faults above active petroleum systems | Not estimated |
| NW Iberian Margin | | Cores; 2D seismic; HSZ modelling | None | Pockmarks; fluid/gas escape structures; seismic blanking; bright spots; chimneys | No hydrate recovered | Not known | Not estimated |
| Offshore South Iberia & NW Africa Margin | Gulf of Cadiz | Cores; 2D seismic | Hydrate sampled; chlorinity anomalies; BSRs | MV; gas chimneys; pockmarks; degassing structures; seismic blanking; backscatter anomalies | Hydrate found in MV; localised deposits and hosted in fine-grained sediments with low permeability | Thermogenic gas migration through focused fluid flow; abiogenic crustal-derived fluids | Saturation of 5-31% in cores |
| | Alborán Sea | Cores | Chlorinity anomalies | Gas release from cores | No hydrate recovered | Thermogenic gas from ~5 km depth | Not estimated |
| Eastern Mediterranean | Anaximander Seamount | Cores; HSZ modelling | Hydrate sampled; chlorinity anomalies; gas seeps | MV; pockmarks | Hydrate found in MV | Thermogenic | mm to cm scale disseminated H; saturation of 0.7-16.7% |
| | Olimpi Field | Cores | Hydrate sampled; chlorinity anomalies; gas seeps | MV; pockmarks | Hydrate found in MV | Mainly thermogenic | c. 5 $GSm^3$ in Milano dome |
| | Nile fan and Levant Basin | 2D & 3D seismic; seafloor video | Possible BSR; gas seeps | Pockmarks, bright spots, seismic blanking | Sandy buried systems | Mostly microbial; thermogenic at MV | Estimated c. 100 Tcf in the Levant Basin |
| Sea of Marmara | | Cores; 2D & 3D seismic | Hydrate sampled; gas seeps | MV; bright spots; gas chimneys; pockmarks | Thermogenic | Thermogenic G migration from deep Oligocene-Eocene reservoirs | Not estimated |

261
262
263
264

Table 1: Continuation

| Region | Location | Data | Direct hydrate indicator | Indirect hydrate indicator | Occurrence and host sediment | Gas source and migration path | Hydrate extent and amount |
|---|---|---|---|---|---|---|---|
| Western Black Sea | Bulgaria & Rumania | Cores; 2D & 3D seismic; OBS; CSEM; HSZ modelling | Hydrate sampled; gas seeps; BSRs | Seismic blanking; gas pipes and chimneys; high resistivity values | H formed in levees or base of channels | Microbial | Saturation from CSEM of 30% and from OBS of 10% or 30-40%. |
| | İğneada | 2D seismic, cores | Hydrate sampled; BSRs | Seismic blanking; bright spots; gas chimneys; possible MV | Hydrate fragments in possible MV | Migration via faults and possible MV | Not estimated |
| | Zonguldak-Amasra | Cores; 2D seismic; HSZ modelling | BSRs | Seismic blanking; MV; gas chimneys | Not known | Thermogenic and microbial | Not estimated |
| Eastern Black Sea | Samsun | Cores; 2D seismic | None | Seismic blanking; gas chimneys; pockmarks | Not known | Possible hydrogen sulphide in the gas | Not estimated |
| | Hopa-Rize-Trabzon-Giresun | 2D & 3D seismic | BSRs | Seismic blanking; MV; gas chimneys | Not known | Deep thermogenic gas migration through faults and microbial gas | Not estimated |

## 3. Offshore Greenland

### 3.1 Geological Setting

The West Greenland margin formed during Cretaceous to Paleogene continental rifting that eventually resulted in seafloor spreading in the Baffin Bay and the Labrador Sea (e.g., Oakey and Chalmers, 2012). A change in spreading direction during the latest Paleocene to Eocene resulted in a general northward drift of Greenland into the Arctic Ocean, resulting in compression and inversion that becomes more pronounced the farther north along the Baffin Bay part of the margin. Significant strike-slope motion along many parts of the margin are also recorded at this time.

After the cessation of the Caledonian Orogeny during Late Silurian–Early Devonian, the northeast Greenland margin experienced repeated episodes of rifting with intervening quiescent periods, and occasionally minor compression and inversion. During the Cretaceous to Paleogene, rifting and breakup resulted in the onset of opening of the North Atlantic, and continued seafloor spreading formed large sedimentary basins (Hopper et al., 2014 and references therein). By early Neogene times, the seafloor spreading resulted in the opening of the Fram Strait and creation of the Atlantic-Arctic gateway (Jokat et al., 2008; Ritzmann and Jokat, 2003).

Along the southeast Greenland margin, no Paleozoic–Jurassic rocks are exposed onshore or otherwise known to exist. Small outcrops of Cretaceous sediments are known both onshore and offshore (e.g.,

Gerlings et al., 2017). Paleocene to Eocene breakup was accompanied by extremely voluminous volcanism as seafloor spreading was established (e.g., Larsen and Saunders, 1998).

In late Neogene, all of Greenland's margins became glaciated, resulting in erosion of the inner and middle shelf areas and deposition of kilometer thick glacigenic wedges on the outer shelf and slope areas, while thick contourite deposition occurred in the basinal areas.

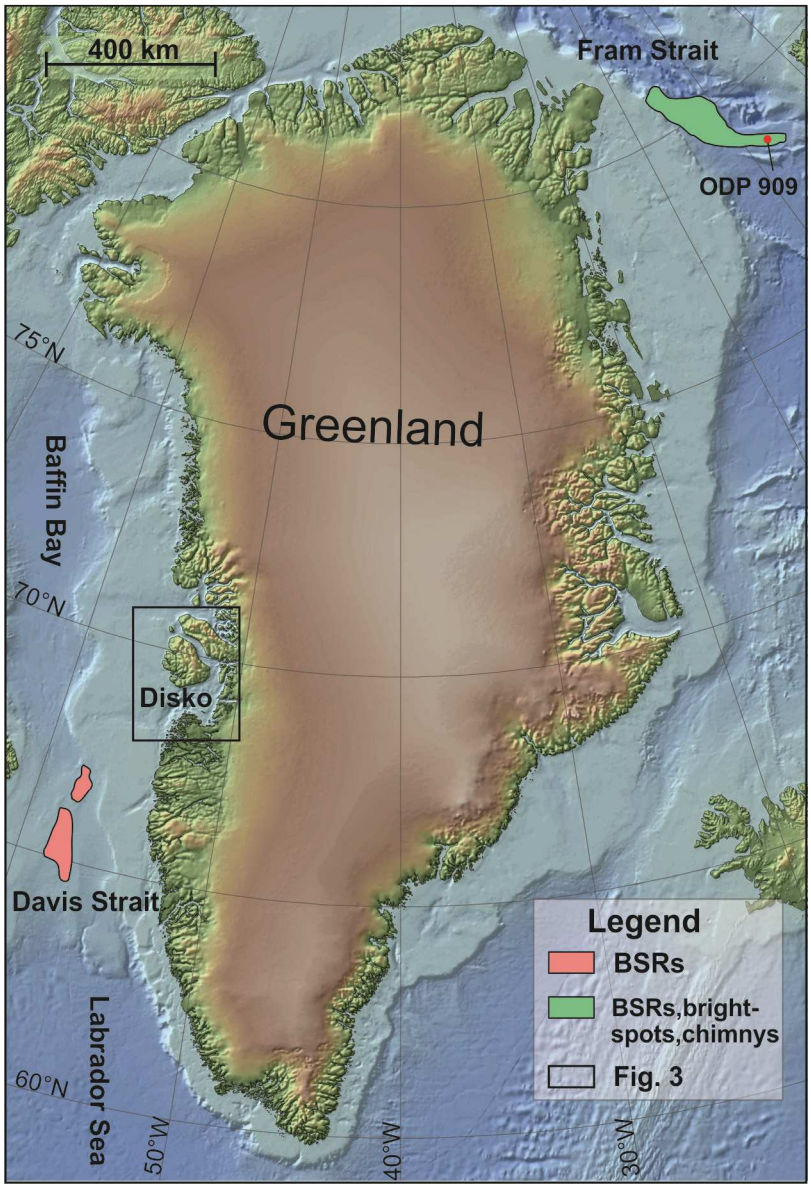


Figure 2: Bathymetric map of the Greenland margins and outline of larger offshore areas with seismic indications of hydrate. Box marks the area shown in Fig. 3.

3.2 Hydrate occurrence

Greenland is surrounded by wide shelf areas with water depths of 200-500 m and 1000-4000 m deep basinal areas (Fig. 2), all swept by cold bottom water currents. Therefore the Greenland continental margins should have physical and oceanographic settings suitable for marine hydrate formation. In addition, a study addressing as yet undiscovered hydrocarbon resources north of the Arctic Circle

suggests that the offshore Mesozoic sedimentary basins on the west and northeast Greenland margins could hold large quantities of oil and gas (Gautier et al., 2011). Due to late Cenozoic uplift and glacial erosion (Japsen et al., 2006), these basins are now exposed on the shelves at or near the seabed (Gregersen and Bidstrup, 2008; Hamann et al., 2005; Hopper et al., 2014), increasing the probability of seepages of gas and thus for formation of hydrate.

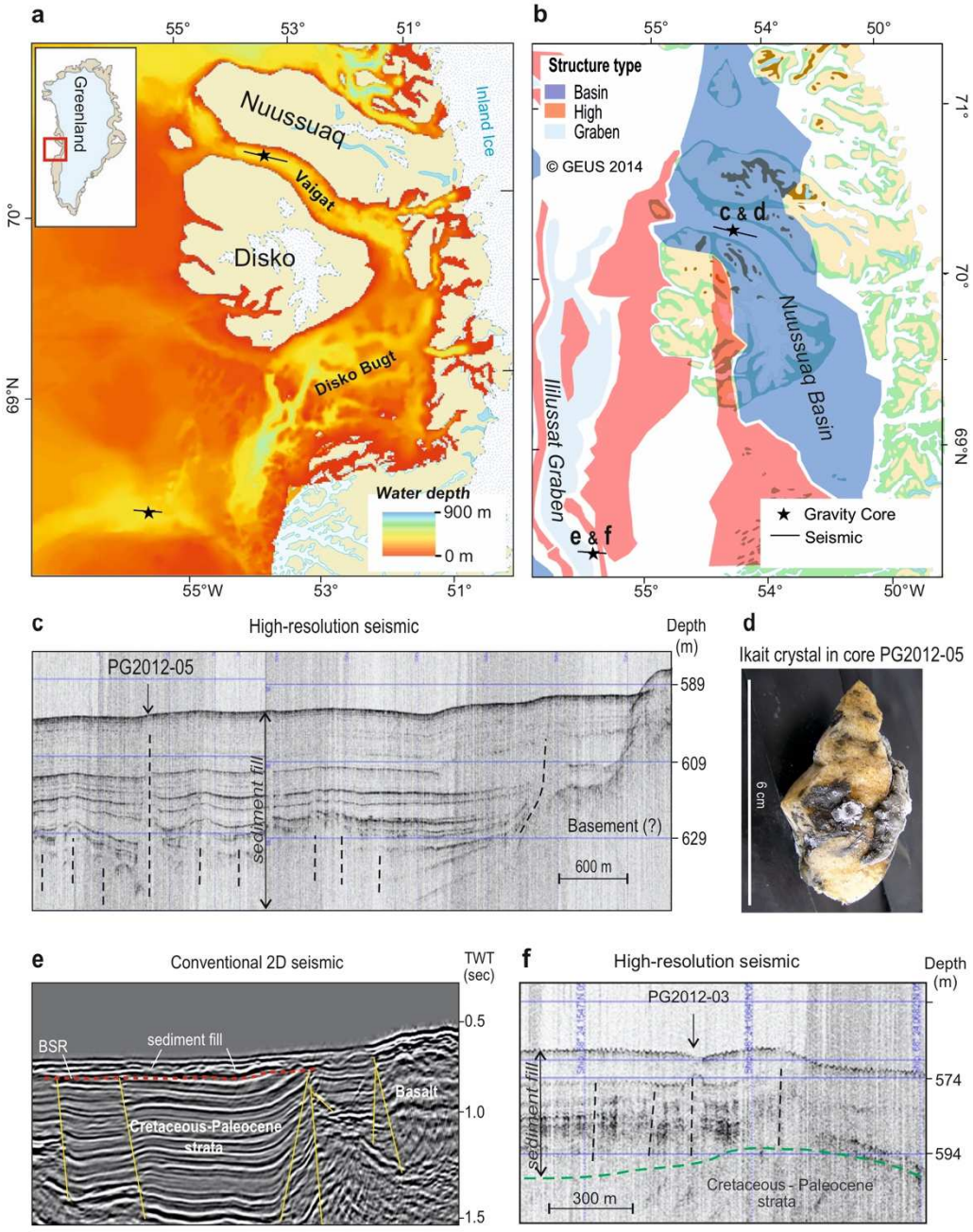


Figure 3: Indications of hydrate occurrence in the Disko area offshore central west Greenland, where bottom water temperature is c. 3°C (after Nielsen et al., 2014) a) Bathymetric map with locations of seismic and cores shown in c)-f) ; b) Simplified map of Cretaceous–Paleogene major structural elements, outlining the hydrocarbon-bearing Nuussuaq Basin (Bojesen-Koefoed et al., 2007) and the likely hydrocarbon-bearing Ilulissat Graben (Gregersen and Bidstrup, 2008), with locations of seismic and cores; c) High-resolution seismic line along Vaigat showing younger sediments with chimneys (dashed black lines) indicating gas/fluid seepage from below, and location of gravity core PG2012-05 taken on top of one of these features; d) 6-cm-long ikaite crystal collected from the core catcher of

gravity core PG2012-05, presumably originating from seepage of methane; e) 2D seismic record showing a seabed depression with sub-cropping faulted Cretaceous–Paleocene strata (yellow lines) and a BSR at about 75 ms sub-bottom depth (red dashed line); f) High-resolution seismic line inside the seabed depression, showing Cretaceous–Paleocene strata overlain by younger sediments that are disrupted by gas/fluid escape features (black dashed lines). Gas-bearing gravity core PG2012-03 was located in a pockmark underlain by a large diapiric feature.

Nevertheless, little work has been done on the hydrate potential of offshore Greenland. At present, most of the available data derive from conventional oil and gas exploration, including more than 100,000 km of 2D seismic reflection data offshore west and northeast Greenland as well as several 3D surveys on the western margin. Some information of heat flow and seabed temperature data offshore Greenland exist, but these are sparse and mostly limited to the few exploration wells that have been drilled along the western margin. Echo-sounder, high-resolution subbottom profiler and swath bathymetry data exist for smaller areas along all the margins, but most are not in the public domain.

Offshore northeast Greenland no commercial wells have been drilled yet. However, in the southern Fram Strait, Ocean Drilling Program (ODP) well 909 encountered gassy sediments (Knies and Mann, 2002), which can be traced up-slope the northeast Greenland margin, where bright spots, chimneys and possible BSRs indicate that hydrate may be present (Fig. 2; Nielsen and Jokat, 2009). Offshore west Greenland, several commercial wells have gas and oil shows, but there have been no significant discoveries so far. Several oil seeps as well as hydrate and gas encountered by shallow onshore drilling demonstrate that working petroleum systems exist in the Nuussuaq Basin (Fig. 3; Bojesen-Koefoed et al., 2007; Christiansen et al., 1994; Pedersen et al., 2006). A pilot study of the marine part of the Nuussuaq Basin found various indirect indicators for the presence of hydrate in shallow seismic and gravity core data (Nielsen et al., 2014; Fig. 3), demonstrating that the offshore part of the Nuussuaq Basin likely contains significant quantities of hydrate. Further offshore west Greenland, in the up to 700 m deep Davis Strait area (Fig. 2), BSRs with associated amplitude variations indicating hydrate above free gas can be seen on several seismic profiles (Nielsen et al., 2000), further demonstrating a possible marine hydrate occurrence in the region.

Direct sampling of hydrate offshore Greenland has not been reported to date and, despite the above-mentioned indications of hydrate presence, no systematic study or compilation has yet been undertaken. In addition, due to the very sparse information on heat flow and seabed temperature, there is currently no published detailed study of the hydrate stability zone offshore Greenland.

## 4. Offshore and onshore Svalbard

### 4.1 Geological Setting

The west Svalbard margin shares a common geological history with the northeast Greenland margin (section 3.1) until the opening of the Fram Strait. Subsequently, deep-water circulation between the

Arctic Ocean and the Norwegian-Greenland Sea led to deposition of thick contourite sequences that extend from the Svalbard margin towards the mid-ocean ridges. Two sediment types dominate the west Svalbard margin: glacigenic debris flows in trough mouth fans beyond the shelf break; and turbiditic, glaciomarine and hemipelagic sediments, which are to some extent reworked by contour currents (Vorren and Laberg, 1997; Vorren et al., 1998). The eastern margins of the Fram Strait were dominated by contourites during the late Miocene to Pleistocene (Mattingsdal et al., 2014) leading to the development of large sediment drifts such as the Vestnesa Ridge (Fohrmann et al., 2001) on young and relatively warm oceanic crust. The Vestnesa Ridge is located in the eastern Fram Strait at ~79°N, north of the Knipovich Ridge and Molloy transform fault (Fig. 4), representing one of the northernmost occurrences of hydrate in the world.

In contrast, the Svalbard archipelago is the most uplifted part of the Barents Shelf and is dominated by older strata providing a "window" into the tectono-stratigraphic evolution of the Barents Sea area. Approximately 60% of the archipelago is covered by glaciers, with the remainder strongly affected by continuous permafrost. Ice caps are found predominantly in northeastern Svalbard, with ice thicknesses of up to 550 m observed for the Austfonna ice cap on Nordaustlandet (Furst et al., 2018). Permafrost thickness varies from less than 100 m in coastal settings to over 500 m in the highlands (Humlum et al., 2003). The nearly complete Devonian-Paleogene stratigraphic record is exceptionally well exposed due to the lack of vegetation, giving insights into reservoir and source rock intervals targeted further south (Henriksen et al., 2011b; Nøttvedt et al., 1993; Worsley, 2008).

## 4.2 Hydrate occurrence

### 4.2.1 Offshore west Svalbard

The presence of a prominent hydrate BSR was revealed by several seismic reflection studies in the Vestnesa basin (e.g., Dumke et al., 2016; Eiken and Hinz, 1993; Vanneste et al., 2005; Fig. 4). The BSR can be traced from the continental slope at c. 800 m water depth to the Molloy Transform Fault and beyond to > 2000 m water depth (Hustoft et al., 2010; Sarkar et al., 2012; Vanneste et al., 2005). It appears as a nearly continuous reflection with amplitudes that vary laterally and generally decrease towards the flanks of sedimentary ridges (Fig. 5). This variation indicates that hydrate and gas accumulations are primarily topographically and structurally controlled (Bünz et al., 2012). The BSR covers the whole of the Vestnesa Ridge (i.e., from c. 1100 m to 1700 m water depth), exhibiting a strong impedance contrast between hydrate-bearing and gas-charged sediments (Bünz et al., 2012; Petersen et al., 2010; Plaza-Faverola et al., 2017). An interconnected zone of free gas beneath the BSR is more prominent along the eastern segment of the Vestnesa Ridge, where currently active gas seepage is concentrated (Hustoft et al., 2009; Panieri et al., 2017; Smith et al., 2014). Faults are identified on seismic profiles, extending from the seafloor to beneath the BSR. These faults control the ascent of fluids and the distribution of gas seeps on the Vestnesa Ridge (Plaza-Faverola et al.,

2015; Vanneste et al., 2005). Basin modeling studies show that generation of thermogenic gas from relatively shallow and young source rocks sustains shallow gas and hydrate accumulations, at least within the eastern part of the Vestnesa basin (Dumke et al., 2016; Knies et al., 2014). In this setting, very close to the mid-ocean ridge, the hydrate system is strongly influenced by the young and hot oceanic crust. Geothermal gradients increase gradually from 70 to 115 °C/km towards the Molloy Transform Fault (Crane et al., 1991; Vanneste et al., 2005).

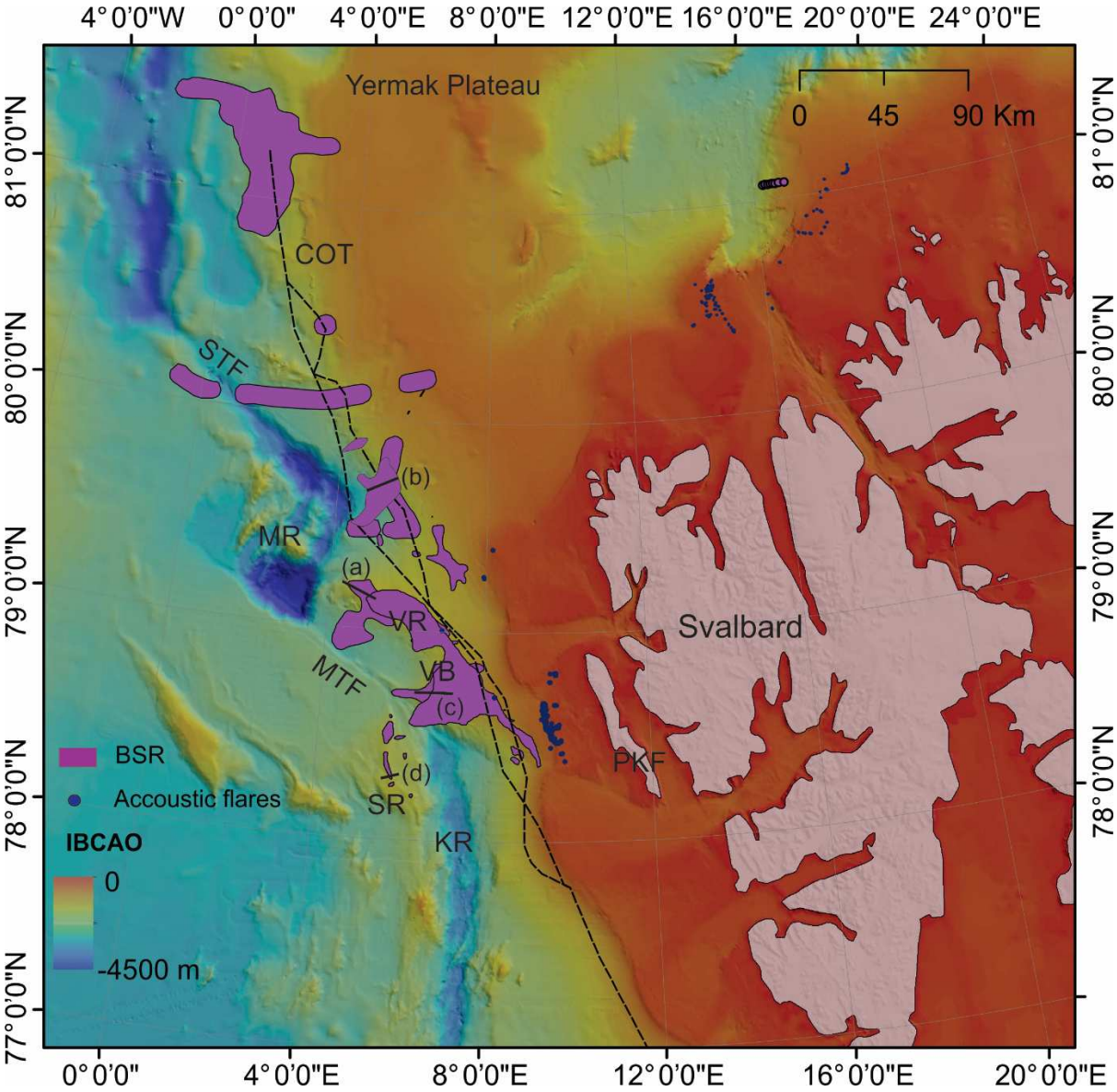


Figure 4: BSR distribution projected over IBCAO bathymetry off Svalbard. The BSR outline corresponds to observations from Vanneste et al. (2005); Petersen et al. (2010); Hustoft et al. (2009); Sarkar et al. (2012); Bünz et al. (2012); Geissler et al. (2014); Johnson et al. (2015); (Dumke et al., 2016);Plaza-Faverola et al. (2017); and Waghorn et al. (2018). Gas flares compiled from multiple expeditions to the area by NOC, AWI, CAGE. PKF=Prins Karl Forland; COT=Continent-Ocean Transition (Engen et al., 2008); KR=Knipovich Ridge; MR=Molloy Ridge; VR=Vestnesa Ridge; VB=Vestnesa Basin; SR=Svyatogor Ridge; MTF=Molloy Transform Fault; STF=Spitsbergen Transform Fault. (a)-(d) mark seismic profiles shown in Fig. 5.

South of the Molloy Transform Fault and to the west of the Knipovich ridge spreading axis, a well-developed hydrate system has been documented along the Svyatogor ridge, a contourite drift similar to the Vestnesa Ridge (Fig. 4, 5). Here the gas hydrate system is believed to be sustained by input of abiotic gas, a product of serpentinization at detachment faults (Johnson et al., 2015; Waghorn et al., 2018).

Elsewhere on the west Svalbard Margin, the BSR is weak and in some areas it is patchy (e.g., Geissler et al., 2014). Observations of shallow gas in accumulations that roughly follow the seafloor further upslope on the continental margin may be linked to hydrate dissociation (Riedel et al., 2018; Sarkar et al., 2012). To the west and east of the Yermak Plateau, relatively weak BSRs and some double BSRs have been documented (e.g., Geissler et al., 2014).

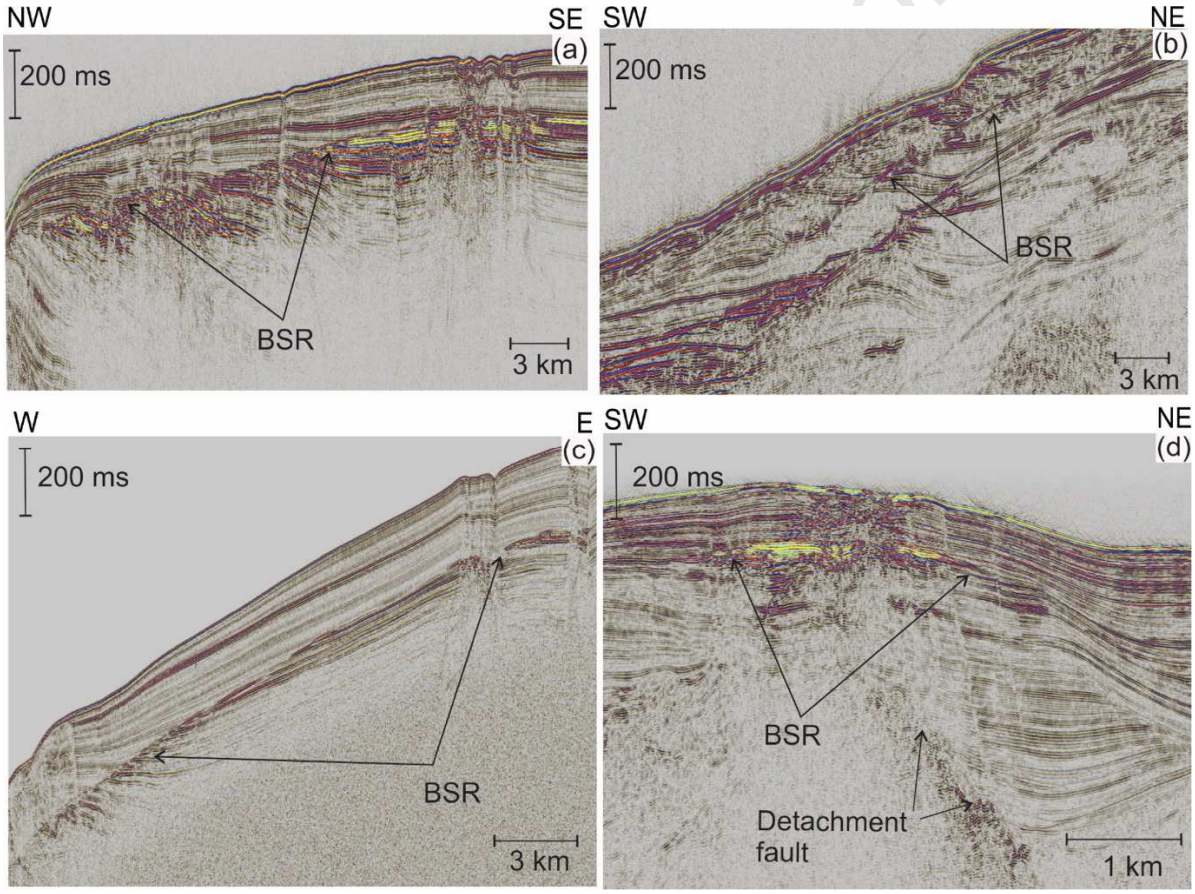


Figure 5: Examples of BSRs offshore west-Svalbard: (a) western segment of the Vestnesa Ridge (Plaza-Faverola et al., 2017); (b) western flank of Yermak Plateau (Geissler et al., 2014); (c) slope between Prins Karl Forland and the Molloy Transform Fault (Vanneste et al., 2005); (d) southern part of the Svyatogor Ridge (Johnson et al., 2015; Waghorn et al., 2018). The location of each example is indicated in Fig. 4. The BSR is continues and strong along the Svyatogor Ridge, the Vestnesa Ridge and its southern flank. The BSR is weak and patchy towards the Yermak Plateau.

Hydrate has been recovered from several of the pockmarks that lie above chimney structures on the eastern Vestnesa Ridge segment. Here, hydrate appears as small, thin chips, in veins or as chunks of several 10s of cm, embedded in the upper 2-4 m of muddy sediments (e.g., Panieri et al., 2017; Smith

et al., 2014). The gas compositions of these hydrate samples and of core head-space gas samples provide strong evidence for a thermogenic input into the HSZ (Plaza-Faverola et al., 2017; Smith et al., 2014). Massive hydrate has been collected in a zone of weak BSRs at a focused fluid flow structure on the continental slope (e.g., Graves et al., 2017; Sarkar et al., 2012). Hydrate is suspected but so far not found in regions where the HSZ pinches out near the shelf break off Prins Karl Forland, where pervasive seepage exists (e.g., Berndt et al., 2014; Wallmann et al., 2018; Westbrook et al., 2009). A HSZ volume of ca. 700 $km^3$ was derived from mapped BSRs in the Vestnesa Basin (Plaza-Faverola et al., 2015).

Several studies provide constraints on hydrate saturations on the eastern Vestnesa Ridge based on P-wave velocity variations from seismic data and resistivity from CSEM data. From P wave velocity anomalies, Hustoft et al. (2009) estimated mean hydrate saturations of ~6% within a 30-100 m thick zone above the BSR, reaching a maximum of 11%. Their velocity model was derived from multi-channel seismic reflection data along an E-W profile that intersects the crest of the Vestnesa ridge at the eastern end of an area of active seepage. They found the highest hydrate saturations at the crest of the ridge and near fault zones. In a more recent study along the ridge crest nearby, Singhroha et al. (2019) estimated hydrate saturations of 10-18% of the pore space within a 100 m thick zone above the BSR, based on P wave velocities and full waveform inversion of wide-angle seismic data from OBSs. By comparison, joint analysis of resistivity from CSEM data and OBS data along a transect in the same area suggests mean hydrate saturations of 20-30% outside of chimney structures and 40-68% in the lowermost c. 80 m of the HSZ within a highly brecciated gas chimney (Goswami et al., 2015). Despite similar velocities to those of Hustoft et al. (2009) and Singroha et al. (2019), these estimated saturations are much higher because free gas is assumed to co-exist with hydrate in the HSZ, contributing positively to the resistivity anomaly and negatively to the velocity anomaly. All three studies systematically found the highest hydrate saturations associated with faults and fractures within the GHZ. The free gas saturations estimated by these studies in zones outside gas chimneys consistently range between 1.5 and 4% of the pore space within a low-velocity zone below the BSR.

#### 4.2.2 Onshore Svalbard

As part of early petroleum exploration of the Barents Sea, eighteen petroleum exploration wells were drilled on Svalbard from 1961 to 1994 (Senger et al., 2017). While none of these wells resulted in commercial discoveries, numerous boreholes encountered gas. In addition, research drilling in Adventdalen and coal exploration in Petuniabukta discovered producible natural gas, some of which is directly associated with permafrost (Senger et al., 2019). These discoveries, as well as the presence of hydrate offshore (Section 4.2.1), prompted efforts to assess the feasibility of finding hydrate onshore Svalbard (Betlem et al., 2019).

Recent modelling efforts constrain a potentially stable marine hydrate stability zone in the fjords around Svalbard (Betlem, 2018; Roy et al., 2012), and a permafrost-associated hydrate stability zone onshore central Spitsbergen (Betlem et al., 2019). The latter has been extended to all unglaciated areas of Svalbard's main islands (Spitsbergen, Nordaustlandet, Prins Karls Forland, Barentsøya and Edgeøya; Fig. 6). Thus far hydrate has not been directly sampled onshore Svalbard, largely due to a lack of dedicated exploration efforts. Circumstantial evidence for probable hydrate presence is provided by long-term gas bubbling in numerous coal exploration boreholes (Jochmann, M., pers. comm. 2017), though these are unfortunately not well documented.

Thus the Svalbard archipelago possesses three important factors contributing to the presence of hydrate: 1) suitable thermobaric conditions, 2) an active petroleum system, and 3) a constant flux of thermogenic and microbial gas. Suitable thermobaric conditions (i.e., shallow-to-deep permafrost) are brought about by laterally changing mean annual air temperatures of between -3.5 °C and -8 °C (Betlem et al., 2019; Przybylak et al., 2014). Where permafrost surpasses 100-125 m depth, subsurface thermal regimes are cold enough to allow hydrate formation under hydrostatic pressure. Thickening of ice caps and glaciers towards the north is likely to contribute further to local regions of hydrate stability as a result of loading (i.e, pressure increase) and favourable thermal regimes at glacier bases. However, the extent of hydrate stability remains difficult to assess due to uncertainties in properties such as sub-glacial thermal state, densities, and local thicknesses, as well as the limited resolution and accuracy of relevant datasets.

Widespread organic-rich source rocks (e.g., Upper Jurassic to Lower Cretaceous Agardhfjellet Formation and Middle-Triassic Botneheia Formation) and coal beds (e.g., Lower Carboniferous Billefjorden Group and Paleogene Firkanten Formation) may act as unconventional reservoirs hosting disseminated or fracture-filled hydrate. These Mesozoic organic rich source rocks have the same origin as those contributing to hydrocarbon discoveries in the Barents Sea (Abay et al., 2014) and have been linked to hydrocarbon finds onshore. Suitable reservoir rocks are found in both sandstone-dominated sequences (e.g., the Paleogene Van Mijenfjorden Group, the Lower Cretaceous Helvetiafjellet Formation and the Upper Triassic-Middle Jurassic Wilhelmøya Subgroup) and carbonates (e.g., the Permian Tempelfjorden and Gipsdalen Groups). Limited reservoir quality, with poor matrix porosity and permability related to extensive diagenesis (e.g., Mork, 2013) is a major challenge. However, pervasive natural fracturing contributes by enhancing fracture-related fluid flow (Ogata et al., 2012).

Significant quantities of thermogenic gas (mixed with microbial gas in shallower intervals) were encountered during research drilling for the Longyearbyen $CO_2$ Lab project in Adventdalen (Ohm et al., 2019) and in petroleum and coal exploration wells (Senger et al., 2019). Furthermore, high

concentrations of microbial gas are observed in onshore pingo discharge waters (Hodson et al., 2019). Gas flares, pockmarks and thermogenic methane are observed in several fjords of Svalbard (Liira et al., 2019; Roy et al., 2019). Thus there is evidence for active fluid seepage both onshore and offshore.

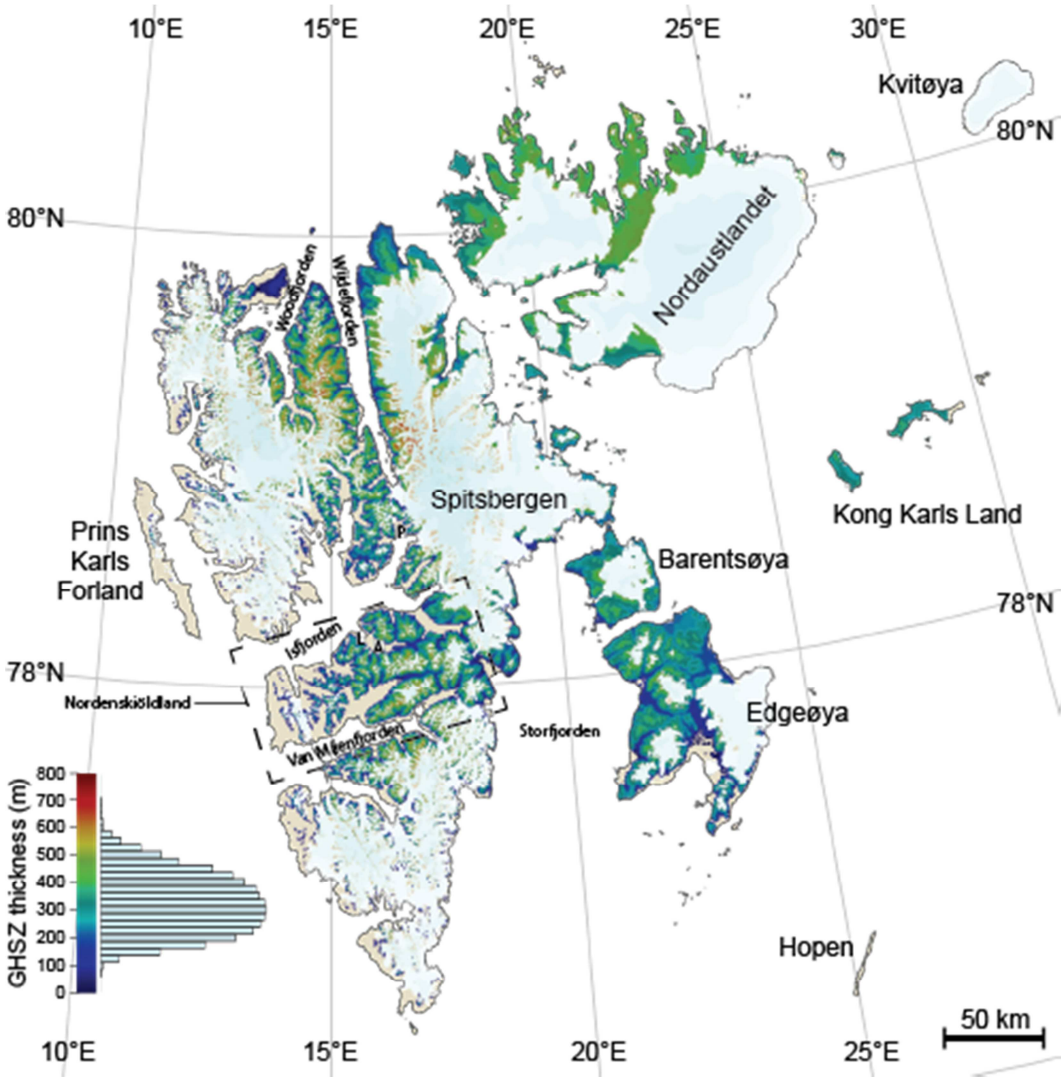


Figure 6: Thickness of the HSZ onshore Svalbard, for a plausible gas composition of 93% methane, 7% ethane and seawater salinity. Geothermal gradients are derived from boreholes and inferred from the depth of the base of permafrost thickness in central Spitsbergen (Betlem, 2018; Betlem et al., 2019). Lapse rate is set at -6 °C/km, and surface air temperatures are incorporated from Przybylak et al. (2014). A: Adventdalen; L: Longyearbyen; P: Petuniabukta. The map uses topographic and coastline data from the Norwegian Polar Institute.

Assuming that structure I hydrate dominates, a zone of hydrate stability likely occurs in the interior of Spitsbergen along a relatively unglaciated corridor stretching from Nordenskiöldland in the centre to Wijdefjorden in the north. Strandflats and valley systems limit hydrate stability on Svalbard's western flanks due to elevated temperatures associated with the West Spitsbergen Current (Przybylak et al., 2014). Mean annual temperatures decrease to the east, so that similar settings on Edgeøya, Barentsøya and Nordaustlandet fall well within the hydrate stability field, even in coastal settings. Most of the

archipelago thus appears to be on the edge of hydrate stability, with vertical and lateral variations tipping particular locations in and out of the hydrate stability field.

## 5. Norwegian Margin

### 5.1 Geological setting

The Barents Sea is a large epi-continental shelf sea bound by the North Atlantic to the west, the Norwegian and Russian landmasses to the south, the Arctic Ocean to the north and Novaya Zemlya to the east. Formed in association with the opening of Norwegian-Greenland Sea and Eurasia Basin during the Cenozoic (Faleide et al., 1984), it is composed of a complex mosaic of basins, platforms, and structural highs and is a major petroleum province (Doré, 1995; Nøttvedt et al., 1988). Tectonic uplift, erosion and multiple glaciations affected the Barents Sea during the Cenozoic and resulted in the removal of up to 2 km of sediments from the region (Henriksen et al., 2011a; Ktenas et al., 2017; Vorren et al., 1991). These processes resulted in the spillage of hydrocarbons from reservoir rocks, and recent exploration has shown predominantly gas reservoirs and underfilled reservoirs with low oil saturation (Doré and Jensen, 1996; Henriksen et al., 2011a).

Along the mid-Norwegian margin, the Møre and the Vøring basins are the two most prominent. They developed as a result of several rifting episodes until Late Paleocene/Early Eocene continental break-up (Brekke, 2000; Lundin and Doré, 1997). Post break-up thermal subsidence during the Cretaceous resulted in up to 10-km-thick sedimentary basin fill. The second youngest sedimentary succession is the Miocene/lowermost Pliocene Kai Formation with predominantly fine-grained hemipelagic sediments (Dalland, 1988; Rise et al., 2005). The overlying Naust formation encompasses sediments of the Plio-Pleistocene glacial-interglacial cycles that significantly changed the sedimentation pattern, yielding a thick wedge of clastic sediments on the shelf (Hjelstuen et al., 1999; Stuevold and Eldholm, 1996). Within this formation, contourites deposited along slope during deglaciation and interglacials frequently interlayer the glacigenic downslope-transported debris flows (Laberg et al., 2001). A mass-wasting event, the Storegga Slide, removed large amounts of sediment within the Møre Basin and along its northern border with the Vøring Plateau at about 8.2 ka (Bryn et al., 2005).

### 5.2 Hydrate occurrence

#### 5.2.1 Barents Sea

Leaking reservoirs in the Barents Sea have given rise to widespread occurrence of fluid-flow features such as shallow gas accumulations, gas seeps, gas chimneys, pockmarks of various sizes, pingos and hydrate (Fig. 7; Andreassen et al., 2017; Chand et al., 2012; Laberg and Andreassen, 1996; Rise et al., 2015; Serov et al., 2017; Vadakkepuliyambatta et al., 2013; Vadakkepuliyambatta et al., 2017). Fluid migration in the area is structurally controlled, with major faults and fractures acting as pathways (Vadakkepuliyambatta et al., 2013).

The presence of hydrate has been inferred at multiple locations in the Barents Sea from BSRs in multi-channel seismic data (Vadakkepuliyambatta et al., 2017 and references therein). BSRs occur in close association with vertical fluid-flow systems, shallow gas accumulations, faults, and fractures (Ostanin et al., 2013; Vadakkepuliyambatta et al., 2013; Vadakkepuliyambatta et al., 2017; Vadakkepuliyambatta et al., 2015). They generally occur in consolidated sediments of Jurassic and younger ages as well as in the glacial sediments of Pleistocene to Holocene age (e.g., Andreassen et al., 1990; Vadakkepuliyambatta et al., 2017). Although multiple active seeps have been detected in the southwest Barents Sea (e.g., Andreassen et al., 2017; Chand et al., 2012), no hydrate sample has been recovered yet. However, in the Storfjordrenna region of the northwest Barents Sea, Serov et al. (2017) reported sampling of hydrate just below the seafloor. Hydrate was also recovered on the continental slope of southwest Barents Sea at the Håkon Mosby mud volcano (Ginsburg et al., 1999).

Results from thermal modelling suggest a prevalence of thermogenic methane and higher order hydrocarbons forming hydrate in the region (Chand et al., 2008; Vadakkepuliyambatta et al., 2017). Methane hydrate is not stable in most parts of the Barents Sea, primarily due to the shallow water depth (<350 m; Chand et al., 2008; Klitzke et al., 2016; Vadakkepuliyambatta et al., 2017). Hydrate occurrence is highly variable, controlled primarily by thermogenic gas discharge into the shallow sediments (Vadakkepuliyambatta et al., 2017). Variations in the geothermal gradient, salt tectonics, and the inflow of warm Atlantic water also influence hydrate stability in the region (Chand et al., 2008; Vadakkepuliyambatta et al., 2017). Major factors controlling hydrate stability, such as the bottom water temperature and geothermal gradient, vary greatly across the various basins and highs of southwest Barents Sea. Bottom-water temperatures can vary between 1 and 6 ºC across the region, where warm Atlantic waters mix with cold Arctic waters (Vadakkepuliyambatta et al., 2017). Seasonal variations in bottom water temperature are up to 2 º C (Ferré et al., 2012). Geothermal gradients vary from 25 to 65 º C/km, mainly due to the presence of salt diapirs on the eastern part of this area (Bugge et al., 2002). The southwest Barents Sea may be a focus of hydrate dissociation due to ocean warming in the near future (Vadakkepuliyambatta et al., 2017).

The volume of hydrate in the Barents Sea is still uncertain, primarily due to the uncertainties related to gas composition, hydrate saturation and hydrate distribution within the host sediments. Based on multi-channel seismic data and well logs, Laberg et al. (1998) estimated ~0.19 $GSm^3$ ($GSm^3 = 10^9$ standard cubic metres) of gas hydrate trapped within the Eocene succession of a small part of Bjørnøya Basin where a BSR was observed. Vadakkepuliyambatta et al. (2017) proposed a hydrate volume of ~93-650 $GSm^3$ in the southwest Barents Sea from hydrate stability models that assumed that the hydrate-forming gas was pure methane. Due to the presence of higher-order hydrocarbons, the hydrate volume could be as high as ~470–3320 $GSm^3$. The patchy occurrence of hydrate systems in

the southwest Barents Sea and their occurrence in consolidated, low-porosity sediments indicates low resource density for economic exploitation.

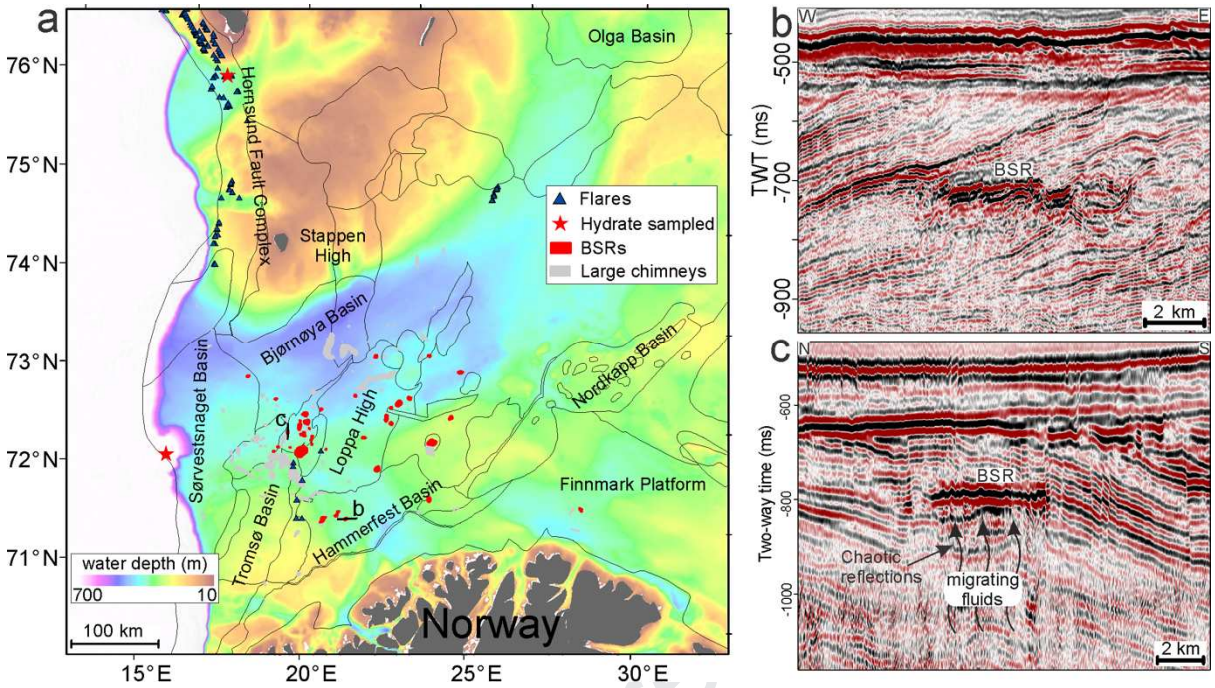


Figure 7: a) Bathymetry of the western Barents Sea with locations of hydrate indicators (compiled from Andreassen et al., 2017; Chand et al., 2012; Mau et al., 2017; Serov et al., 2017; Vadakkepuliyambatta et al., 2013; Vadakkepuliyambatta et al., 2017). b) and c) Seismic examples of a BSR in the southwest Barents Sea clearly cross-cutting the tilted sedimentary strata and showing reversed polarity compared to the seafloor reflection (modified from Vadakkepuliyambatta et al., 2017).

5.2.2 Mid-Norwegian margin

Bugge et al. (1988) first recognised evidence for hydrate in the northern Storegga Slide area of the mid-Norwegian Margin in the form of a weak BSR. Later, Posewang and Mienert (1999) and Bouriak et al. (2000) confirmed the geophysical evidence that hydrate exists in this area. In high-resolution seismic data, the BSR is generally characterised as an abrupt upper boundary of increased reflection amplitude (Fig. 8a; Bouriak et al., 2000; Bünz et al., 2003). In areas of dipping seafloor the BSR is readily identified cross-cutting the almost horizontally layered strata.

A double BSR observed in a small area along the northern flank of the Storegga Slide is attributed to a hydrate structure involving high-order hydrocarbons (Andreassen et al., 2000; Posewang and Mienert, 1999). Analysis of multi-component seismic data does not show a BSR in shear-wave components, indicating that hydrate here does not increase the shear stiffness of the sediments (Andreassen et al., 2003; Bünz et al., 2005). The presence of a BSR inside the slide area indicates that the hydrate system is dynamically adjusting to post-slide pressure-temperature equilibrium conditions (Fig. 8b; Bouriak et al., 2000; Bünz et al., 2003).

Bünz et al. (2003) mapped the extent of the BSR, which predominantly occurs over an area of about 4000 km$^2$ on the mid-Norwegian margin along the northern flank of the Storegga Slide (Fig. 8c). The glacial evolution of this margin resulted in widespread deposition of glacial sediments that built out the continental shelf (e.g., Hjelstuen et al., 2005; Stuevold and Eldholm, 1996). These low-permeability sediments are not conducive to hydrate growth and limit the extent of hydrate to the northern flank of the Storegga Slide, where they occur in marine contourite deposits. The large-scale distribution of hydrate in this area can be classified as a stratigraphic accumulation. The hydrate occurrence coincides with a vertical fluid flow system as documented by features such as pockmarks on the seafloor and pipe and chimney structures in subsurface seismic data (Bouriak et al., 2000; Bünz et al., 2003; Hustoft et al., 2010; Hustoft et al., 2007). A hydrate stability model was developed by Mienert et al. (2005), who speculated that ocean warming since the last deglaciation promoted the development of instabilities along the mid-Norwegian margin.

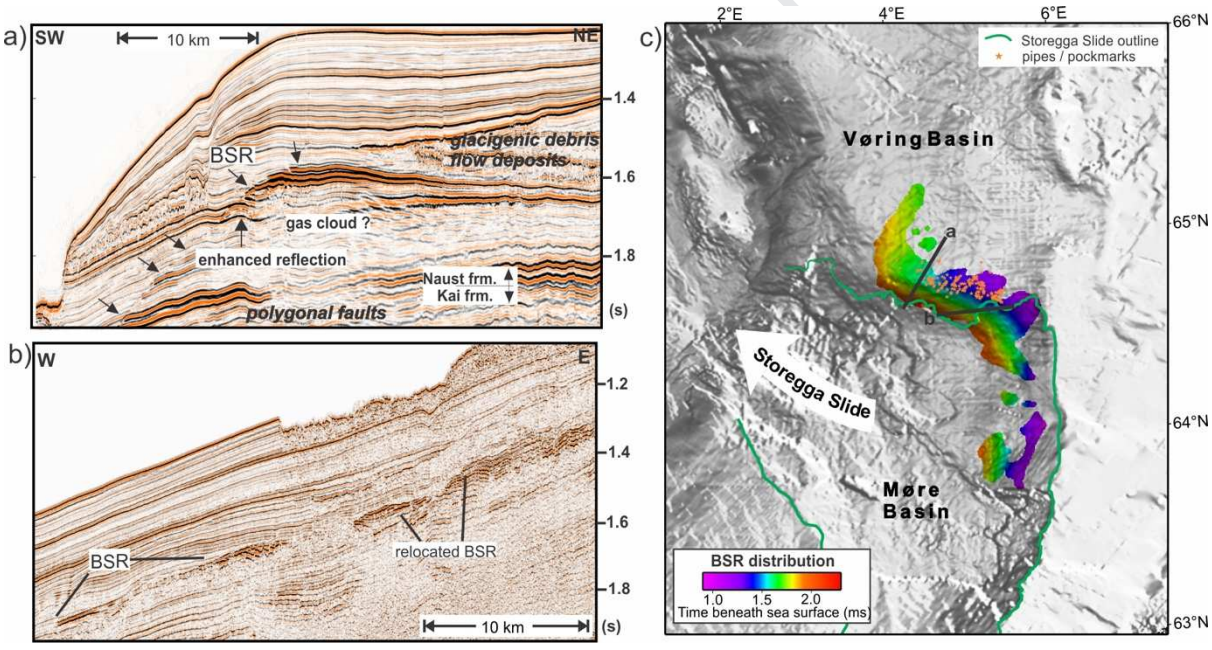


Figure 8: Examples of BSRs on the mid-Norwegian margin (modified from Bünz and Mienert, 2004): a) typical expression of a BSR identified as an abrupt upper boundary of increased reflection amplitude, occurring in glaciomarine contourite deposits along the northern flank of the Storegga Slide (vertical exaggeration ~35). b) The BSR also occurs inside the Storegga Slide area where it has readjusted to post-slide pressure-temperature equilibrium conditions (vertical exaggeration ~33). c) The BSR predominantly occurs along the northern Storegga Slide flank and patchily west of the Storegga Slide headwall over a total area of 4000 km$^2$.

Velocity analyses of seismic data provided evidence for the existence of hydrate in sub-seafloor sediments (Bünz and Mienert, 2004; Bünz et al., 2005; Plaza-Faverola et al., 2010; Westbrook et al., 2008). Hydrate saturations have been estimated from OBS data and range from 2 to 15% of pore space. The first hydrate sample in this area was from a pockmark in the Nyegga area, located at the northeastern corner of the Storegga Slide (Ivanov et al., 2007). Isotopic analysis of the gas in hydrate

649 from this pockmark suggests a primarily microbial origin but with a significant thermogenic
650 component (Vaular et al., 2010). In the Nyegga area, many focused fluid flow structures pierce the
651 HSZ (Hjelstuen et al., 2010; Hustoft et al., 2010; Plaza-Faverola et al., 2011) and form such
652 pockmarks at the seafloor (Hovland et al., 2005; Mazzini et al., 2006). Analysis of velocities from
653 wide-angle seismic data and resistivities from CSEM data showed that these chimneys likely contain
654 much larger amounts of gas hydrate than the surrounding stratified sediments (Attias et al., 2016;
655 Plaza-Faverola et al., 2010).
656
657 Senger et al. (2010) compiled a large database of geophysical and geotechnical borehole data for a
658 resource evaluation of the Norwegian Sea gas hydrate prospect. Their method was based on a
659 stochastic approach and closely followed that of conventional hydrocarbon prospect evaluation. The
660 calculated in-place volume has a large uncertainty, primarily due to the lateral variations in reservoir
661 parameters. Senger et al. (2010) estimated that the prospect (both hydrate and free-gas zones) contains
662 625 $GSm^3$ of gas. The amount of gas is significant compared to conventional hydrocarbon reservoirs
663 in the Norwegian Sea (e.g. the Ormen Lange field with about 439 $GSm^3$). However, the resource
664 density is rather low, so future economic exploitation is unlikely.
665
666 **6. Offshore Ireland**
667 6.1 Geological Setting
668 The continental margin offshore Ireland bears the imprints and structures resulting from Variscan,
669 Caledonian and older orogenic events (Naylor and Shannon, 2011). The nature of the basement
670 successions, together with their inherent lineaments and structural fabrics, had a major influence on
671 the location and structural segmentation of the basins. Basins of various geometries, sizes and ages,
672 filled with thick Cenozoic successions, occur in the western Irish Atlantic shelf, in water depths of
673 400 m to more than 4500 m. Four kilometres of Cenozoic strata occur in the Porcupine Basin and up
674 to 2 km have been identified on seismic profiles in the Rockall Basin (Shannon et al., 1993). Fluid
675 flow within the basins is likely to have been controlled by the overall basin geometry and by the
676 distribution and linkage of permeable strata with fault systems and unconformities. Active petroleum
677 systems in the Rockall and Porcupine basins have been documented by oil and gas exploration since
678 the 1970s.
679
680 Potential source rocks include the Upper Carboniferous, Middle and Upper Jurassic successions,
681 which are generally mature throughout these basins. The Cretaceous and Cenozoic successions also
682 have some potential for oil and gas generation. The Kimmeridgian succession (Upper Jurassic) is a
683 good proven source rock that is well distributed in the Porcupine Basin. It has total organic carbon
684 (TOC) values of 3 - 4%. The Lower Cretaceous succession has TOC values of 1.8 – 2.7% (Naylor and
685 Shannon, 2011). The Dooish gas condensate discovery on the eastern margin of the Rockall Basin

demonstrates the presence there of a thermogenic petroleum system. Middle Jurassic lacustrine mudstone is anticipated as a potential source as in the Porcupine Basin. Other source rocks are the Lower Cretaceous with TOC values of 3-14%, and Albian lacustrine mudstones with TOC values of 2.04% (Hitchen, 2004).

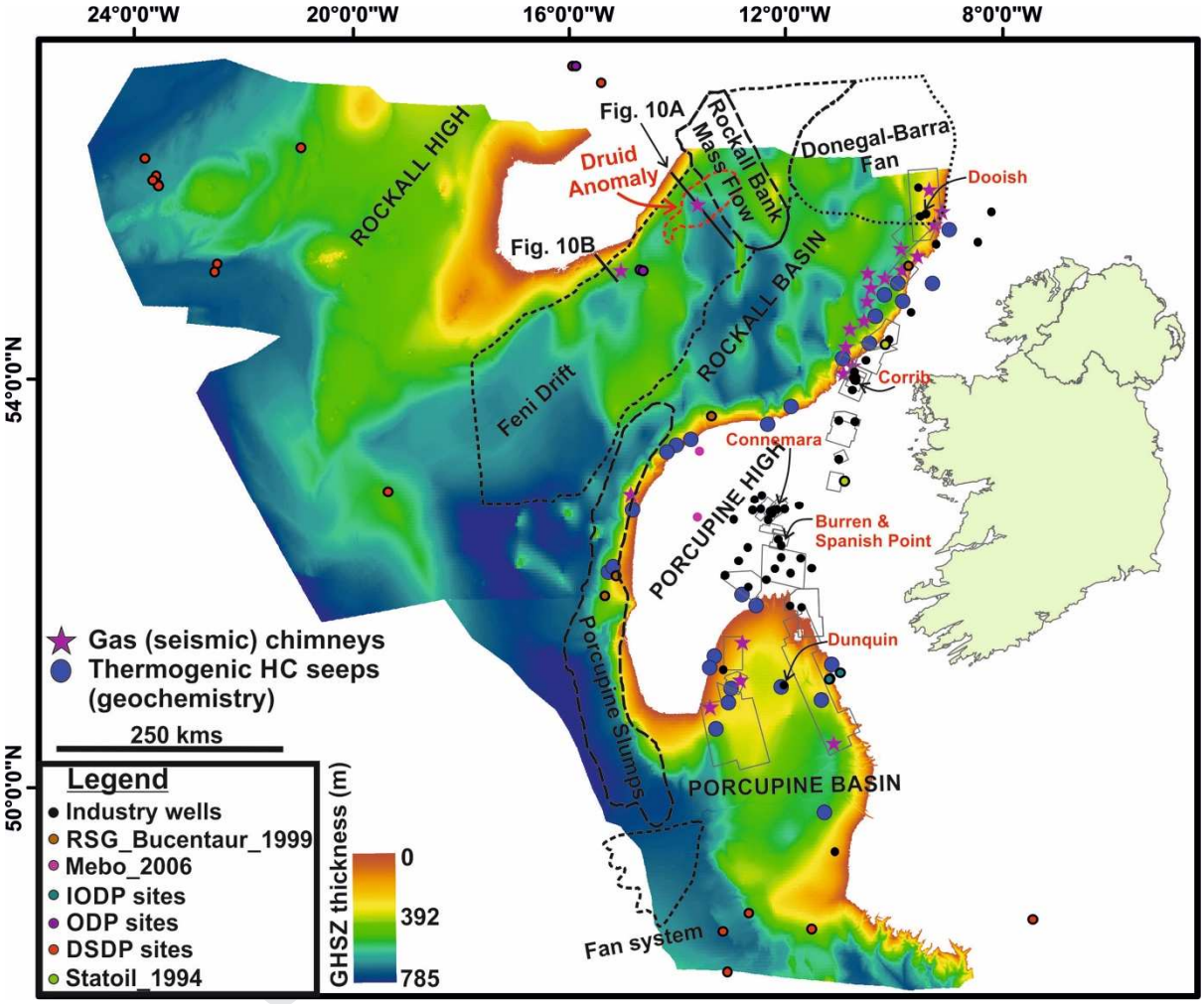


Figure 9: Calculated HSZ of Irish basins, for pure methane and 3.5% salinity and using seabed temperature from a compilation of oceanographic data and a geothermal gradient of 30-35°C/km (Roy et al., 2017). Also shown are locations of 3D seismic cubes, boreholes, gas chimneys, hydrocarbon (HC) seeps, and proven hydrocarbon systems (text in red).

## 6.2 Hydrate Occurrence

High resolution bathymetric data (100 m resolution), seabed temperature from 4760 CTD casts, and geothermal data from four boreholes have been used to calculate the HSZ offshore western Ireland (Roy and Max, 2018; Fig. 9). An extensive set of geophysical and geological data was integrated for the assessment of lithology, migration pathways of natural gas-saturated water in the form of chimney structures (Van Rensbergen et al., 2005b), presence of source rocks or conventional reservoirs, as well as host rocks for hydrate within its stability zone. A brief summary of the datasets used is provided below, with locations shown in Fig. 9:

a) Industry scale exploration data: 31 2D multichannel seismic surveys, 11 3D seismic cubes, and 18 exploration wells drilled within the HSZ.
b) Scientific drilling campaigns: Integrated Ocean Drilling Programme (2 sites), Ocean Drilling Programme (2 sites) and 12 Deep Sea Drilling Project (12 sites) within the HSZ.
c) Shallow drilling campaigns: Statoil 1994 (1 site), Rockall Study Group Bucentaur 1999 (3 sites), and Mebo 2006 (1 site).

The HSZ extends up to 645 m below the seafloor in the Rockall Basin, and 784 m in Porcupine Basin (Fig. 9). Fluid escape features, gas chimneys, bright spots indicating shallow gas accumulations, and faults that act as pathways for fluid migration, have been interpreted above potential source rocks and active petroleum systems. Three types of depositional systems have been identified as potential hosts for hydrate accumulations in Irish basins:

a) Mass transport deposits (MTDs): Slope failures are widespread along both the western and eastern margins of the Rockall Basin. Sidescan sonar images show a broad interplay of along-slope and downslope sediment transport, with sediment sourced from the northeastern margin and redistributed by currents along the western margin (Unnithan et al., 2001). Along the western margin, the Rockall Bank Mass Flow is a large, multi-phase submarine slope failure comprising of several MTDs, with failure scarps extending over *c.* 6100 km$^2$. It lies upslope a series of mass flow lobes covering *c.* 18,000 km$^2$ of the Rockall Basin seafloor (Elliott et al., 2010). Low- to medium-porosity turbidites have been found in shallow gravity cores of the lobes, which could be ideal hydrate reservoirs (Roy and Max, 2018).
b) Feni contourite drift: The Feni drift lies along the northwest flank of Rockall Basin, formed under the influence of deep, geostrophic currents formed by intermittent overflows of Arctic Intermediate Water from the Norwegian Sea. Sites 980 and 981 from ODP Leg 162 are located on the Feni Drift sediments. It is predominantly composed of rapidly accumulated nannofossil oozes with variable amounts of clay and silt. The lithology of Feni Drift is similar to that of Blake Ridge sediments but bed differentiation may be better. Extensive fluid escape features from deeper Lower Jurassic source rocks extend over an area ~ 2000 km$^2$, known as the Druid Anomaly (Fig. 9). Gas chimneys terminate beneath polygonal faults observed partly within the HSZ, which has an average thickness of 225 m (Roy and Max, 2017; Fig. 10).
c) Turbidite and contourite deposits: Isolated sand bodies, contourite furrows (erosional features), and turbidite channel systems have been mapped from 3D seismic data within the HSZ in the Porcupine Basin (Roy and Max, 2018). Associated gas chimneys and fault systems mark upwelling fluid migration from deeper sources to these potential hydrate reservoirs.

BSRs have not been identified in the Irish basins. A reason for the absence of a BSR in the available seismic data could be that these data were processed to better identify deeper structural and

stratigraphic geological traps. The processing sequence may have obscured shallower structures. Various seismic amplitude anomalies (e.g., bright spots, seismic gas pipes and chimneys, reverse polarity) have been observed in close proximity to the calculated base of the HSZ (Fig. 10b). Possible BSRs have been documented within contourite deposits in the southern and central parts of Porcupine Basin, at water depths of 1500 - 2200 m (Roy and Max, 2018).

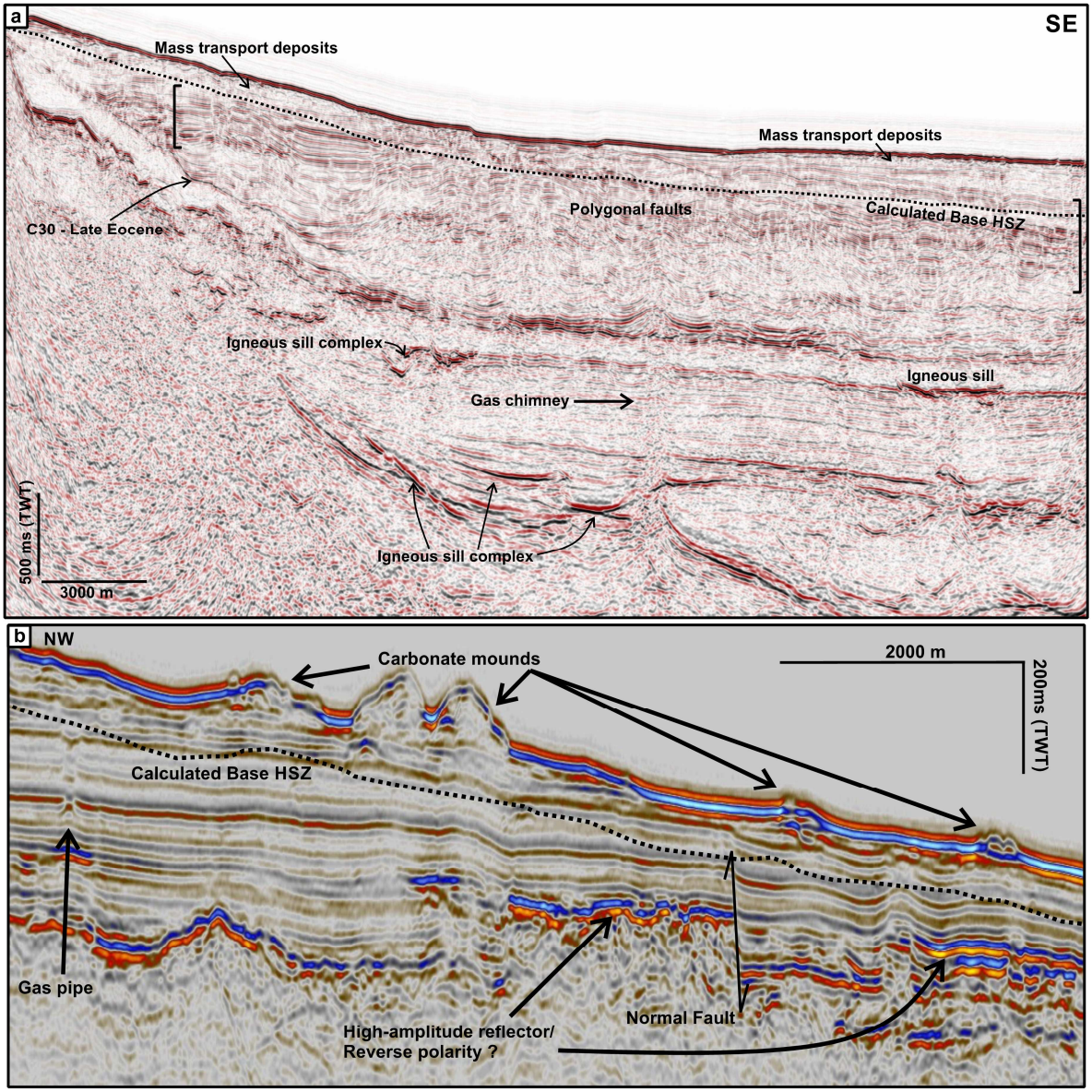


Figure 10: a) Seismic reflection profile showing gas chimney (part of the Druid anomaly) in the Rockall Basin, originating from potential source rock, with polygonal faults, sill complexes, mass transport deposits (Rockall Mass Flow), and C30 late Eocene unconformity (Roy et al., 2017). The extent of polygonal faults, which extend into the HSZ in the southeast, is shown by square brackets. These faults could act as potential fluid migration pathways for deeper fluids to reach the HSZ (interpolated from the grid of Fig. 9). b) Interpretation of suspected shallow gas accumulation (enhanced high-amplitude reflections) beneath the calculated base of HSZ, and fluid migration pathways such as gas pipes and normal faults in Rockall Basin. Locations are marked in Fig. 9.

## 7. Northwest Iberian Margin

### 7. 1 Geological Setting

The northwest Iberia continental margin developed during the northward propagation of the North Atlantic Ocean rift system (Boillot, 1995; Boillot et al., 1979; Pérez-Gussinyé and Reston, 2001). Several extensional phases from the Triassic to the Early Cretaceous lead to a complex fault system formed by north-south to northwest-southeast normal faults and northeast-southwest to east-west transfer faults (Pinheiro et al., 1996; Wilson et al., 1989). North-south compression during the Alpine orogeny resulted in the reactivation and partial inversion of previous rift structures and the generation of new compressional structures (Murillas et al., 1990; Pinheiro et al., 1996; Vázquez et al., 2008).

The present-day northwest Iberia continental margin is characterised by a roughly north-south, ~40 km wide continental shelf and a relatively steep slope down to ~2000 m water depth. Beyond the continental slope, the continental margin can be divided into three main geomorphological provinces (Fig. 11; Reston, 2005): 1) the Galicia Interior Basin (GIB); 2) the Western Banks – an area of seamounts that includes the Galicia Bank; and 3) the Deep Galicia Margin (DGM). The sedimentary cover ranges from 0 to 4 km, with maximum thickness in the Galicia Interior Basin depocenter (Pérez-Gussinyé et al., 2003).

### 7.3 Hydrate Occurrence

The data available for determining the likelihood of methane hydrate stability and presence on the northwest Iberia margin come from diverse sources of varying resolution. Bathymetry data with a minimum 250 x 250 m resolution are publicly available on the EMODnet bathymetry data portal ( EMODnet Bathymetry Consortium, 2016). A higher resolution bathymetric grid (100 x100 m) compiled by the Spanish Naval Hydrographic Institute has limited public availability (Druet et al., 2018; Maestro et al., 2018; Somoza et al., 2014). Only two research cruises have been focused on shallow gas occurrence there (Rey and Gran Burato Science Team, 2010, 2011). These cruises acquired high-resolution multichannel and very-high-resolution single channel (3.5 kHz) seismic data and multibeam data to characterise three giant pockmarks depressions in the Transitional Zone (Fig. 11) between the highly thinned crust of the Galicia Interior Basin and the relatively unthinned crust of the Galicia Bank.

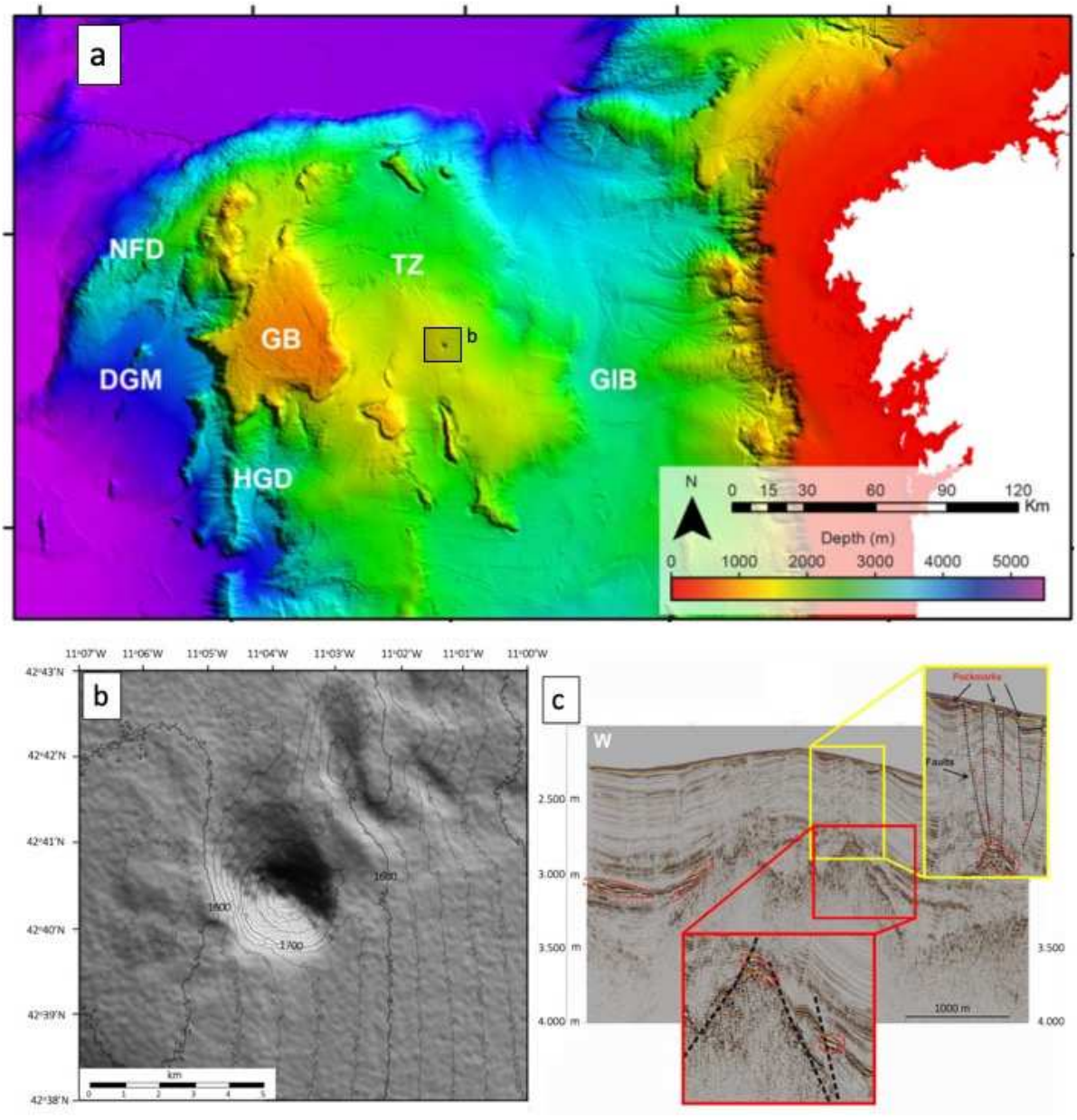


**Figure 11:** a) Bathymetry of the northwest Iberian Margin. GIB: Galicia Interior Basin, TZ: Transitional Zone, GB: Galicia Bank, NFD: Northwest Flank Domain, DGM: Deep Galicia Margin, HGD: Half-graben Domain. Note the three large circular structures in the Transitional Zone; b) Detail of the Gran Burato (GB) giant pockmark (after Druet, 2015) corresponding to grey square in a); c) Seismic line located south of the Gran Burato pockmark in b) showing how amplitude anomalies (circled in red) sourced fluid activity (after Ribeiro, 2011).

Evidence for shallow gas in the proximal northwest Iberia continental margin has been described since the early 2000s (Durán et al., 2007; Ferrín et al., 2003; García-García et al., 2003; García-Gil et al., 2015). However, the possibility of hydrate occurrence did not emerge until a decade later based on the presence of several seabed features related to fluid escape imaged in the Transitional Zone (Druet, 2015; Ercilla et al., 2011; López Pérez et al., 2019; Ribeiro, 2011). Some of the fluid escape structures have a seafloor expression (e.g., pockmarks), while others were detected by seismic amplitude

anomalies. Pockmarks were identified with a wide range of size and depths, on almost all the seismic profiles acquired in the Transitional Zone (Rey and Gran Burato Science Team, 2010, 2011; Ribeiro, 2011). The three biggest pockmarks, in water depths of 1600-1850 m, correspond to semicircular depressions that have depths up to 375 m and diameters between 2 and 5 km. A detailed study of the Gran Burato (Fig. 11b), the northernmost and largest pockmark in the Transitional Zone, showed evidence for fluid (most likely gas) migration and accumulation in both deep and shallow stratigraphic units (Ribeiro, 2011). Additionally, two fields of medium-size pockmarks with a density of more than five pockmarks per square kilometer were described (Rey and Gran Burato Science Team, 2011). Stratigraphic analysis of seismic data suggests that some these pockmarks are related to middle Miocene to Quaternary sedimentary units. Some of the pockmarks still appear to be active (Ribeiro, 2011). The most recent and intense fluid escape takes place in the northernmost sector. An estimate of the HSZ based on the regional geothermal gradient suggests widespread hydrate stability in the area (Rey and Gran Burato Science Team, 2011).

Various seismic amplitude anomalies (e.g., areas of seismic blanking, bright spots, chimney structures) have been identified close to the pockmark fields and are interpreted as evidence of gas presence within the sediments (Ribeiro, 2011). Fig. 11c shows high-amplitude anomalies on a structural high that pinch out against faults. Pockmarks observed immediately above may result from extensive structurally controlled fluid seepage via faults and fractures (Ribeiro, 2011). A high-amplitude reflector that mimics the seabed was observed in some seismic profiles at the estimated hydrate phase boundary depth, but the polarity inversion typically associated with BSRs could not be identified, so its origin remains uncertain (Rey and Gran Burato Science Team, 2011).

Analysis of sediment samples from piston cores collected close to the Gran Burato were inconclusive (Rey and Gran Burato Science Team, 2011). Some signs of liquefaction were observed in one piston core, but no associated thermal anomalies were registered, though long core travel times may have attenuated such anomalies. Also, no evidence for chlorinity anomalies or significant sulphate depletion was reported (Rey and Gran Burato Science Team, 2010, 2011). Benthic fauna associated with gas seepage were reported, although the observed species are not exclusive to these environments.

## 8. South Iberia and Northwest African Margin

### 8.1 Geological Setting

The South Iberia and Northwest Africa margins are located in the context of the Betic–Rif orogen either side of the Gibraltar Strait: the Gulf of Cádiz (Eastern Atlantic) and Alborán Sea basin (Western Mediterranean) (Fig. 12). The Atlantic margins of the Gulf of Cádiz were formed during Mesozoic rifting close to the boundary between the Central and North Atlantic. From the late

Oligocene to the early Tortonian, these margins were deformed by north-south convergence between the African and Eurasian plates due to the westward drift of the Alborán Domain and development of the Betic-Rif belt (Platt et al., 2003). Simultaneously the Alborán Basin was developed by extensional normal faulting and crustal thinning in the back-arc area of the Alborán Domain. Northwest-southeast convergence caused a post-Tortonian compressive regime that produced the progressive inversion of the basin, Betic-Rif range uplift, two sets of strike–slip faults, reverse faults and folds (Estrada et al., 2018; Martinez-Garcia et al., 2017). There was subsequent mud diapirism and related mud volcanism and the formation of pockmark fields (Pérez-Belzuz et al., 1997; Somoza et al., 2012), which occur mainly in the western part of the Alborán Basin (Pérez-Belzuz et al., 1997).

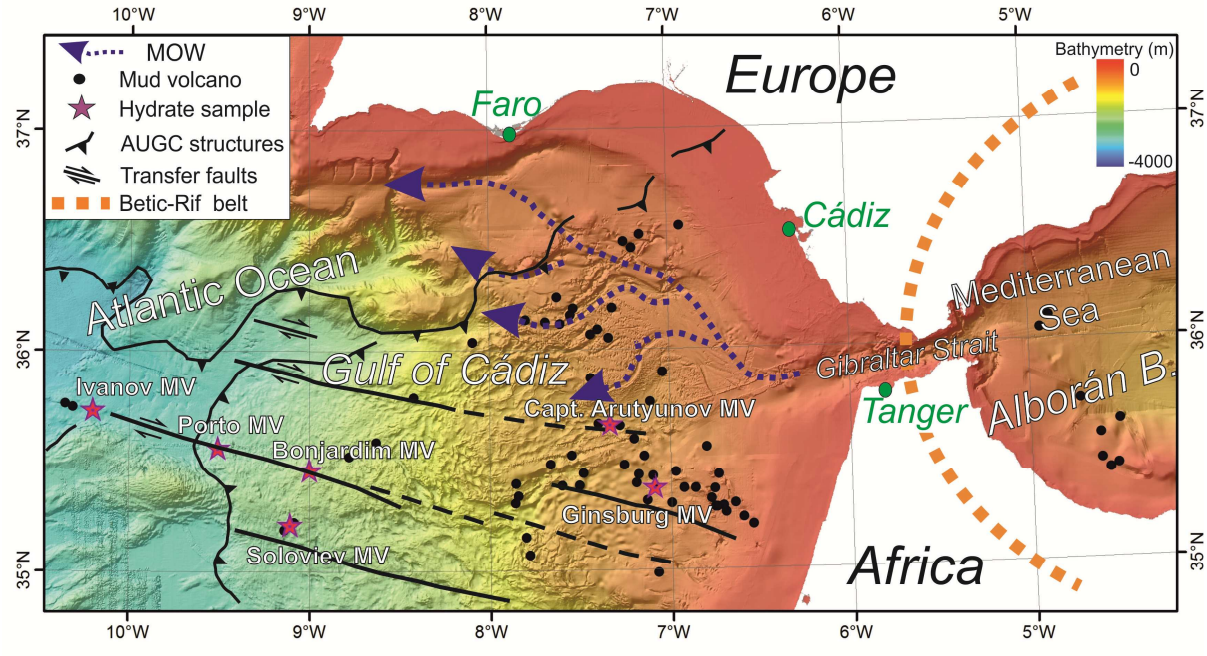


Figure 12. Bathymetry of the South Iberia and Northwest Africa margins. Arrows mark flow directions of Mediterranean outflow water. Stars mark mud volcanoes (MV) at which hydrate has been sampled. Black dots mark other mud volcanoes. The boundaries of the Allochthonous Unit of the Gulf of Cádiz (AUGC) are modified from Medialdea et al. (2009). Black lines mark southwest Iberia Margin (SWIM) faults (dashed where discontinuous).

In the Gulf of Cádiz, the westward migration of the Alborán Domain forced the emplacement of a large tectono-sedimentary allochthonous unit in the continental margin and oceanic realm of the Gulf of Cádiz, generally known as the allochthonous unit of the Gulf of Cádiz (AUGC) (Medialdea et al., 2009). The AUGC is responsible for diapirism of huge volumes of mud and salt of Triassic units and also for under-compacted early to middle Miocene plastic marls and shales (Fernandez-Puga et al., 2007; Maldonado et al., 1999; Medialdea et al., 2009). Numerous seabed fluid escape structures result from this diapirism, including mud volcanoes, of which some bear hydrate (León et al., 2012; Mazurenko et al., 2002; Pinheiro et al., 2003; Somoza et al., 2003; Van Rensbergen et al., 2005a), hydrocarbon-derived authigenic carbonate (HDAC)-bearing chimneys (Diaz-del-Rio et al., 2003; Magalhaes et al., 2012; Palomino et al., 2016) and pockmarks (Baraza and Ercilla, 1996; León et al.,

2014; León et al., 2010; León et al., 2006). The distribution of these fluid migration and escape structures is also related to the arcuate wedge and the west-northwest to east-southeast SWIM transcurrent fault system (Fig. 12; Hensen et al., 2015). The deeper mud volcanoes (2500-4500 m water depth), located in the Southwest Iberia Margin segment of the Gulf of Cádiz area, are closely linked to the presence of the active strike-slip SWIM faults, which provide pathways for deep-seated fluids sourced from oceanic crust older than 140 Ma (Hensen et al., 2015). A local and discontinuous BSR has been observed only in the upper slope (between 200 and 400 m water depth) on the Iberian margin of the Gulf (Casas et al., 2003) and within a mud volcano in the Moroccan slope (Depreiter et al., 2005). Hydrate and hydrocarbon gases sampled from mud volcano sediments include both microbial and thermogenic components (Mazurenko et al., 2002; Stadnitskaia et al., 2006).

8.2 Hydrate Occurrence

Direct evidence for hydrate in the Gulf of Cádiz has been detected only in association with the mud volcanoes. The first sample was recovered in 1999 at the Ginsburg mud volcano (Gardner, 2001; Mazurenko et al., 2002). Subsequent work confirmed the presence of hydrate in six other mud volcanoes at 930-4500 m water depth (Hensen et al., 2015; Mazurenko et al., 2002; Pinheiro et al., 2003; Fig. 12). Hydrate appears in various morpho-stratigraphical types, including a tabular shape of irregular thickness (up to 1-2 mm), forming layers within the sediment; or isometric sub-rounded aggregates or individual clast-like occurrences, from millimetre size to several centimetres. The biggest samples (> 5cm) have been recovered in the Porto and Michael Ivanov mud volcanoes (Hensen et al., 2015). They comprise disseminated clasts inside a homogeneous mud breccia of grey or dark grey color, saturated in gas and with a porous structure resulting of degasification. In some of the mud volcanoes (e.g. Ginsburg and Captain Arutyunov), based on chlorinity anomalies in sediment cores, hydrate content can reach 3-16% of the sediment volume and 5-31% of the pore space volume (Mazurenko et al., 2002). Hydrocarbon gases from gravity cores collected from Ginsburg mud volcano indicate allochthonous natural gases of thermogenic origin, with 81% methane and 19% higher hydrocarbons (Mazurenko et al., 2002; Stadnitskaia et al., 2006). The ratio iso-C4/n-C4 points to focused fluid flow as the principal mechanism of gas migration (Stadnitskaia et al., 2006). Differences in the composition of hydrocarbon gases between the deep Portuguese margin and the Atlantic Morocco middle continental slope suggest two groups with distinctive fluid venting environments and geochemical behavior/properties of migrating fluids, resulting from a complex of secondary migrated, microbially altered and mixed hydrocarbons (Stadnitskaia et al., 2006).

Indirect evidence for hydrate has been found in other mud volcanoes and mud mounds in the Gulf of Cádiz. The most common indirect evidence is liquefied and degassing structures in the mud breccia sediments (Fig. 13). These structures have been detected in most mud volcanoes below 1000 m water depth and in some carbonate mounds such as Cornide. In the Alborán Sea, degassing structures have

been detected only in one gravity core from the Carmen mud volcano. Coherent reversed-polarity reflections beneath the slopes of mud volcanoes, interpreted as BSRs have been detected in the Atlantic Moroccan margin below Mercator mud volcano (Depreiter et al., 2005). Similar reflections that are quasi-parallel to the seafloor and interpreted as BSRs have been detected in seismic profiles from the Portuguese continental upper slope seaward the city of Faro. Finally, the presence of chloride ion concentrations below 450 mM, indicating the presence of dissociated hydrate (Hesse and Harrison, 1981), has been detected in the hydrate-bearing mud volcanoes, as well as in the Yuma, Carlos Ribeiro and Olenin mud volcanoes, where hydrate was not recovered (Mazurenko et al., 2002).

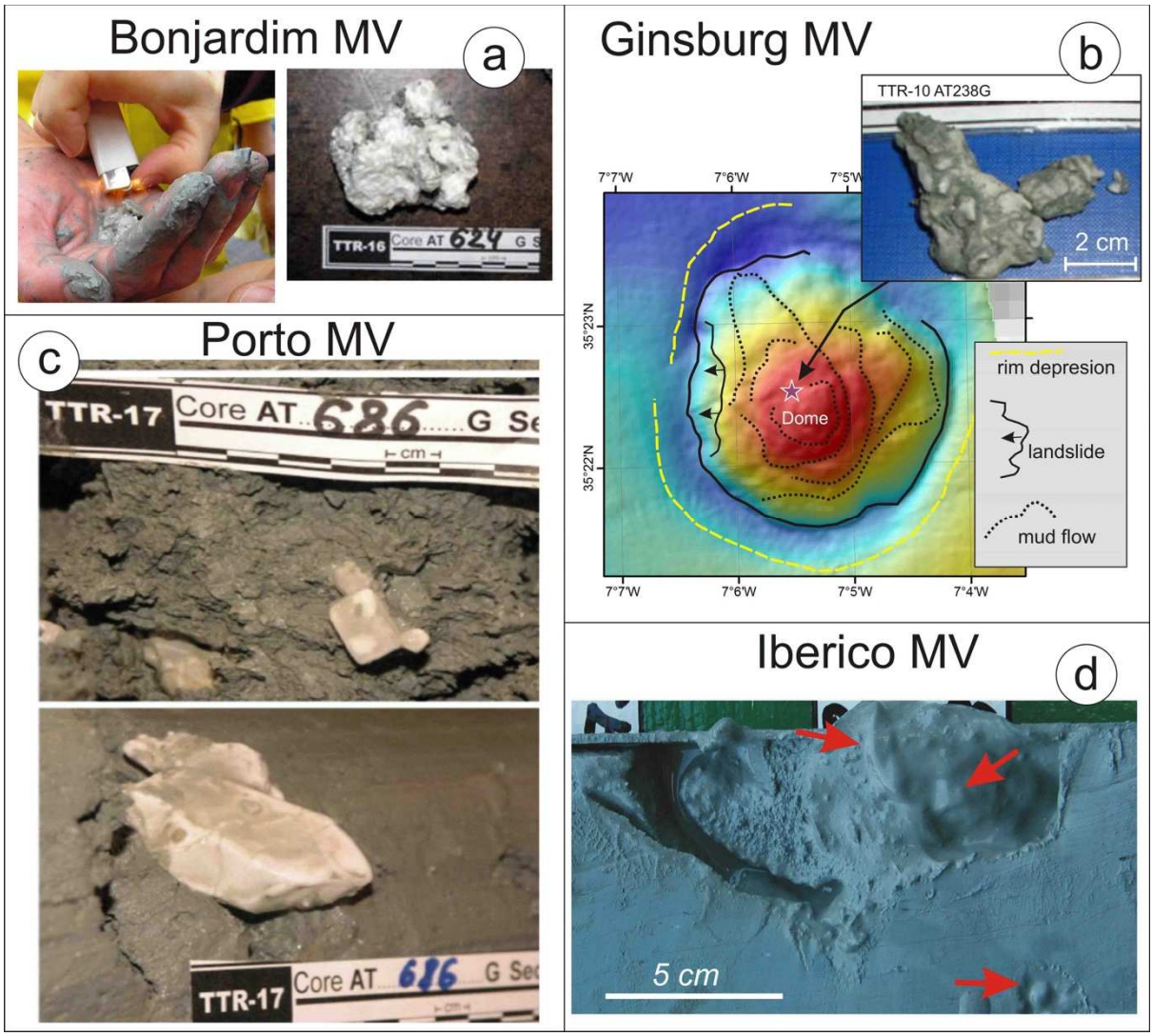


Figure 13. Direct and indirect hydrate evidence of the South Iberia and Northwest Africa margins. a) Hydrate sample from the Bonjardim mud volcano (AT624 from Akhmetzhanov et al., 2008); b) Bathymetry and geological interpretation of the Ginsburg mud volcano (modified from Toyos et al., 2016) with the location of the first hydrate sample recovered in the Gulf of Cádiz (AT238G from Kenyon et al., 2001); c) Hydrate crystals from a gravity core at Porto mud volcano (Ivanov et al., 2010); d) Liquefied structures (red arrows) inferred to represent hydrate dissociation in a gravity core from Ibérico mud volcano (Leon, 2007).

Thus, hydrate in the Gulf of Cádiz seems to be present in localised deposits and hosted in fine-grained sediments with low permeability, although the thickness and extent of hydrate present are poorly known. This type of occurrence cannot be considered to be of significant resource potential. No hydrate has been detected in any other geological features, such as pockmarks in the Gulf of Cádiz, nor in the Estremadura Spur of the west Iberia margin (Duarte et al., 2017). Hydrate indications are also absent in the sandy or muddy contourite deposits of the continental slope of the Gulf of Cádiz. The lack of hydrate evidence in pockmarks could also be related to the insufficient data collected on these sites. HDACs recovered in pockmarks show an isotopic composition (depletion in $\delta^{13}C$ and enrichment in $\delta^{18}O$) compatible with possible past massive hydrate dissociation episodes (Diaz-del-Rio et al., 2003).

Moreover, the BSRs that were identified occur only locally, without regional continuity, and in close association with fluid escape areas (Casas et al., 2003; Depreiter et al., 2005). In multichannel seismic profiles, areas of blanking and amplitude anomalies below pockmark fields, collapse structures and mud volcanoes reflect the presence of fluids (very possibly hydrocarbon fluids) in the sediment column (Medialdea et al., 2009). Suitable reservoirs for hydrate, comprising thick sandy contourite deposits generated by the Mediterranean outflow water (MOW), exist in the Gulf of Cádiz at 400-1200 m water depth. However, this water mass warms the seafloor and results in variation of the hydrate stability field through time. Global sea-level changes and subsequent episodic warming by the MOW undercurrents are the most plausible scenarios for massive hydrate dissociation in the Gulf of Cádiz during the Quaternary (León et al., 2010). Thus, hydrate could extend beyond the seabed fluid escape structures where it has been observed, and ultimately the amount of hydrate present is unknown.

Although hydrate has not been sampled in the mud volcanoes of the Alborán Sea, their presence has been proposed due to indirect evidence from some mud volcano structures (e.g., Blinova et al., 2011). Here, hydrate occurrence was inferred from the large gas release during core sampling. Pore water geochemistry provided further evidence, with a 160 to 600 mMol chlorinity anomaly. The gas was inferred to be thermogenic and from a deep (around 5 km) source (Blinova et al., 2011).

## 9. Eastern Mediterranean

### 9.1 Geological Setting

The Eastern Mediterranean Sea (Fig. 14) is a diverse composite of tectonic elements, which evolved through the Mesozoic formation and fragmentation of the northern passive margin of Gondwanaland and subsequent collision with Eurasia to form a subduction and accretionary complex (e.g., Garfunkel, 2004). An increasing supply of clastic sediments since the Oligocene formed the extensive

present-day Nile fan, extending into the Herodotus and Levant basins and reaching thicknesses of >8 km (Macgregor, 2012). Restricted connectivity with the Atlantic Ocean during the Messinian salinity crisis resulted in the deposition of evaporites across the Mediterranean basin and accumulation of ~2 km of salt within the Levant and Herodotus basins (CIESM, 2008).

The Eastern Mediterranean Sea is expected to host a significant amount of hydrate (e.g., Merey and Longinos, 2018) because large areas of the seabed are located within the HSZ (Fig. 1). The geological variability of this region offers a variety of potential hydrate depositional environments. The deep-water temperature ranges between 13 and 14 °C (e.g., Zavatarelli and Mellor, 1995), so that hydrate is only stable at water depths of >1000 m (Praeg et al., 2011). The geothermal gradient varies significantly between 20-30 °C/km in the Nile fan and associated deep basins to the south and ~60 °C/km in the Aegean (e.g., Makris and Stobbe, 1984), resulting in a variable sub-seafloor depth of the base HSZ across the area. The Eastern Mediterranean is extremely oligotrophic (Krom et al., 2004). The major potential sources for hydrocarbon formation are Tethyan deposits, late Messinian shallow water deposits and Miocene to recent sapropels and other organic-rich intervals (e.g., Merey and Longinos, 2018).

9.2 Hydrate Occurrence

Multiple observations indicate the availability of gas, required for the formation of hydrate, across the seafloor. In particular, numerous mud volcanoes are present, primarily along the accretionary complex and to a lesser degree in the Nile fan (e.g., Mascle et al., 2014; Zitter et al., 2005). Mud volcanoes in the Olimpi Field and at Anaximander Seamount exhibit gas seeps and broad degassing areas, with associated chemosynthetic fauna and authigenic carbonates (Aloisi et al., 2000; Zitter et al., 2005). In both locations, pockmarks have been identified and some of these are filled with brines characterized by high gas content (Dimitrov and Woodside, 2003). The gas seeps have clear thermogenic signatures, indicating deep-rooted fluid expulsion sources (e.g., Pape et al., 2010). Away from mud volcanoes, an abundance of gas, predominantly microbial methane (e.g., Römer et al., 2014; Rubin-Blum et al., 2014), is indicated by a multitude of deep sea seafloor gas seepage features that have been identified over the last two decades across the Nile fan (Dupre et al., 2010; Loncke et al., 2004), Levant basin (Tayber et al., 2019) and Eratosthenes Seamount (Mitchell et al., 2013). These features include gas bubbling, pockmarks, and authigenic carbonates at the seafloor, and a variety of seismic reflection anomalies beneath the seabed, including bright spots and seismic blanking. The scope of known seepage is continuously expanding as new data become available, providing further evidence for the potential for hydrate formation.

To date, hydrate has been sampled only in several mud volcanoes of the accretionary complex, starting in the Anaximander Seamount region (Fig. 14). These include the Kula mud volcano

(Woodside et al., 1997), the nearby Amsterdam, Kazan, Athina, and Thassaloniki mud volcanoes (Lykousis et al., 2009; Pape et al., 2010; Perissoratis et al., 2011), and those in the Olimpi field offshore Crete, including the Napoli, Milano, Maidstone and Moscow mud volcanoes (Fig. 14; e.g., Aloisi et al., 2000). Most hydrate samples are within predominantly relatively fine muddy sediments. In most cases the presence and dissolution of hydrate was indicated by the soupy texture of the sampled sediments (e.g., Lykousis et al., 2009) or their signatures in pore water chlorinity and chemistry (e.g., de Lange and Brumsack, 1998a; Pape et al., 2010).

Analysis of sediments collected at the Mediterranean Ridge (ODP Leg 160, Site 971) suggests locally massive hydrate occurrence at depths of 1 to over 40 m below seafloor across the summit of Milano mud volcano (de Lange and Brumsack, 1998a). Based on a porosity of 60% to 40% (ODP Leg 160, hole 970A), the total amount of methane stored in this mud volcano as hydrate and free gas equal is estimated to be $5 \times 10^9$ $m^3$ (De Lange and Brumsack, 1998b). In contrast, hydrate samples retrieved at Kazan mud volcano had a mm-scale rice-like appearance. Those from the summit of Amsterdam mud volcano occurred as several-cm scale flaky lumps resembling compacted snow, estimated to occupy a volume fraction of 16.7% within the sediment interval between the sulphate base and the maximum sampling depth of 2.5 m (Pape et al., 2010). This estimate is based on the analysis of four pressurized near-surface sediment cores (following e.g., Heeschen et al., 2007). In addition, pore-water analysis was used to assess the upper limit of hydrate stability. Both of the above hydrate morphologies were found on the Thessaloniki mud volcano, but the estimated volume fraction in a single 70-cm autoclave core was only 0.7% (Perissoratis et al., 2011). Lykousis et al. (2009) and Perissoratis et al. (2011) note that on Thassaloniki mud volcano, located at about 1260 m water depth, methane hydrate is present mostly just below the calculated upper limit of the HSZ. Thus, hydrate may dissociate due to small increases in temperature or decreases in pressure or salinity, which might occur due to climate change or local sediment transport.

In spite of the broad coverage of the Eastern Mediterranean by 2D and 3D commercial and academic seismic data, only a single observation of a BSR has been reported (Fig. 14; Praeg et al., 2008; Praeg et al., 2011). The suggested BSR appears as a discontinuous negative polarity reflection, 220-330 ms below the seafloor at water depths of 2000–2500 m on the distal part of the western deep sea Nile fan. If a mean seismic velocity of 1.6-1.8 km/s is assumed above the reflection, its depth agrees well with the modelled base of the HSZ (Praeg et al., 2017). Direct indications of hydrate stability, and of the presence of gas within the HSZ, in the Nile deep sea fan were provided by Römer et al. (2014). They observed formation of hydrate within a funnel during the collection of gas emitted from the seafloor. In addition, hydrate coating formed on ascending bubbles and dissolved below the modeled top of the HSZ. This latter result was supported by echo-sounder imaging. Geochemical analyses of vented gas

suggest that it predominantly originates from microbial methanogenesis, with traces of thermogenic input (Römer et al., 2014).

Based on a statistical analysis of a large 3D dataset covering a significant portion of the Levant basin, Tayber et al. (2019) suggest that observed scattered high-amplitude reflectivity there marks a pseudo BSR, representing the presence of hydrate and associated underlying gas within localised sandy buried channel systems. Tayber et al. (2019) estimated the hydrate volume associated with these presumed accumulations at ~100 Tcf (~3000 $GSm^3$) and its carbon content at ~1.5 Gt.

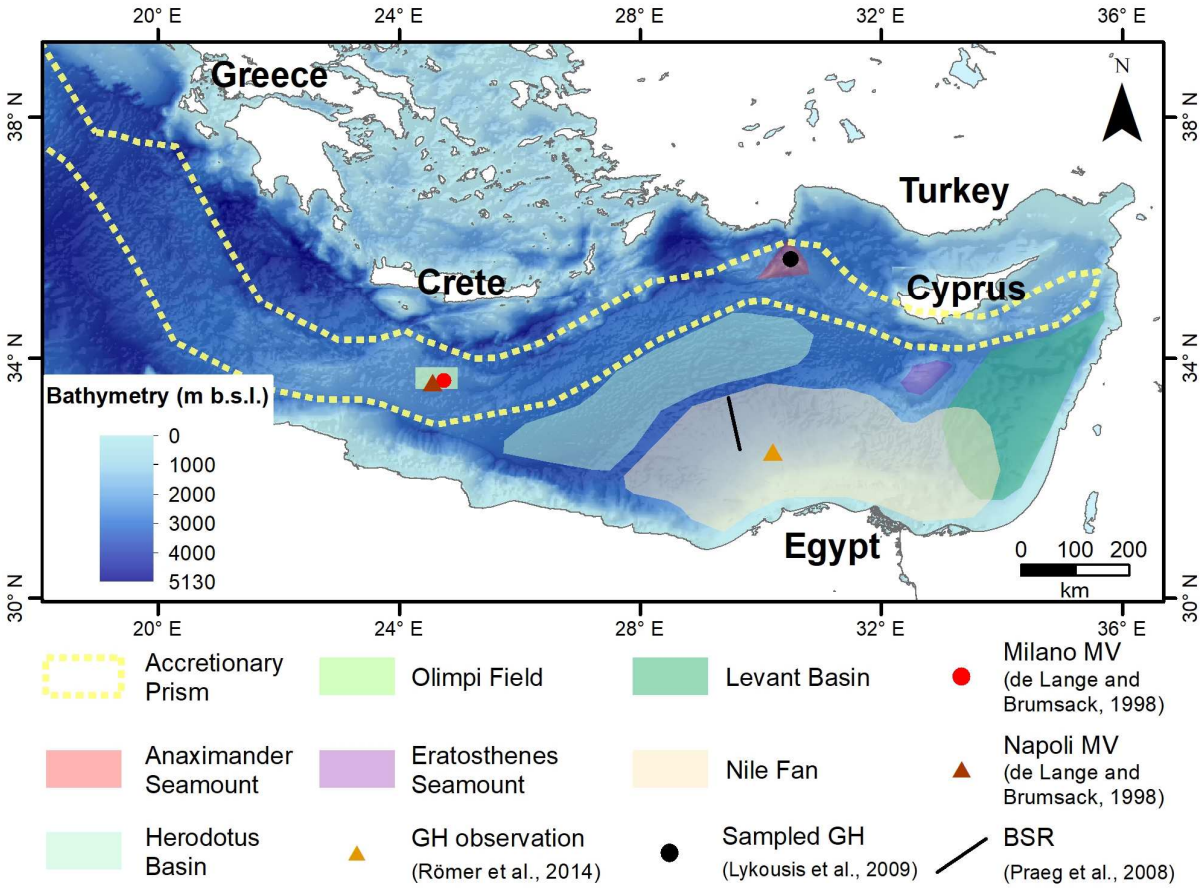


Figure 14: Bathymetry of the Eastern Mediterranean Sea (from https://www.gmrt.org/GMRTMapTool) with a range of seafloor features (e.g., Mascle et al., 2014). Filled circles mark sites where hydrate has been sampled and coloured triangles mark other hydrate indicators, as detailed in the text. Black line marks the seismic profile along which Praeg et al. (2008) reported a BSR.

## 10. Sea of Marmara

### 10.1 Geological Setting

The Sea of Marmara is a pull-apart basin linking the onshore North Anatolian Fault with more distributed extensional deformation in the Aegean. The current basin geometry appears to have formed since 5 Ma by the rotation of several lithospheric blocks (Armijo et al., 1999). The basin reaches a depth of over 1300 m and is subdivided into three sub-basins, from west to east named the Tekirdağ, Central and Çınarcık basins, separated by basement highs named the Western and Central

High, respectively (e.g., Le Pichon et al., 2001). It has been extensively studied over the past two decades because of the hazardous active fault system that crosses its centre.

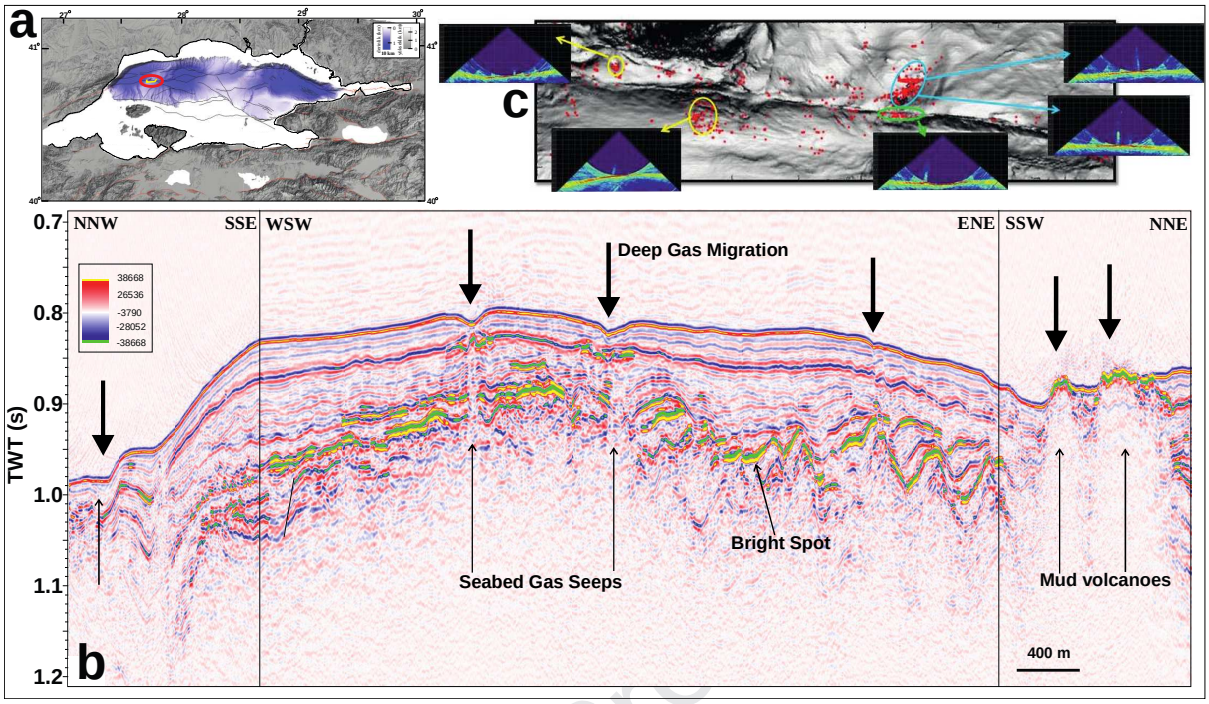


Figure 15: a) Faults, bathymetry and topography of the Sea of Marmara. Bathymetry is from Rangin et al. (2001) and faults from Sorlien et al. (2012). Red circle shows the study area and yellow line inside shows the location of the seismic profile in b). b) Seismic reflection profile showing evidence of shallow gas (Sarıtaş et al., 2018). Thick black arrows show gas seeps to seabed. The amount of gas seeps is the highest at mud volcano area. Hydrate of thermogenic origin is sampled in the mud volcanoes on the western high. High amplitude and reverse polarity bright spots are formed due to gas accumulations. c) Seabed morphology of the central Sea of Marmara calculated from 3D seismic data with red dots showing gas flares (Saritas, 2013). Yellow circles mark gas seeps from pockmarks, blue circle marks seeps from mud volcanoes and green circle marks seeps from the North Anatolian Fault.

## 10.2 Hydrate occurrence

Only small areas of the Sea of Marmara are deep enough to fall within the methane HSZ (Fig. 1). However, hydrate has been sampled directly (Bourry et al., 2009) on the Western High, where indications of sub-seabed fluid escape have been widely observed in seismic profiles around the North Anatolian Fault system (e.g., Sarıtaş et al., 2018; Thomas et al., 2012; Fig. 15). Oil seeps have also been observed (Crémière et al., 2012). Unequivocal BSRs have not been observed, but high-amplitude reflections with reversed polarity that roughly mimic the seabed were clearly imaged in 2D and 3D high-resolution multichannel seismic reflection data (e.g., Thomas et al., 2012). The reflections do not cross-cut sedimentary strata, which also roughly parallel the seabed, so they may or may not mark the base of the HSZ. They are similar to reflections seen in the Sorokin Trough in the Black Sea (Krastel et al., 2003). Mud volcanoes, zones of seismic blanking and chimneys reaching the seabed were also clearly imaged, suggesting the presence of abundant free gas in the shallow sedimentary column.

Gas sampled from hydrate and bubble plumes was predominantly methane, but ethane, propane and i-butane were also present, indicating a thermogenic source (Bourry et al., 2009). This thermogenic gas may have migrated into shallow sediments via the North Anatolian Fault system from Oligocene to Eocene reservoirs like those in the Thrace basin. Based on the gas compositions observed, both structure I and structure II hydrate may be present.

## 11. Black Sea

### 11.1 Geological Setting

The Black Sea (Fig. 16) is a semi-isolated extensional basin with a maximum water depth of 2212 m. Its deep waters (87% of the total volume) form the largest anoxic, hydrogen sulphide and methane reservoirs in the world. The amount of dissolved methane contained in the basin (96 Tg) is 2.4-6 times greater than the global annual geological methane contribution to the atmosphere (Reeburgh et al. 1991). 91% of its seafloor is within the range of hydrate stability (Vassilev and Dimitrov, 2002), making the Black Sea an interesting target for a European hydrate field study.

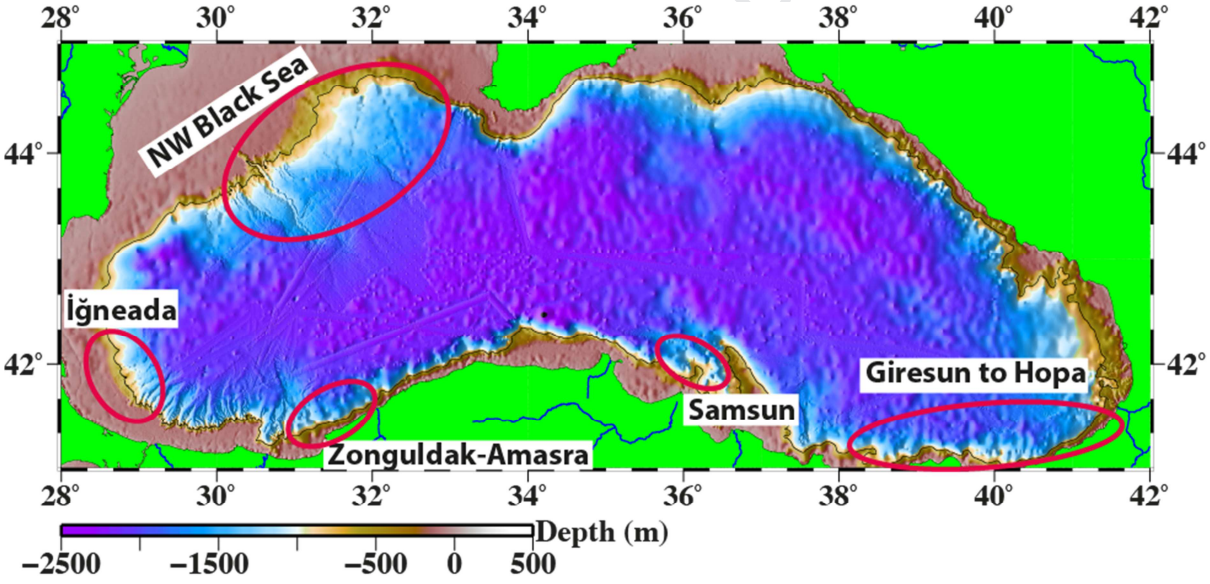


Figure 16: Bathymetry of the Black Sea (Smith and Sandwell, 1997) with study areas described in the text.

The Black Sea basin is generally thought to have formed in a back-arc environment because of its spatial association with subduction of both the Paleo- and Neo-Tethys oceans (Letouzey et al., 1977). The timing and style of this opening history remain controversial, partly because the thick sediment cover means that the oldest sedimentary fill has not been drilled (e.g., Nikishin et al., 2015; Zonenshain and Le Pichon, 1986). The Black Sea is subdivided into eastern and western basins separated by the Mid Black Sea High, a SW-NE system of buried basement ridges (e.g, Nikishin et al., 2015). Sediments in the Western basin may reach a thickness of up to 19 km (Nikishin et al., 2003). They include 4-5 km of folded organic-rich Maikopian deposits (Oligocene to lower Miocene)

and 2-3 km of Cenozoic deposits (e.g., Finetti et al., 1988; Nikishin et al., 2015), which become thinner or disappear on the basin margin. Sediments in the eastern basin are thinner – perhaps only 8-9 km (Shillington et al., 2008).

11.2 Hydrate occurrence in the western Black Sea

11.2.1 Offshore Romania and Bulgaria

The northwestern Black Sea forms the transition zone between the Moesian Platform in the west, Scythian Platform in the north and the Western Black Sea Basin in the southeast. Structural styles of the Moesian and Scythian Platforms, which correspond to the Bulgarian and Romanian-Ukrainian EEZs, are significantly different. The former is quite structured and features normal faults with tilted blocks, while the latter is a mosaic of structural styles, with mainly Miocene gravity-driven thrusting, folding, toe-thrust and growth and tectonic deformation (Bega and Ionescu, 2009).

The northwest margin of the Black Sea (Fig. 17) is made up of the two largest and thickest organic-rich fan complexes in the Black Sea, the Danube and Dniepr fans, built up by the rivers Danube, Dniepr, Dniestr and Bug. Sediment deposition and the evolution of these fan systems has been controlled by climate and sea-level change (e.g., Ryan et al., 1997). The Danube and Dniepr fans developed from a significant stack of paleo-channels and levee deposits (Popescu et al., 2001; Winguth et al., 2000). Periodic seabed anoxia made conditions favourable for gas generation, as documented by the presence of more than 3000 gas plumes in the water column (Egorov et al., 2011), arranged in a circum-Black-Sea belt of gas flares. The majority of flares occur in water depths shallower than 665 m, which marks the present-day upper limit of the gas hydrate stability zone in the Black Sea. Exceptions are the underwater mud volcanoes, generally located in deeper waters, which can expel significant amounts of fluids, including methane. However, only 1.9% of the total methane escape from the seafloor reaches the atmosphere (Egorov et al., 2011).

Hydrate was first discovered in the area in a core sample by Yefremova and Zhizchenko (1974), with the first hydrate sample in the Romanian sector recovered in 2017 (Riboulot et al., 2018). The existence of hydrate at depth was inferred from BSRs. However their distribution is not continuous and is limited to a few areas (e.g., Popescu et al., 2007; Zander et al., 2017). Hydrate there is of microbial origin, with methane $\delta^{13}C$ values of −84‰ to −70‰ and concentrations of 99.1–99.9% (Haeckel et al., 2017). Organic-rich Maykopian sedimentary deposits are not in a productive state yet and do not provide an observable thermogenic methane component.

The HSZ in the northwestern Black Sea is coincident with the Danube and Dniepr fans. Hydrate formation in the levees or channel base of these fans is inferred from the presence of BSRs, for example in the Danube fan, where multiple BSRs have been observed beneath ancient levee systems

(e.g., Popescu et al., 2007; Zander et al., 2017; Fig. 18). Zander et al. (2017) inferred that these multiple BSRs do not reflect gas composition changes or overpressured compartments, but rather past pressure and temperature conditions. Results from thermal models suggest that temperature changes related to rapid sediment deposition, rather than bottom-water temperature or sea level variations, have a primary influence over the pressure and temperature conditions resulting in the formation of multiple BSRs (Zander et al. 2017).

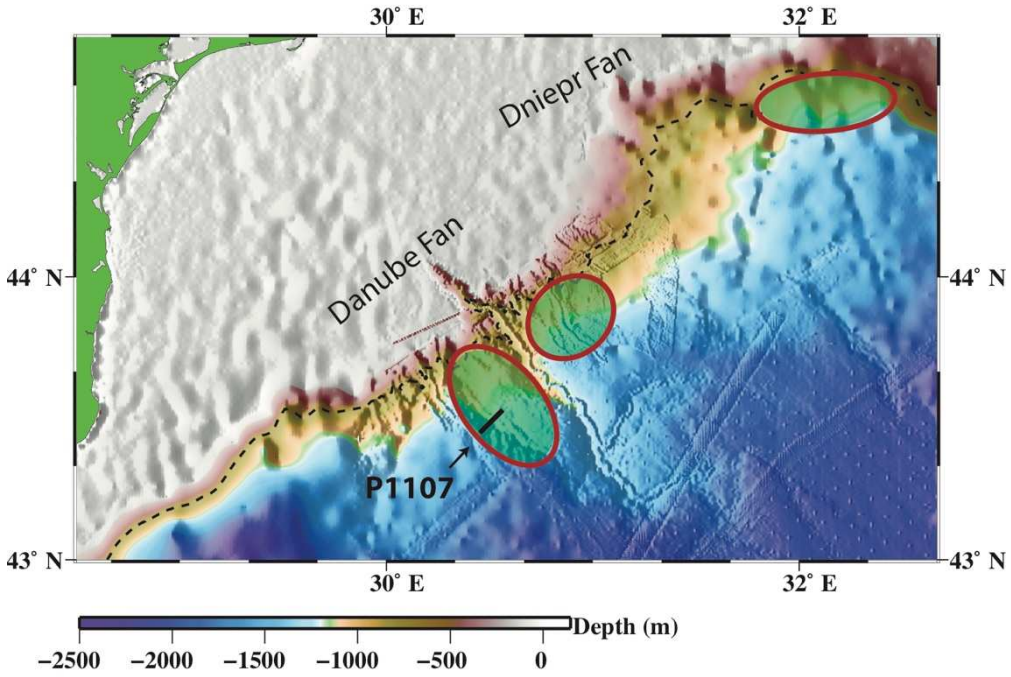


Figure 17: Bathymetric map of the northwest Black Sea. Background shaded bathymetry from Smith and Sandwell (1997) is overlain with shipboard bathymetry compiled by MARUM and GEOMAR. Areas with reported gas hydrate indications are marked with shade ellipses. Dashed contour marks the upper depth limit of the HSZ at 650 m water depth. Hydrate distribution is derived from Zillmer et al. (2005), Popescu et al. (2006), Zander et al. (2017) and Hillman et al. (2018a).

CSEM data collected across and within the channel levee system shown in Fig. 18 revealed highly anomalous resistivity values at various depths within the HSZ, which are partly attributed to lower pore water salinities (around 4 ppm; Bohrmann et al., 2018), but also suggest a high hydrate saturation of possibly up to 20-30% within the channel filling sediments and below the western levee.

The availability of structural and stratigraphic constraints from deep-penetrating seismic data has enabled the development of a basin scale numerical model to investigate the production and migration of gas and resulting hydrate distribution (Hillman et al., 2018a). Sediment structure, slope failures and distribution of BSRs are imaged on shallow seismic data (Hillman et al., 2018b; Popescu et al., 2007; Zander et al., 2017). These data have enabled the development of a stratigraphy for the slope deposits and mass transport events inferred from that of Winguth et al. (2000), although in the absence of sufficient sediment samples there remains some uncertainty in the dating of these deposits. Dating has come from the ASSEMBLAGE project (Lericolais et al., 2013) and DSDP Leg 42 (Stoffers et al.,

1978). Mapping of active gas seeps using water column imaging, and gas-related structures in seismic profiles, have been used to describe the plumbing system in the canyon and levee systems (Hillman et al., 2018b). Many of the active gas seeps correlate with sub-seafloor gas migration structures such as chimneys or pipes. There is an apparent correlation between gas vents and submarine landslide features, but there are insufficient data to determine whether gas migration has played a causative role in triggering such slope failure events (Hillman et al., 2018b). Changes in climate, resulting in changes in the HSZ, and the identification of paleo seafloors, have together been used to explain the origin of the multiple BSRs (Zander et al., 2017). Modelling of the HSZ using inputs from 2D and 3D seismic data has indicated that the hydrate system may be in a transient state, with factors such as topographic focusing of heat flow playing a significant role in controlling the location and distribution of hydrate (Hillman et al., 2018a).

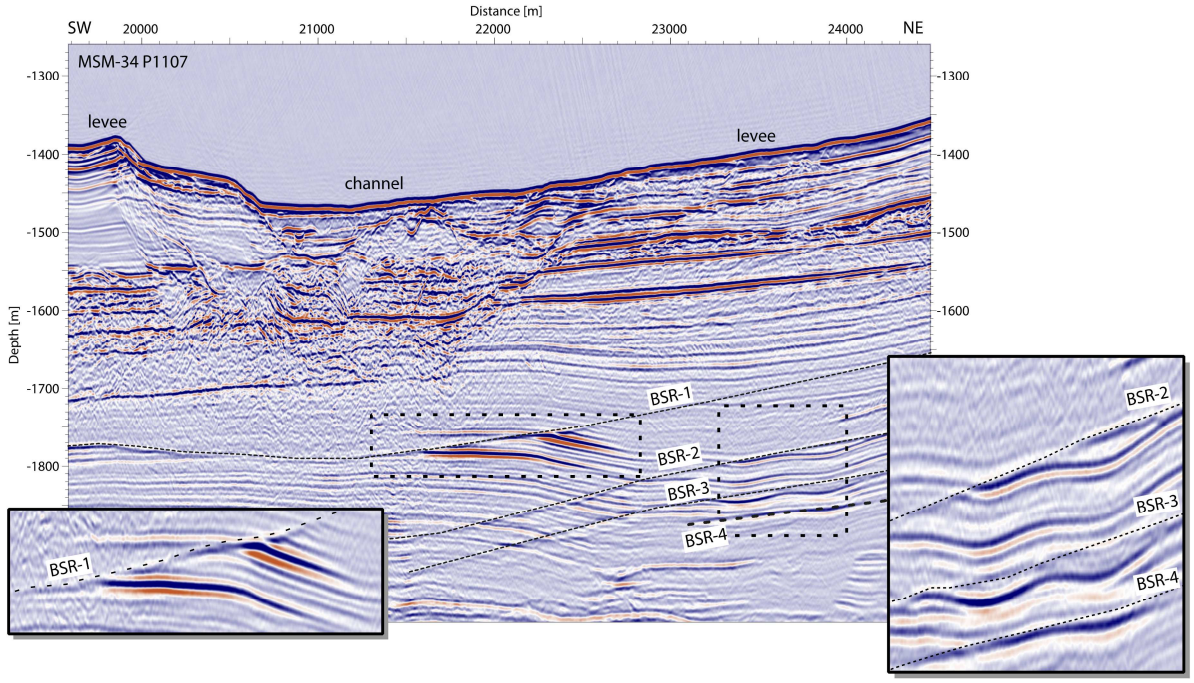


Figure 18: Multichannel seismic data example of today's BSR (BSR 1) and multiple BSR occurrences (BSR 2 to 4) in the Danube fan. While BSR 1 extends over the entire channel levee system the multiple BSRs disappear towards the channel structure (SUGAR channel). Insets zoom into the BSR events and highlight the increased reflection amplitudes where inversion point and termination indicate the BSR position. Data acquired during cruise MSM34 (Bialas et al., 2014).

Seismic velocities from analysis of OBS data were used to provide the first estimates of possible gas and hydrate concentrations in the Bulgarian sector of the northwestern Black Sea. The resulting velocity-depth sections represent average velocities for sediment packages of about 100 m thickness. Estimates of average hydrate saturations in the pore space based on these seismic velocity distributions are up to 10% or 30-40%, depending on the hydrate morphology assumed. CSEM data were acquired to further investigate gas and hydrate distribution in the sediments. Hydrate saturation estimates derived from CSEM datasets depend on the porosity and pore water salinity, and the

appropriate choice of Archie parameters. These studies suggest saturations in the range of 20-30% in parts of the HSZ. It is likely that the highest hydrate saturations are be located within coarser grained, sand-rich sediments in the channel systems and intermittently distributed through the levees (Zander et al., 2017).

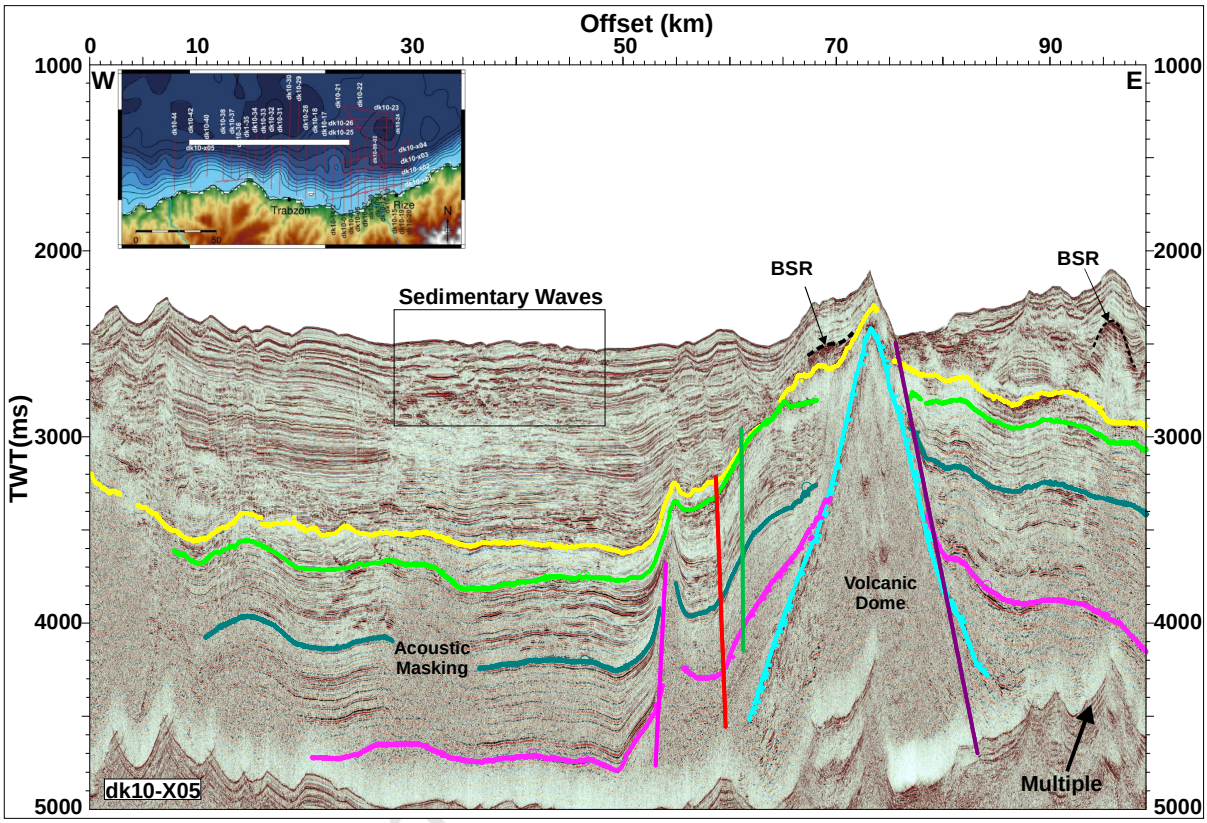


Figure 19: Seismic line parallel to coastline offshore Trabzon area, showing fault related volcanic dome structure at the eastern side of the section and a BSR at around 300 ms below the seafloor (Gunduz, 2015). The Trabzon fault is a strike-slip fault. Acoustic blanking below the BSR may indicate free gas. Acoustic blanking is also present in deeper parts of the section.

11.2.2 Offshore İğneada

Regional seismic data acquired across the continental shelf and slope offshore İğneada (Fig. 16) show folded sediments with gas accumulations beneath structural highs, evidenced by seismic blanking zones, fluid escape structures and a reef structure (Özel, 2012). Fault systems penetrate the shallow sediments beneath these ridges and cross the gas-charged lithologies, suggesting the presence of hydrocarbon migration pathways. One profile displays BSRs across the continental slope. However, the distribution of hydrate at this site is not well understood due to large inline and cross-line intervals. Other profiles show high-amplitude, reversed-polarity reflections that mimic the seabed but do not cross-cut stratigraphy, at a depth that is significantly different from that of the unequivocal BSRs. The origin of these features remains uncertain. Hydrate was recovered at an acoustically transparent feature observed in sub-bottom profiler data that protrudes from beneath the hemipelagic

cover, interpreted as a mud volcano (Fokin et al., 2005). Numerous carbonate-cemented layers and a mousse-like breccia below were also observed.

11.2.3 Offshore Zonguldak-Amasra

The Zonguldak-Amasra area is one of the best-studied in terms of shallow gas and hydrate. Geological and geophysical investigations, including conventional and high-resolution seismic data, chirp sub-bottom profiler data, multibeam bathymetry and direct sampling, have shown the presence of gas and indications of gas hydrate (Küçük et al., 2015). Dissolved gas in the shallow sediments contains hydrocarbons ranging from methane to hexane, suggesting a thermogenic gas source in addition to microbial gas in the shallow sediments. Seismic evidence for the presence of seven different mud volcanoes and a large number of buried and active gas chimneys was found in this region. Widespread seismic blanking zones were observed also beneath the HSZ, with up to 25 km lateral extent. Chirp sub-bottom profiler data show many chimney structures in the first 40-50 m below the seabed and sparse gas anomalies were observed on seismic data in various locations. Both continuous and discontinuous BSRs have been widely observed at this site. Multiple BSRs were also imaged, with up to five successive BSRs. These additional BSRs may have a similar origin to those imaged in the Danube fan (section 11.2.1) or may be attributed to a variety of different gas compositions with different stability limits. In addition to structure I and structure II hydrate, structure H hydrate might be present at this site, indicated by the presence of i-Pentane gas in a gas composition similar to that observed in the Gulf of Mexico (Sassen and MacDonald, 1994).

11.3 Hydrate occurrence in the eastern Black Sea

11.3.1 Offshore Samsun

High-resolution seismic data and sediment cores are available from this region (e.g., Dondurur and Çifçi, 2009). Indications of shallow gas, such as buried and active pockmarks and seismic blanking zones, were imaged in seismic data. Here, hydrate may be present at relatively shallow water depth (250-700 m). Bright reflections on the upper slope have been interpreted as hydrate-bearing sedimentary units. The presence of hydrate at such shallow water depths could be explained by the presence of hydrogen sulphide in the gas, which shifts the phase boundary to higher temperatures and lower pressures (Dondurur and Çifçi, 2009).

11.3.2 Offshore Hopa-Rize-Trabzon-Giresun

Three-dimensional seismic data offshore Hopa show the presence of a widespread BSR that is most prominent beneath structural highs (Minshull and Keddie, 2010). A dense grid of seismic data offshore Rize and Trabzon showed widespread indications of shallow gas and gas hydrate (Fig. 19). Chimneys, seismic blanking zones, gas charged sediments, mud diapirs and mud volcanoes are all present. These were observed around crustal-scale faults that suggest migration from depth. Both continuous and discontinuous BSRs have been clearly imaged. No hydrate indicators have been identified in regional seismic data offshore Giresun.

## 12. Discussion

Although methane hydrate is stable in large areas of European margins, numerical models of microbial gas generation suggest that significant microbial hydrate accumulations are unlikely to be widespread (e.g., Archer et al., 2009; Wallmann et al., 2012). This result is a consequence of low predicted organic carbon accumulation rates in the parts of European margins that are deep enough for hydrate stability. This prediction is supported by observations of particulate organic carbon concentrations in surface sediments (Wallmann et al., 2012). Consistent with these modelling considerations, most of the hydrate occurrences described above are associated with conventional hydrocarbon provinces, and where there are data available on hydrate-forming gas compositions or isotopic ratios, these data commonly suggest the presence of gas that is at least partly of thermogenic origin. Direct sampling of hydrate is mostly at fluid escape features such as pockmarks or mud volcanoes, so we cannot rule out the possibility that the sample locations are unrepresentative.

Offshore Greenland, the search for hydrate is still at an early stage, although the physical and oceanographic settings of these margins are perfect for hydrate formation. Investigations suggest a high potential for oil and gas within out- or shallow sub-cropping sedimentary basins in the west and northeast Greenland margins. The onshore observations of oil seeps in central west Greenland confirm the existence of an active hydrocarbon system here and the discovery of onshore hydrate indicates that gas is migrating from the system and likely forms hydrate. Such gas migration is also suggested by indirect evidence from seismic and shallow cores offshore. Further offshore on the west Greenland margin, observed BSRs and seismic blanking may also provide evidence of hydrate occurrence. Thus it is likely that hydrate is present on the central west Greenland margin and, based on the onshore oil discoveries, the hydrate could contain a high portion of thermogenic gas. Hydrate has not yet been reported on the east Greenland margin, which is likely due to the lack of research and wells on this margin. However, a gas-show in ODP well 909, together with the presence of BSRs and other seismic indicators, may provide evidence for an active hydrocarbon system forming hydrate in the northeast Greenland margin.

Offshore Svalbard, the hydrate system has characteristics that may be unique among hydrate systems worldwide. It stretches from the continental slope onto the mid-ocean ridge, thereby experiencing significant changes in thermodynamic conditions, and it may be the only hydrate system in the world that forms from hydrocarbon gas of three different sources, namely microbial, thermogenic and abiotic gas. However, the relative contribution of each of these sources is still unknown and may show significant local variations. The structural-stratigraphic development of this area has led to the formation of distinct sedimentary depocentres and fluid migration pathways, thereby controlling the distribution of hydrate. At present, the total distribution extends over approximately 4000 $km^2$ with

the main accumulation in the Vestnesa Ridge and many smaller patches of hydrate in close vicinity. Yet large parts of this area remain unmapped and potentially hold much more hydrate if the hypothesized abiotic origin of gas in hydrate is confirmed as a potential hydrate play. Nonetheless, current estimates of hydrate saturations so far are sufficiently low that the economic value of hydrate offshore Svalbard is questionable.

Onshore Svalbard, on average, the modelled HSZ thickness reaches 300 m, with the thickest zones extending from about 75 m to up to 725 m below the surface, which are the minimum and maximum depths at which hydrate is expected to form, based on regionally constrained thermobaric conditions. Variable pore water salinities, anomalous regional pressure regimes, uncertainties in regional geothermal gradients and changing temperature conditions put a limit on the model's accuracy further away from Nordenskiöldland, where regional datasets and constraints afford good control. In addition, the model takes no account of factors likely to control hydrate presence, such as fluid migration pathways and local biogeochemistry. The ongoing study of the onshore HSZ in central Spitsbergen and archipelago-wide is pivotal to the mapping of the potential occurrence of onshore hydrate accumulations and compliments the significant findings made offshore.

The Barents Sea exhibits widespread evidence for thermogenic hydrate occurrence and is a unique region where hydrate is hosted in consolidated sedimentary formations and likely co-exists with conventional petroleum reservoirs. Seismic data analysis by Laberg et al. (1998) and patchy BSR distribution indicate relatively low resource potential, but the free gas trapped beneath the BSR could still be of commercial interest. Despite increased petroleum exploration activities in recent years, none of the BSRs identified in the southwest Barents Sea have yet been drilled or sampled. The presence of hydrate stability conditions within the major shallow reservoirs in the region, however, has attracted increased attention towards hydrate from commercial exploration companies (Norwegian Petroleum Directorate, 2018).

On the mid-Norwegian Margin, the BSR only occurs within finely bedded contouritic and hemipelagic deposits (mainly silty clays) of the Quarternary Naust formation, which seem to be the favourable host sediments for hydrate. The extent of hydrate is geologically controlled by hydrate stability conditions that exclude hydrate on the continental shelf, and the availability of the suitable host rock elsewhere. Bünz et al. (2003) suggest that hydrate on the mid-Norwegian margin develops from fluids that originate far beneath the HSZ. Deep-seated Cenozoic dome structures with inferred hydrocarbon reservoirs might be one source of gas, though gas compositions from limited sampling suggest a primarily microbial origin. Using the approach of Max and Johnson (2016), hydrate on the mid-Norwegian margin can be classified as a low grade deposit with little economic value.

Offshore Ireland, the Druid Anomaly over the Feni Drift in the Rockall Basin, and contourite deposits in the Porcupine Basin, have been identified as potential targets for further hydrate exploration. Furthermore, exploration in deep water for conventional hydrocarbons in the South Porcupine Basin requires better definition of the HSZ to mitigate against the risk of hydrate dissociation while drilling and consequent uncontrolled gas release. More seismic interpretation, followed by seabed sampling and shallow drilling, are required to identify hydrate. As more conventional oil and gas wells are drilled offshore Ireland, new geothermal gradient data will be acquired that will contribute to a better definition of the HSZ.

On the northwest continental margin of Iberia, the occurrence of hydrate is uncertain. Although some data suggest that the sedimentary and geomorphological evolution of the area is controlled by fluid dynamics associated with gas seepage, and occasional weak indicators of gas have been described (e.g., possible BSR, seismic bright spots and liquefaction of a sediment core), none are conclusive.

On the South Iberia and Northwest Africa margins, direct evidence for hydrate has been found only in the mud volcanoes of the Gulf of Cádiz. Indirect evidence has been detected on both sides of the Straits of Gibraltar, mostly associated with mud volcanoes and mud diapirs, but also in the form of localised BSRs, degassing and liquefied sediments in cores, and by the presence of chlorinity anomalies. The preferred migration pathways for fluids into the basin are the main tectonic structures such as diapirs, folds and faults. The composition of the pore fluids and hydrate sampled in the Gulf of Cádiz indicate generally a mixture of microbial and thermogenic sources. However, in some mud volcanoes associated with the deep SWIM strike-slip faults, an abiotic source is also possible, connected to hydrothermal fluids in the oceanic domain. Thus the Gulf of Cádiz has a variety of sources of gas and geological settings for hydrate formation. In the case of the Alborán Sea, gas is present in diapiric formations originating in the basal allochthonous unit and is likely to be thermogenic.

In the Eastern Mediterranean, hydrate sampling is also limited to mud volcanoes. There is little published work on seismic indicators of hydrate presence, although extensive exploration datasets provide opportunities for further analysis. The high sensitivity of the ocean here to climate and oceanographic changes may provide a natural laboratory to investigate the influence of these changes on hydrate stability, as well as the potential impacts.

In the Sea of Marmara, there is abundant evidence for the presence of gas within the HSZ and hydrate has been directly sampled in the top of a mud volcano, but unequivocal BSRs have not been observed, so the amount of the hydrate present is difficult to assess.

In the Black Sea offshore Romania and Bulgaria, diverging results on possible hydrate saturations demonstrate the need to ground-truth models by collecting samples from deep drilling with logging and core sampling. Physical sediment parameters, heat-flow measurements, geochemical data and sediment dating are required to calibrate the remote sensing techniques and to enable the extension of available models along the margin. Changes in climate such as the last glacial maxima (LGM) caused a bottom water temperature decrease from 9° C to about 4-6° C, a sea-level decrease of about 120 m and the development of limnic conditions as the Bosphorus interface to the Mediterranean was closed. These changes caused a decrease in the maximum thickness of the hydrate stability field by about 33%, from 550 m to 370 m (Zander et al. 2017). This change may have released 1.1-4.6 Gt of methane carbon as the hydrate dissociated (Poort et al. 2005). Ongoing salinity increases in the Black Sea sediments will shift the top of the HSZ in the future, causing further hydrate dissociation (Riboulot et al., 2018). Furthermore, a mis-match between modeled HSZ limits and observed BSR depths suggests that the hydrate system of the Black Sea is currently not in equilibrium but is approaching steady state (Hillman et al., 2018a).

On the southern continental slope and rise of Black Sea, BSR occurrences are mapped in water depths of 750-2000 meters from high resolution multichannel seismic reflection data. Also, chirp data suggest the presence of gas accumulations at shallow sediment depths (30-40 m). Slope failures are widespread along both the western and eastern steep canyon systems. The presence of hydrate is not restricted to these areas but is probably much more extensive. Hydrate samples have been reported widely across the Turkish Black Sea margin in BSR and mud volcano areas. Free gas is inferred to occur beneath the BSR, as indicated by seismic bright spots and areas of seismic blanking. The presence of gas seeps to the seabed through the hydrate stability zone, via mud volcanoes and fault zones, provides evidence for free gas below the hydrate zone. Mapping of active gas seeps using water column imaging and sampling of free gas in water samples and sediments will give information about the origin of the gas, which could be microbial or thermogenic or both, as in the Amasra area.

Thus we can categorise areas covered by our study into three types:

1. Areas of widespread BSRs: the Davis Strait, Fram Strait, the mid-Norwegian margin, and the southern margin of Black Sea.
2. Areas where there is no BSR, or the BSR is localised rather than widespread, but hydrate has been directly sampled: the Barents Sea, the Gulf of Cadiz, the Eastern Mediterranean, the Sea of Marmara, and the Black Sea offshore Bulgaria and Romania.
3. Areas with neither a clearly identified BSR nor direct sampling of hydrate, but where other more indirect hydrate indicators are present: the Disko area offshore west Greenland, the northeast Greenland margin, onshore Svalbard, offshore Ireland, and offshore northwest Iberia.

Where hydrate has been sampled, it usually contains higher hydrocarbons, indicating a thermogenic component; an exception is the Black Sea offshore Romania and Bulgaria, where only trace amounts of higher hydrocarbons are present.

## 13. Conclusions

From our review of hydrate occurrence around Europe, we conclude:

1. There is direct or indirect evidence for the presence of hydrate in several European locations including the western and eastern margins of Greenland, onshore and offshore Svalbard, the Barents Sea, the mid-Norwegian margin, the Atlantic margin of Ireland, the eastern Mediterranean Sea, the Sea of Marmara, and the western and southern margins of the Black Sea.
2. Hydrate is observed to be particularly widespread offshore Svalbard and Norway and in the Black Sea.
3. Areas with strong evidence for the presence of hydrate commonly coincide with conventional thermogenic hydrocarbon provinces.
4. Although hydrate systems are well explored in a few small areas, for most European margins, significant further research is needed to determine the regional abundance of hydrate beneath the seabed.

## Acknowledgements

This work was supported by the European Commission via ESSEM COST action ES1405, entitled Marine gas hydrate – an indigenous source of natural gas for Europe (MIGRATE). We thank Jack Schuenmeyer for advice and Ingo Pecher and two anonymous reviewers for constructive comments. TAM was supported by a Wolfson Research Merit Award. ALC was supported by the 'Programa de axudas á etapa posdoutoral da Xunta de Galicia'. LMP thanks CESAM (UID/AMB/50017/2019) and FCT/MCTES for financial support. DR thanks the Ministerio de Ciencia Innovación y Tecnología of Spain and Consellería de Industria of the Xunta de Galicia for funding data acquisition offshore Galicia and A. E. López Pérez for his help with the Galician Marine bathymetry. AV was supported by the Bulgarian National Science Fund (Project KP-06-OPR04/7 GEOHydrate). Metadata associated with this review are available at https://www.migrate-cost.eu/wg1-reports.

**References**

Abay, T.B., Karlsen, D.A. and Pedersen, J.H. (2014) Source Rocks at Svalbard: An Overview of Jurassic and Triassic Formations and Comparison with Offshore Barents Sea Time Equivalent Source Rock Formations, AAPG International Conference & Exhibition, Istanbul, Turkey.

Akhmetzhanov, A.M., Kenyon, N.H., Ivanov, M.K., Westbrook, G.K. and Mazzini, A. (2008) Deep-water depositional systems and cold seeps of the Western Mediterranean, Gulf of Cadiz and Norwegian continental margins. Preliminary results of investigations during the TTR-16 cruise of RV Professor Logachev May-July, 2006, Intergovernmental Oceanographic Commission (IOC) Technical Series. UNESCO, Paris, France, p. 91.

Aloisi, G., Pierre, C., Rouchy, J.M., Foucher, J.P., Woodside, J. and Party, M.S. (2000) Methane-related authigenic carbonates of eastern Mediterranean Sea mud volcanoes and their possible relation to gas hydrate destabilisation. Earth and Planetary Science Letters 184, 321-338.

Andreassen, K., Berteussen, K.A., Sognnes, H., Henneberg, K., Langhammer, J. and Mienert, J. (2003) Multicomponent ocean bottom cable data in gas hydrate investigation offshore of Norway. Journal of Geophysical Research: Solid Earth 108, 2399, doi:2310.1029/2002JB002245.

Andreassen, K., Hogstad, K. and Berteussen, K.A. (1990) Gas hydrate in the southern Barents Sea, indicated by a shallow seismic anomaly. First Break 8, 235-245.

Andreassen, K., Hubbard, A., Winsborrow, M., Patton, H., Vadakkepuliyambatta, S., Plaza-Faverola, A., Gudlaugsson, E., Serov, P., Deryabin, A., Mattingsdal, R., Mienert, J. and Bünz, S. (2017) Massive blow-out craters formed by hydrate-controlled methane expulsion from the Arctic seafloor. Science 356, 948-953.

Andreassen, K., Mienert, J., Bryn, P. and Singh, S.C. (2000) A Double Gas-Hydrate Related Bottom Simulating Reflector at the Norwegian Continental Margin. Annals of the New York Academy of Sciences 912, 126-135.

Archer, D., Buffett, B. and Brovkin, V. (2009) Ocean methane hydrates as a slow tipping point in the global carbon cycle. Proceedings of the National Academy of Sciences 106, 20596-20601.

Armijo, R., Meyer, B., Hubert, A. and Barka, A. (1999) Westward propagation of the North Anatolian fault into the northern Aegean: Timing and kinematics. Geology 27, 267-270.

Attias, E., Weitemeyer, K., Minshull, T.A., Best, A.I., Sinha, M., Jegen-Kulcsar, M., Hölz, S. and Berndt, C. (2016) Controlled-source electromagnetic and seismic delineation of sub-seafloor fluid flow structures in a gas hydrate province, offshore Norway. Geophysical Journal International 206, 1093-1110.

Baraza, J. and Ercilla, G. (1996) Gas-charged sediments and large pockmark-like features on the Gulf of Cadiz slope (SW Spain). Marine and Petroleum Geology 13, 253-261.

Bega, Z. and Ionescu, G. (2009) Neogene structural styles of the NW Black Sea region, offshore Romania. The Leading Edge 9, 1082-1089.

Berndt, C., Bunz, S., Clayton, T., Mienert, J. and Saunders, M. (2004) Seismic character of bottom simulating reflectors: examples from the mid-Norwegian margin. Marine and Petroleum Geology 21, 723-733.

Berndt, C., Feseker, T., Treude, T., Krastel, S., Liebetrau, V., Niemann, H., Bertics, V.J., Dumke, I., Dunnbier, K., Ferre, B., Graves, C., Gross, F., Hissmann, K., Huhnerbach, V., Krause, S., Lieser, K.,

1467 Schauer, J. and Steinle, L. (2014) Temporal Constraints on Hydrate-Controlled Methane Seepage off
1468 Svalbard. Science 343, 284-287.

1469 Betlem, P. (2018) 3D Thermo-baric Modelling of Central Spitsbergen: Implications for Gas Hydrate
1470 Occurrence. MSc thesis, University of Iceland, Reykjavik.

1471 Betlem, P., Senger, K. and Hodson, A. (2019) 3D thermobaric modelling of the gas hydrate stability
1472 zone onshore central Spitsbergen, Arctic Norway. Marine and Petroleum Geology 100, 246-262.

1473 Bialas, J., Klaucke, I. and Haeckel, M. (2014) FS Maria S. Merian Fahrtbericht/Cruise Report
1474 MSM34/1 and 2, SUGAR site. GEOMAR, Kiel, Germany.

1475 Blinova, V.N., Comas, M.C., Ivanov, M.K., Poludetkina, E.N. and Matveeva, T.V. (2011) Active
1476 mud volcanism in the West Alboran Basin: Geochemical evidence of hydrocarbon seepage. Marine
1477 and Petroleum Geology 28, 1483-1504.

1478 Bohrmann, G., Ahrlich, F., Bachmann, K., Bergenthal, M., Beims, M., Betzler, C., Brünjes, J.,
1479 Deusner, C., Domeyer, B., Düßmann, R., Ewert, J., Gaide, S., Frank, C., Freudenthal, T., Fröhlich, S.,
1480 Greindl, T., Haeckel, M., Heitmann-Bacza, C., Ion, G., Kaszemeik, K., Keil, H., Kinski, O., Klein, T.,
1481 Kossel, E., Linowski, E., Malnati, J., Mau, S., Meyer, B., Pape, T., Popa, A., Renken, J., Reuter, J.,
1482 Reuter, M., Riedel, M., Riemer, P., Rohleder, C., Rosiak, U., Rotaru, S.-G., Rothenwänder, T.,
1483 Stachowski, A., Schmidt, W., Seiter, C., Utecht, C., Vasilev, A., Wallmann, K., Wegwerth, A.,
1484 Wintersteller, P. and Wunsch, D. (2018) R/V Meteor Cruise Report M142: Drilling gas hydrates in
1485 the Danube deep-sea fan, Black Sea, Varna–Varna–Varna, 04 November–22 November–09
1486 December 2017. MARUM – Center for Marine Environmental Sciences, Bremen, Germany, p. 121.

1487 Boillot, G. (1995) A lithospheric syn-rift shear zone at the ocean-continent transition: preliminary
1488 results of the GALINAUTE II cruise (Nautile dives on the Galicia Bank, Spain). Comptes Rendus -
1489 Academie des Sciences, Serie II: Sciences de la Terre et des Planetes 321, 1171-1178.

1490 Boillot, G., Dupeuble, P.A. and Malod, J. (1979) Subduction and tectonics on the continental margin
1491 off northern Spain. Marine Geology 32, 53-70.

1492 Bojesen-Koefoed, J.A., Bidstrup, T., Christiansen, F.G., Dalhoff, F., Gregersen, U., Nytoft, H.P.,
1493 Nohr-Hansen, H., Pedersen, A.K. and Sonderholm, M. (2007) Petroleum seepages at Asuk, Disko,
1494 West Greenland: Implications for regional petroleum exploration. Journal of Petroleum Geology 30,
1495 219-236.

1496 Boswell, R. and Collett, T.S. (2011) Current perspectives on gas hydrate resources. Energy &
1497 Environmental Science 4, 1206-1215.

1498 Boswell, R., Shipp, C., Reichel, T., Shelander, D., Saeki, T., Frye, M., Shedd, W., Collett, T.S. and
1499 McConnell, D.R. (2016) Prospecting for marine gas hydrate resources. Interpretation 4, SA13-SA24.

1500 Bouriak, S., Vanneste, M. and Saoutkine, A. (2000) Inferred gas hydrates and clay diapirs near the
1501 Storegga Slide on the southern edge of the Vøring Plateau, offshore Norway. Marine Geology 163,
1502 125-148.

1503 Bourry, C., Chazallon, B., Charlou, J.L., Pierre Donval, J., Ruffine, L., Henry, P., Geli, L., Çagatay,
1504 M.N., Inan, S. and Moreau, M. (2009) Free gas and gas hydrates from the Sea of Marmara, Turkey.
1505 Chemical and structural characterization. Chemical Geology 264, 197-206.

1506 Brekke, H. (2000) The tectonic evolution of the Norwegian Sea Continental Margin with emphasis on
1507 the Vøring and Møre Basins. Geological Society, London, Special Publications 167, 327-378.

Bryn, P., Berg, K., Forsberg, C.F., Solheim, A. and Kvalstad, T.J. (2005) Explaining the Storegga Slide. Marine and Petroleum Geology 22, 11-19.

Bugge, T., Belderson, R.H. and Kenyon, N.H. (1988) The Storegga slide. Philosophical Transactions of the Royal Society of London A325, 357-388.

Bugge, T., Elvebakk, G., Fanavoll, S., Mangerud, G., Smelror, M., Weiss, H.M., Gjelberg, J., Kristensen, S.E. and Nilsen, K. (2002) Shallow stratigraphic drilling applied in hydrocarbon exploration of the Nordkapp Basin, Barents Sea. Marine and Petroleum Geology 19, 13-37.

Bünz, S. and Mienert, J. (2004) Acoustic imaging of gas hydrate and free gas at the Storegga Slide. Journal of Geophysical Research 109, B04102, doi:04110.01029/02003JB002863.

Bünz, S., Mienert, J. and Berndt, C. (2003) Geological controls on the Storegga gas-hydrate system of the mid-Norwegian continental margin. Earth and Planetary Science Letters 209, 291-307.

Bünz, S., Mienert, J., Vanneste, M. and Andreassen, K. (2005) Gas hydrates at the Storegga Slide: Constraints from an analysis of multicomponent, wide-angle seismic data. Geophysics 70, B19-B34.

Bünz, S., Polyanov, S., Vadakkepuliyambatta, S., Consolaro, C. and Mienert, J. (2012) Active gas venting through hydrate-bearing sediments on the Vestnesa Ridge, offshore W-Svalbard. Marine Geology 332-334, 189-197.

Casas, D., Ercilla, G. and Baraza, J. (2003) Acoustic evidences of gas in the continental slope sediments of the Gulf of Cadiz (E Atlantic). Geo-Mar Lett 23, 300-310.

Chand, S., Mienert, J., Andreassen, K., Knies, J., Plassen, L. and Fotland, B. (2008) Gas hydrate stability zone modelling in areas of salt tectonics and pockmarks of the Barents Sea suggests an active hydrocarbon venting system. Marine and Petroleum Geology 25, 625-636.

Chand, S., Thorsnes, T., Rise, L., Brunstad, H., Stoddart, D., Bøe, R., Lågstad, P. and Svolsbru, T. (2012) Multiple episodes of fluid flow in the SW Barents Sea (Loppa High) evidenced by gas flares, pockmarks and gas hydrate accumulation. Earth and Planetary Science Letters 331–332, 305-314.

Christiansen, F.G., Dam, G., Nørh-Hansen, H. and Sønderholm, M. (1994) Shallow core drilling summary sheets: Cretaceous sediments of Nuussuaq and Svartenhuk Halvø (GGU 400701-400712), GGU Open File Series.

CIESM (2008) Impacts of acidification on biological, chemical and physical systems in the Mediterranean and Black Seas, in: Briand, F. (Ed.), CIESM Workshop Monographs, Monaco, p. 124.

Collett, T.S., Johnson, A., Knapp, C. and Boswell, R. (2009) Natural gas hydrates: a review, in: Collett, T., Johnson, A., Knapp, C., Boswell, R. (Eds.), Natural Gas Hydrates: Energy Resource Potential and Associated Geologic Hazards. American Association of Petroleum Geologists Memoir 89.

Crane, K., Sundvor, E., Buck, R. and Martinez, F. (1991) Rifting in the northern Norwegian-Greenland Sea - Thermal tests of asymmetric spreading. Journal of Geophysical Research 96, 14529-14550.

Crémière, A., Pierre, C., Blanc-Valleron, M.M., Zitter, T., Çağ atay, M.N. and Henry, P. (2012) Methane-derived authigenic carbonates along the North Anatolian fault system in the Sea of Marmara (Turkey). Deep-Sea Research Part I: Oceanographic Research Papers 66, 114-130.

1547 Dai, J., Snyder, F., Gillespie, D., Koesoemadinata, A. and Dutta, N. (2008) Exploration for gas
1548 hydrates in the deepwater, northern Gulf of Mexico: Part I. A seismic approach based on geologic
1549 model, inversion, and rock physics principles. Marine and Petroleum Geology 25, 830-844.

1550 Dalland, A., Worsley, D., Ofstad, K. (1988) A lithostratigraphical scheme for the Mesozoic and
1551 Cenozoic succession offshore mid- and northern Norway. Norwegian Petroleum Directorate Bulletin
1552 4.

1553 de Lange, G. and Brumsack, H.-J. (1998a) Pore-water indications for the occurrence of gas hydrates
1554 in eastern Mediterranean mud dome structures. Proceedings of the Ocean Drilling Program, Scientific
1555 Results 160, 569-574.

1556 De Lange, G.J. and Brumsack, H.J. (1998b) The occurrence of gas hydrates in Eastern Mediterranean
1557 mud dome structures as indicated by pore-water composition. Geological Society Special Publication
1558 137, 167-175.

1559 Depreiter, D., Poort, J., Van Rensbergen, P. and Henriet, J.P. (2005) Geophysical evidence of gas
1560 hydrates in shallow submarine mud volcanoes on the Moroccan margin. Journal of Geophysical
1561 Research: Solid Earth 110, doi:10.1029/2005JB003622.

1562 Diaz-del-Rio, V., Somoza, L., Martinez-Frias, J., Mata, M.P., Delgado, A., Hernandez-Molina, F.J.,
1563 Lunar, R., Martin-Rubi, J.A., Maestro, A., Fernandez-Puga, M.C., León, R., Llave, E., Medialdea, T.
1564 and Vázquez, J.T. (2003) Vast fields of hydrocarbon-derived carbonate chimneys related to the
1565 accretionary wedge/olistostrome of the Gulf of Cadiz. Marine Geology 195, 177-200.

1566 Dimitrov, L. and Woodside, J. (2003) Deep sea pockmark environments in the eastern Mediterranean.
1567 Marine Geology 195, 263-276.

1568 Dondurur, D. and Çifçi, G. (2009) Anomalous strong reflections on high resolution seismic data from
1569 the Turkish shelf of the Eastern Black Sea: Possible indicators of shallow hydrogen sulphide-rich gas
1570 hydrate layers. Turkish Journal of Earth Sciences 18, 299-313.

1571 Doré, A.G. (1995) Barents Sea geology, petroleum resources and commercial potential. Arctic 48,
1572 207-221.

1573 Doré, A.G. and Jensen, L.N. (1996) The impact of late Cenozoic uplift and erosion on hydrocarbon
1574 exploration: offshore Norway and some other uplifted basins. Global and Planetary Change 12, 415-
1575 436.

1576 Druet, M. (2015) Geodinámica del Margen Continental de Galicia: Estructura Profunda y
1577 Morfotectónica. PhD thesis, Madrid Complutense University.

1578 Druet, M., Muñoz-Martín, A., Granja-Bruña, J.L., Carbó-Gorosabel, A., Acosta, J., Llanes, P. and
1579 Ercilla, G. (2018) Crustal Structure and Continent-Ocean Boundary Along the Galicia Continental
1580 Margin (NW Iberia): Insights From Combined Gravity and Seismic Interpretation. Tectonics 37,
1581 1576-1604.

1582 Duarte, D., Magalhaes, V.H., Terrinha, P., Ribeiro, C., Madureira, P., Pinheiro, L.M., Benazzouz, O.,
1583 Kim, J.H. and Duarte, H. (2017) Identification and characterization of fluid escape structures
1584 (pockmarks) in the Estremadura Spur, West Iberian Margin. Marine and Petroleum Geology 82, 414-
1585 423.

1586 Dumke, I., Burwicz, E.B., Berndt, C., Klaeschen, D., Feseker, T., Geissler, W.H. and Sarkar, S.
1587 (2016) Gas hydrate distribution and hydrocarbon maturation north of the Knipovich Ridge, western
1588 Svalbard margin. Journal of Geophysical Research: Solid Earth 121, 1405-1424.

1589 Dupre, S., Woodside, J., Klaucke, I., Mascle, J. and Foucher, J.P. (2010) Widespread active seepage
1590 activity on the Nile Deep Sea Fan (offshore Egypt) revealed by high-definition geophysical imagery.
1591 Marine Geology 275, 1-19.

1592 Durán, R., García-Gil, S., Diez, R. and Vilas, F. (2007) Stratigraphic framework of gas accumulations
1593 in the Ría de Pontevedra (NW Spain). Geo-Mar Lett 27, 77-88.

1594 Egorov, V., Artemov, Y.G., Gulin, S.B. and Polikarpov, G.G. (2011) Methane seeps in the Black Sea:
1595 discovery, quantification and environmental assessment. J. Black Sea Mediterranean Environment 17,
1596 171-185.

1597 Eiken, O. and Hinz, K. (1993) Contourites in the Fram Strait. Sedimentary Geology 82, 15-32.

1598 Elliott, G.M., Shannon, P.M., Haughton, P.D.W. and Ovrebo, L.K. (2010) The Rockall Bank Mass
1599 Flow: Collapse of a moated contourite drift onlapping the eastern flank of Rockall Bank, west of
1600 Ireland. Marine and Petroleum Geology 27, 92-107.

1601 EMODnet Bathymetry Consortium (2016) EMODnet Digital Bathymetry (DTM),
1602 http://doi.org/10.12770/c7b53704-999d-4721-b1a3-04ec60c87238.

1603 Engen, Ø., Faleide, J.I. and Dyreng, T.K. (2008) Opening of the Fram Strait gateway: A review of
1604 plate tectonic constraints. Tectonophysics 450, 51-69.

1605 Ercilla, G., Casas, D., Vázquez, J.T., Iglesias, J., Somoza, L., Juan, C., Medialdea, T., León, R.,
1606 Estrada, F., García-Gil, S., Farran, M., Bohoyo, F., García, M. and Maestro, A. (2011) Imaging the
1607 recent sediment dynamics of the Galicia Bank region (Atlantic, NW Iberian Peninsula). Mar Geophys
1608 Res 32, 99-126.

1609 Estrada, F., Galindo-Zaldivar, J., Vázquez, J.T., Ercilla, G., D'Acremont, E., Alonso, B. and Gorini,
1610 C. (2018) Tectonic indentation in the central Alboran Sea (westernmost Mediterranean). Terra Nova
1611 30, 24-33.

1612 Faleide, J.I., Gudlaugsson, S.T. and Jacquart, G. (1984) Evolution of the western Barents Sea. Marine
1613 and Petroleum Geology 1, 123-150.

1614 Fernandez-Puga, M.C., Vázquez, J.T., Somoza, L., del Rio, V.D., Medialdea, T., Mata, M.P. and
1615 Leon, R. (2007) Gas-related morphologies and diapirism in the Gulf of Cadiz. Geo-Mar Lett 27, 213-
1616 221.

1617 Ferré, B., Mienert, J. and Feseker, T. (2012) Ocean temperature variability for the past 60 years on the
1618 Norwegian-Svalbard margin influences gas hydrate stability on human time scales. Journal of
1619 Geophysical Research 117, C10017, doi:10010.11029/12012JC008300.

1620 Ferrín, A., Durán, R., Dieaz, R., García-Gil, S. and Vilas, F. (2003) Shallow gas features in the
1621 Galician Rías Baixas (NW Spain). Geo-Mar Lett 23, 207-214.

1622 Finetti, I., Bricchi, G., Del Ben, A., Pipan, M. and Xuan, Z. (1988) Geophysical Study of the Black
1623 Sea. Bollettino Di Geofisica Teorica ed Applicata 30, 197-324.

1624 Fohrmann, H., Backhaus, J.O., Blaume, F., Haupt, B.J., Kämpf, J., Michels, K., Mienert, J.,
1625 Posewang, J., Ritzrau, W., Rumohr, J., Weber, M. and Woodgate, R. (2001) Modern Ocean Current-
1626 Controlled Sediment Transport in the Greenland-Iceland-Norwegian (GIN) Seas, in: Schäfer, P.,
1627 Ritzrau, W., Schlüter, M., Thiede, J. (Eds.), The Northern North Atlantic: A Changing Environment.
1628 Springer Berlin Heidelberg, Berlin, Heidelberg, pp. 135-154.

Fokin, I., Klaucke, I. and Akhmethanov, A. (2005) Side Scan Sonar data, Trakya Area, 2005,Deep Water cold seeps, sedimentary environments and ecosystems of the Black and Tyrrhenian Seas and the Gulf of Cadiz, Intergovernmental Oceanographic Commission (IOC) Technical Series. UNESCO, Paris, France.

Furst, J.J., Navarro, F., Gillet-Chaulet, F., Huss, M., Moholdt, G., Fettweis, X., Lang, C., Seehaus, T., Ai, S.T., Benham, T.J., Benn, D.I., Bjornsson, H., Dowdeswell, J.A., Grabiec, M., Kohler, J., Lavrentiev, I., Lindback, K., Melvold, K., Pettersson, R., Rippin, D., Saintenoy, A., Sanchez, G., Schuler, T.V., Sevestre, H., Vasilenko, E. and Braun, M.H. (2018) The Ice-Free Topography of Svalbard. Geophysical Research Letters 45, 11760-11769.

Gabitto, J.B., M. (2010) Gas hydrates research programs: an international review. Office of Scientific and Technical Information, US Department of Energy, https://www.osti.gov/servlets/purl/978338/.

García-García, A., García-Gil, S. and Vilas, F. (2003) Monitoring the Spanish gas fields in the Ría de Vigo (1991-2001). Geo-Mar Lett 23, 200-206.

García-Gil, S., Cartelle, V., De Blas, E., De Carlos, A., Díez, R., Durán, R., Ferrín, A., García-Moreiras, I., García-García, A., Iglesias, J., Martínez-Carreño, N., Muñoz Sobrino, C. and Ramírez-Pérez, A.M. (2015) Shallow gas in the Iberian continental margin. Boletin Geologico y Minero 126, 575-608.

Gardner, J.M. (2001) Mud volcanoes revealed and sampled on the Western Moroccan continental margin. Geophysical Research Letters 28, 339-342.

Garfunkel, Z. (2004) Origin of the Eastern Mediterranean basin: a reevaluation. Tectonophysics 391, 11-34.

Gautier, D.L., Bird, K.J., Charpentier, R.R., Grantz, A., Houseknecht, D.W., Klett, T.R., Moore, T.E., Pitman, J.K., Schenk, C.J., Schuenemeyer, J.H., Sørensen, K., Tennyson, M.E., Valin, Z.C. and Wandrey, C.J. (2011) Chapter 9: Oil and gas resource potential north of the Arctic Circle, Geological Society Memoir 35. Geological Society, London, pp. 151-161.

Geissler, W.H., Pulm, P.V., Jokat, W. and Gebhardt, A.C. (2014) Indications for the Occurrence of Gas Hydrates in the Fram Strait from Heat Flow and Multichannel Seismic Reflection Data. Journal of Geological Research 2014, doi:10.1155/2014/582424.

Gerlings, J., Hopper, J.R., Fyhn, M.B.W. and Frandsen, N. (2017) Mesozoic and older rift basins on the SE Greenland Shelf offshore Ammassalik, in: PeronPinvidic, G., Hopper, J.R., Funck, T., Stoker, M.S., Gaina, C., Doornenbal, J.C., Arting, U.E. (Eds.), NE Atlantic Region: A Reappraisal of Crustal Structure, Tectonostratigraphy and Magmatic Evolution. Geological Soc Publishing House, Bath, pp. 375-392.

Ginsburg, G.D., Milkov, A.V., Soloviev, V.A., Egorov, A.V., Cherkashev, G.A., Vogt, P.R., Crane, K., Lorenson, T.D. and Khutorskoy, M.D. (1999) Gas hydrate accumulation at the Håkon Mosby Mud Volcano. Geo-Mar Lett 19, 57-67.

Goswami, B.K., Weitemeyer, K.A., Minshull, T.A., Sinha, M.C., Westbrook, G.K., Chabert, A., Henstock, T.J. and Ker, S. (2015) A joint electromagnetic and seismic study of an active pockmark within the hydrate stability field at the Vestnesa Ridge, West Svalbard margin. Journal of Geophysical Research: Solid Earth 120, 6797-6822.

Graves, C.A., James, R.H., Sapart, C.J., Stott, A.W., Wright, I.C., Berndt, C., Westbrook, G.K. and Connelly, D.P. (2017) Methane in shallow subsurface sediments at the landward limit of the gas hydrate stability zone offshore western Svalbard. Geochimica Et Cosmochimica Acta 198, 419-438.

Gregersen, U. and Bidstrup, T. (2008) Structures and hydrocarbon prospectivity in the northern Davis Strait area, offshore West Greenland. Petroleum Geoscience 14, 151-166.

Gunduz, S. (2015) Investigation of active tectonism structure of the Eastern Black Sea with using multichannel seismic data, Masters Thesis, Institute of Marine Sciences and Technology. Dokuz Eylul University.

Haeckel, M., Zander, T., Burwicz, E., Bialas, J., Berndt, C., Dannowski, A., Hensen, C., Hölz, S., Jegen, M., Klaucke, I., Rottke, W. and Schwalenberg, K. (2017) The gas hydrate system of the Danube deep-sea fan in the Black Sea, 9th International Conference on Gas Hydrates, Denver, Colorado, USA.

Hamann, N.E., Whittaker, R.C. and Stemmerik, L. (2005) Geological development of the Northeast Greenland shelf. Petroleum Geology Conference Proceedings 6, 887-902.

Heeschen, K.U., Hohnberg, H.J., Haeckel, M., Abegg, F., Drews, M. and Bohrmann, G. (2007) In situ hydrocarbon concentrations from pressurized cores in surface sediments, Northern Gulf of Mexico. Marine Chemistry 107, 498-515.

Henriksen, E., Bjørnseth, H.M., Hals, T.K., Heide, T., Kiryukhina, T., Kløvjan, O.S., Larssen, G.B., Ryseth, A.E., Rønning, K., Sollid, K. and Stoupakova, A. (2011a) Uplift and erosion of the greater Barents Sea: impact on prospectivity and petroleum systems. Geological Society, London, Memoir 35, 271-281.

Henriksen, E., Ryseth, A.E., Larssen, G.B., Heide, T., Rønning, K., Sollid, K. and Stoupakova, A.V. (2011b) Tectonostratigraphy of the greater Barents Sea: Implications for petroleum systems. Geological Society, London, Memoir 35, 163-195.

Hensen, C., Scholz, F., Nuzzo, M., Valadares, V., Gracia, E., Terrinha, P., Liebetrau, V., Kaul, N., Silva, S., Martinez-Loriente, S., Bartolome, R., Pinero, E., Magalhaes, V.H., Schmidt, M., Weise, S.M., Cunha, M., Hilario, A., Perea, H., Rovelli, L. and Lackschewitz, K. (2015) Strike-slip faults mediate the rise of crustal-derived fluids and mud volcanism in the deep sea. Geology 43, 339-342.

Hesse, R. and Harrison, W.E. (1981) Gas hydrates (clathrates) causing pore-water freshening and oxygen isotope fractionation in deep-water sedimentary sections of terrigenous continental margins. Earth and Planetary Science Letters 55, 453-462.

Hillman, J.I.T., Burwicz, E., Zander, T., Bialas, J., Klaucke, I., Feldman, H., Drexler, T. and Awwiller, D. (2018a) Investigating a gas hydrate system in apparent disequilibrium in the Danube Fan, Black Sea. Earth and Planetary Science Letters 502, 1-11.

Hillman, J.I.T., Klaucke, I., Bialas, J., Feldman, H., Drexler, T., Awwiller, D., Atgin, O., Cifci, G. and Badhani, S. (2018b) Gas migration pathways and slope failures in the Danube Fan, Black Sea. Marine and Petroleum Geology, 1-16.

Hitchen, K. (2004) The geology of the UK Hatton-Rockall margin. Marine and Petroleum Geology 21, 993-1012.

Hjelstuen, B.O., Eldholm, O. and Skogseid, J. (1999) Cenozoic evolution of the northern Vøring margin. GSA Bulletin 111, 1792-1807.

Hjelstuen, B.O., Haflidason, H., Sejrup, H.P. and Nygård, A. (2010) Sedimentary and structural control on pockmark development—evidence from the Nyegga pockmark field, NW European margin. Geo-Mar Lett 30, 221-230.

1713 Hjelstuen, B.O., Petter Sejrup, H., Haflidason, H., Nygård, A., Ceramicola, S. and Bryn, P. (2005)
1714 Late Cenozoic glacial history and evolution of the Storegga Slide area and adjacent slide flank
1715 regions, Norwegian continental margin. Marine and Petroleum Geology 22, 57-69.

1716 Hodson, A.J., Nowak, A., Redeker, K.R., Holmlund, E.S., Christiansen, H.H. and Turchyn, A.V.
1717 (2019) Seasonal Dynamics of Methane and Carbon Dioxide Evasion From an Open System Pingo:
1718 Lagoon Pingo, Svalbard. Frontiers in Earth Science 7, doi:10.3389/feart.2019.00030.

1719 Honoré, A. (2014) The outlook for natural gas demand in Europe, Oxtord, UK, p. 174pp.

1720 Hopper, J.R., Funck, T., Stoker, M., Árting, U., Peron-Pindivic, G., Gaina, C. and Doornenbal, H.
1721 (2014) Tectonostratigraphic Atlas of the North- East Atlantic Region, Geological Survey of Denmark
1722 and Greeland (GEUS), Copenhagen.

1723 Hovland, M., Svensen, H., Forsberg, C.F., Johansen, H., Fichler, C., Fosså, J.H., Jonsson, R. and
1724 Rueslåtten, H. (2005) Complex pockmarks with carbonate-ridges off mid-Norway: Products of
1725 sediment degassing. Marine Geology 218, 191-206.

1726 Humlum, O., Instanes, A. and Sollid, J.L. (2003) Permafrost in Svalbard: a review of research history,
1727 climatic background and engineering challenges. Polar Res 22, 191-215.

1728 Hustoft, S., Bünz, S. and Mienert, J. (2010) Three-dimensional seismic analysis of the morphology
1729 and spatial distribution of chimneys beneath the Nyegga pockmark field, offshore mid-Norway. Basin
1730 Research 22, 465-480.

1731 Hustoft, S., Bünz, S., Mienert, J. and Chand, S. (2009) Gas hydrate reservoir and active methane-
1732 venting province in sediments on <20 Ma young oceanic crust in the Fram Strait, offshore NW-
1733 Svalbard. Earth and Planetary Science Letters 284, 12-24.

1734 Hustoft, S., Mienert, J., Bünz, S. and Nouzé, H. (2007) High-resolution 3D-seismic data indicate
1735 focussed fluid migration pathways above polygonal fault systems of the mid-Norwegian margin.
1736 Marine Geology 245, 89-106.

1737 Ivanov, M., Blinova, V., Kozlova, E., Westbrook, Graham K., Mazzini, A., Minshull, T. and Nouzé,
1738 H. (2007) First sampling of gas hydrate from the Vøring Plateau. Eos, Transactions American
1739 Geophysical Union 88, 209-212.

1740 Ivanov, M.K., Kenyon, N.H., Laberg, J.S. and Blinova, V.N. (2010) Cold seeps, coral mounds and
1741 deep-water depositional systems of the Alborán Sea, Gulf of Cadiz and Norwegian Continental
1742 Margin. Preliminary results of investigations during the TTR-17 cruise of RV Professor Logachev,
1743 June–July, 2008, in: UNESCO (Ed.), Intergovernmental Oceanographic Commission (IOC) Technical
1744 Series. UNESCO, Paris, France, p. 144.

1745 Japsen, P., Bonow, J.M., Green, P.F., Chalmers, J.A. and Lidmar-Bergström, K. (2006) Elevated,
1746 passive continental margins: Long-term highs or Neogene uplifts? New evidence from West
1747 Greenland. Earth and Planetary Science Letters 248, 330-339.

1748 Johnson, J.E., Mienert, J., Plaza-Faverola, A., Vadakkepuliyambatta, S., Knies, J., Bünz, S.,
1749 Andreassen, K. and Ferré, B. (2015) Abiotic methane from ultraslow-spreading ridges can charge
1750 Arctic gas hydrates. Geology 43, 371-374.

1751 Jokat, W., Geissler, W. and Voss, M. (2008) Basement structure of the north-western Yermak Plateau.
1752 Geophysical Research Letters 35, L05309, doi:05310.01029/02007GL032892.

Judd, A., Davies, G., Wilson, J., Holmes, R., Baron, G. and Bryden, I. (1997) Contributions to atmospheric methane by natural seepages on the UK continental shelf (vol 137, pg 165, 1997). Marine Geology 140, 427-455.

Kenyon, N.H., Ivanov, M.K., Akhmetzhanov, A.M. and Akhmanov, G.G. (2001) Interdisciplinary approaches to geoscience on the north east Atlantic margin and Mid-Atlantic Ridge. Preliminary results of investigations during the TTR-10 cruise of RV Professor Logachev. July-August, 2000, in: UNESCO (Ed.), Intergovernmental Oceanographic Commission (IOC) technical series. UNESCO, Paris, France, p. 104.

Klitzke, P., Luzi-Helbing, M., Schicks, J.M., Cacace, M., Jacquey, A.B., Sippel, J., Scheck-Wenderoth, M. and Faleide, J.I. (2016) Gas Hydrate Stability Zone of the Barents Sea and Kara Sea Region. Energy Procedia 97, 302-309.

Knies, J. and Mann, U. (2002) Depositional environment and source rock potential of Miocene strata from the central Fram Strait: introduction of a new computing tool for simulating organic facies variations. Marine and Petroleum Geology 19, 811-828.

Knies, J., Mattingsdal, R., Fabian, K., Grøsfjeld, K., Baranwal, S., Husum, K., De Schepper, S., Vogt, C., Andersen, N., Matthiessen, J., Andreassen, K., Jokat, W., Nam, S.-I. and Gaina, C. (2014) Effect of early Pliocene uplift on late Pliocene cooling in the Arctic–Atlantic gateway. Earth and Planetary Science Letters 387, 132-144.

Krastel, S., Spiess, V., Ivanov, M., Weinrebe, W., Bohrmann, G., Shashkin, P. and Heidersdorf, F. (2003) Acoustic investigations of mud volcaneos in the Sorokin Trough, Black Sea. Geo-Mar Lett 23, 230-238.

Krom, M.D., Herut, B. and Mantoura, R.F.C. (2004) Nutrient budget for the Eastern Mediterranean: Implications for phosphorus limitation. Limnology and Oceanography 49, 1582-1592.

Ktenas, D., Henriksen, E., Meisingset, I., Nielsen, J.K. and Andreassen, K. (2017) Quantification of the magnitude of net erosion in the southwest Barents Sea using sonic velocities and compaction trends in shales and sandstones. Marine and Petroleum Geology 88, 826-844.

Küçük, H.M., Dondurur, D., Özel, O., Atgun, O., Sınayuç, Ç., Merey, Ş. and Çifçi, G. (2015) Acoustic Investigations of Gas and Gas Hydrate Formations, Offshore Southwestern Black Sea, American Geophysical Union Fall Meeting, San Francisco, USA.

Laberg, J.S. and Andreassen, K. (1996) Gas hydrate and free gas indications within the Cenozoic succession of the Bjornoya Basin, western Barents Sea. Marine and Petroleum Geology 13, 921-940.

Laberg, J.S., Andreassen, K. and Knutsen, S.M. (1998) Inferred gas hydrate on the Barents Sea shelf — a model for its formation and a volume estimate. Geo-Mar Lett 18, 26-33.

Laberg, J.S., Dahlgren, T., Vorren, T.O., Haflidason, H. and Bryn, P. (2001) Seismic analyses of Cenozoic contourite drift development in the Northern Norwegian Sea. Mar Geophys Res 22, 401-416.

Larsen, H.C. and Saunders, A.D. (1998) Tectonism and volcanism at the Southeast Greenland rifted margin; a record of plume impact and later continental rupture. Proceedings of the Ocean Drilling Program, Scientific Results 152, 1-503.

Le Pichon, X., Sengor, A.M.C., Demirbag, E., Rangin, C., Imren, C., Armijo, R., Gorur, N., Cagatay, N., de Lepinay, B.M., Meyer, B., Saatcilar, R. and Tok, B. (2001) The active Main Marmara Fault. Earth and Planetary Science Letters 192, 595-616.

Lee, J.H., Baek, Y.S., Ryu, B.J., Riedel, M. and Hyndman, R.D. (2005) A seismic survey to detect natural gas hydrate in the East Sea of Korea. Mar Geophys Res 26, 51-59.

Leon, R. (2007) Modelo SIG del campo de estabilidad de los hidratos de gas: aplicación a las estructuras geológicas ligadas a las emisiones submarinas de fluidos hidrocarburos en el Golfo de Cádiz. Instituto Geológico y Minero de España, Madrid, Spain.

León, R., Somoza, L., Medialdea, T., Gonzalez, F.J., Gimenez-Moreno, C.J. and Perez-Lopez, R. (2014) Pockmarks on either side of the Strait of Gibraltar: formation from overpressured shallow contourite gas reservoirs and internal wave action during the last glacial sea-level lowstand? Geo-Mar Lett 34, 131-151.

León, R., Somoza, L., Medialdea, T., Hernandez-Molina, F.J., Vázquez, J.T., Diaz-del-Rio, V. and Gonzalez, F.J. (2010) Pockmarks, collapses and blind valleys in the Gulf of Cadiz. Geo-Mar Lett 30, 231-247.

León, R., Somoza, L., Medialdea, T., Maestro, A., Diaz-del-Rio, V. and Fernandez-Puga, M.D. (2006) Classification of sea-floor features associated with methane seeps along the Gulf of Cadiz continental margin. Deep-Sea Research Part II - Topical Studies in Oceanography 53, 1464-1481.

León, R., Somoza, L., Medialdea, T., Vázquez, J.T., Gonzalez, F.J., Lopez-Gonzalez, N., Casas, D., Mata, M.D., Fernandez-Puga, M.D., Gimenez-Moreno, C.J. and Diaz-del-Rio, V. (2012) New discoveries of mud volcanoes on the Moroccan Atlantic continental margin (Gulf of Cadiz): morpho-structural characterization. Geo-Mar Lett 32, 473-488.

Lericolais, G., Bourget, J., Popescu, I., Jermannaud, P., Mulder, T., Jorry, S. and Panin, N. (2013) Late Quaternary deep-sea sedimentation in the western Black Sea: New insights from recent coring and seismic data in the deep basin. Global and Planetary Change 103, 232-247.

Letouzey, J., Biju-Duval, B., Dorkel, A., Gonnard, R., Kristchev, K., Montadert, L. and Sungurlu, O. (1977) The Black Sea: A Marginal Basin, Geophysical and Geological Data, in: Biju-Duval, B., Montadert, L. (Eds.), International Symposium of the Mediterranean Basins. Editions Technip, Paris, pp. 363-376.

Liira, M., Noormets, R., Sepp, H., Kekišev, O., Maddison, M. and Olaussen, S. (2019) Sediment geochemical study of hydrocarbon seeps in Isfjorden and Mohnbukta: a comparison between western and eastern Spitsbergen, Svalbard. Arctos 1, 49-62.

Loncke, L., Mascle, J. and Fanil Scientific, P. (2004) Mud volcanoes, gas chimneys, pockmarks and mounds in the Nile deep-sea fan (Eastern Mediterranean): geophysical evidences. Marine and Petroleum Geology 21, 669-689.

López Pérez, A.E., Rey, D., Martins, V., Plaza-Morlote, M. and Rubio, B. (2019) Application of multivariate statistical analyses to Itrax (TM) core scanner data for the identification of deep-marine sedimentary facies: A case study in the Galician Continental Margin. Quaternary International 514, 152-160.

Lundin, E.R. and Doré, A.G. (1997) A tectonic model for the Norwegian passive margin with implications for the NE Atlantic: Early Cretaceous to break-up. Journal of the Geological Society 154, 545-550.

Lykousis, V., Alexandri, S., Woodside, J., de Lange, G., Dahlmann, A., Perissoratis, C., Heeschen, K., Ioakim, C., Sakellariou, D., Nomikou, P., Rousakis, G., Casas, D., Ballas, D. and Ercilla, G. (2009) Mud volcanoes and gas hydrates in the Anaximander mountains (Eastern Mediterranean Sea). Marine and Petroleum Geology 26, 854-872.

1838 Macgregor, D.S. (2012) The development of the Nile drainage system: integration of onshore and
1839 offshore evidence. Petroleum Geoscience 18, 417-431.

1840 Maestro, A., Jané, G., Llave, E., López-Martínez, J., Bohoyo, F. and Druet, M. (2018) The role of
1841 tectonic inheritance in the morphostructural evolution of the Galicia continental margin and adjacent
1842 abyssal plains from digital bathymetric model (DBM) analysis (NW Spain). International Journal of
1843 Earth Sciences 107, 1267-1286.

1844 Magalhaes, V.H., Pinheiro, L.M., Ivanov, M.K., Kozlova, E., Blinova, V., Kolganova, J.,
1845 Vasconcelos, C., McKenzie, J.A., Bernasconi, S.M., Kopf, A.J., Diaz-del-Rio, V., Gonzalez, F.J. and
1846 Somoza, L. (2012) Formation processes of methane-derived authigenic carbonates from the Gulf of
1847 Cadiz. Sedimentary Geology 243, 155-168.

1848 Majumdar, U., Cook, A.E., Shedd, W. and Frye, M. (2016) The connection between natural gas
1849 hydrate and bottom-simulating reflectors. Geophysical Research Letters 43, 7044-7051.

1850 Makris, J. and Stobbe, C. (1984) Physical properties and state of the crust and upper mantle of the
1851 Eastern Mediterranean Sea deduced from geophysical data. Marine Geology 55, 347-363.

1852 Maldonado, A., Somoza, L. and Pallares, L. (1999) The Betic orogen and the Iberian-African
1853 boundary in the Gulf of Cadiz: geological evolution (central North Atlantic). Marine Geology 155, 9-
1854 43.

1855 Marín-Moreno, H., Giustiniani, M., Tinivella, U. and Pinero, E. (2016) The challenges of quantifying
1856 the carbon stored in Arctic marine gas hydrate. Marine and Petroleum Geology 71, 76-82.

1857 Marín-Moreno, H., Sahoo, S.K. and Best, A.I. (2017) Theoretical modeling insights into elastic wave
1858 attenuation mechanisms in marine sediments with pore-filling methane hydrate. Journal of
1859 Geophysical Research: Solid Earth 122, 1835-1847.

1860 Martinez-Garcia, P., Comas, M., Lonergan, L. and Watts, A.B. (2017) From Extension to Shortening:
1861 Tectonic Inversion Distributed in Time and Space in the Alboran Sea, Western Mediterranean.
1862 Tectonics 36, 2777-2805.

1863 Mascle, J., Mary, F., Praeg, D., Brosolo, L., Camera, L., Ceramicola, S. and Dupre, S. (2014)
1864 Distribution and geological control of mud volcanoes and other fluid/free gas seepage features in the
1865 Mediterranean Sea and nearby Gulf of Cadiz. Geo-Mar Lett 34, 89-110.

1866 Mattingsdal, R., Knies, J., Andreassen, K., Fabian, K., Husum, K., Grøsfjeld, K. and De Schepper, S.
1867 (2014) A new 6 Myr stratigraphic framework for the Atlantic–Arctic Gateway. Quaternary Science
1868 Reviews 92, 170-178.

1869 Mau, S., Römer, M., Torres, M.E., Bussmann, I., Pape, T., Damm, E., Geprägs, P., Wintersteller, P.,
1870 Hsu, C.W., Loher, M. and Bohrmann, G. (2017) Widespread methane seepage along the continental
1871 margin off Svalbard - from Bjørnøya to Kongsfjorden. Scientific Reports 7, 42997.

1872 Max, M.D. and Johnson, A.H. (2014) Hydrate petroleum system approach to natural gas hydrate
1873 exploration. Petroleum Geoscience 20, 187-199.

1874 Max, M.D. and Johnson, A.H. (2016) Valuation of NGH deposits, Exploration and Production of
1875 Oceanic Natural Gas Hydrate Springer, New York, pp. 157-172.

1876 Mazurenko, L.L., Soloviev, V.A., Belenkaya, I., Ivanov, M.K. and Pinheiro, L.M. (2002) Mud
1877 volcano gas hydrates in the Gulf of Cadiz. Terra Nova 14, 321-329.

1878 Mazzini, A., Svensen, H., Hovland, M. and Planke, S. (2006) Comparison and implications from
1879 strikingly different authigenic carbonates in a Nyegga complex pockmark, G11, Norwegian Sea.
1880 Marine Geology 231, 89-102.

1881 McGlade, C. and Ekins, P. (2015) The geographical distribution of fossil fuels unused when limiting
1882 global warming to 2° C. Nature 517, 187-190.

1883 Medialdea, T., Somoza, L., Pinheiro, L.M., Fernandez-Puga, M.C., Vázquez, J.T., León, R., Ivanov,
1884 M.K., Magalhaes, V., Diaz-del-Rio, V. and Vegas, R. (2009) Tectonics and mud volcano
1885 development in the Gulf of Cadiz. Marine Geology 261, 48-63.

1886 Merey, S. and Longinos, S.N. (2018) Does the Mediterranean Sea have potential for producing gas
1887 hydrates? Journal of Natural Gas Science and Engineering 55, 113-134.

1888 Mienert, J., Vanneste, M., Bünz, S., Andreassen, K., Haflidason, H. and Sejrup, H.P. (2005) Ocean
1889 warming and gas hydrate stability on the mid-Norwegian margin at the Storegga slide. Marine and
1890 Petroleum Geology 22, 233-244.

1891 Minshull, T.A. and Keddie, A. (2010) Measuring the geotherm with gas hydrate bottom-simulating
1892 reflectors: a novel approach using three-dimensional seismic data from the eastern Black Sea. Terra
1893 Nova 22, 131-136.

1894 Mitchell, G., Mayer, L., Bell, K.L.C., Ballard, R.D., Raineault, N.A., Roman, C., Ballard, W.B.A.,
1895 Cornwell, K., Hine, A., Shinn, E., Dimitriadis, I. and Bogdan, O. (2013) Exploration of Eratosthenes
1896 Seamount-A Continental Fragment Being Forced Down an Oceanic Trench. Oceanography 26, 36-41.

1897 Moridis, G. (2003) Numerical studies of gas production from methane hydrates. SPE Journal 8, 359-
1898 370.

1899 Mork, M.B.E. (2013) Diagenesis and quartz cement distribution of low-permeability Upper Triassic-
1900 Middle Jurassic reservoir sandstones, Longyearbyen CO2 lab well site in Svalbard, Norway. AAPG
1901 Bulletin 97, 577-596.

1902 Murillas, J., Mougenot, D., Boulot, G., Comas, M.C., Banda, E. and Mauffret, A. (1990) Structure
1903 and evolution of the Galicia Interior Basin (Atlantic western Iberian continental margin).
1904 Tectonophysics 184, 297-319.

1905 Naylor, D. and Shannon, P. (2011) Petroleum Geology of Ireland. Dunedin Academic Press Limited,
1906 Edinburgh, UK.

1907 Nielsen, T. and Jokat, W. (2009) Petroleum potential in southern Fram Strait?, AAPG 3-P Arctic
1908 Conference and Exhibition. AAPG, Moscow, Russia.

1909 Nielsen, T., Laier, T., Kuijpers, A., Rasmussen, T.L., Mikkelsen, N.E. and Norgard-Pedersen, N.
1910 (2014) Fluid flow and methane occurrences in the Disko Bugt area offshore West Greenland:
1911 indications for gas hydrates? Geo-Mar Lett 34, 511-523.

1912 Nielsen, T., Marcusses, C., Konradi, P., Kuijpers, A. and Christiansen, F.G. (2000) Geohazard desk
1913 study offshore West Greenland - Pilot project, GEUS Report 2000/21.

1914 Nikishin, A.M., Korotaev, M.V., Ershov, A.V. and Brunet, M.-F. (2003) The Black Sea basin:
1915 tectonic history and Neogene-Quaternary rapid subsidence modelling. Sedimentary Geology 156,
1916 149-168.

Nikishin, A.M., Okay, A.I., Tuysuz, O., Demirer, A., Amelin, N. and Petrov, E. (2015) The Black Sea basins structure and history: New model based on new deep penetration regional seismic data. Part 1: Basins structure and fill. Marine and Petroleum Geology 59, 638-655.

Norwegian Petroleum Directorate (2018) Resources for the future: Seabed minerals and gas hydrates, Resource Report Exploration 2018. Norwegian Petroleum Directorate, Stavanger, Norway, pp. 67-72.

Nøttvedt, A., Berglund, L.T., Rasmussen, E. and Steel, R.J. (1988) Some aspects of Tertiary tectonics and sedimentation along the western Barents Shelf. Geological Society, London, Special Publications 39, 421-425.

Nøttvedt, A., Livbjerg, F., Midbøe, P.S. and Rasmussen, E. (1993) Hydrocarbon potential of the Central Spitsbergen Basin, in: Vorren, T.O., Bergsager, E., Dahl-Stamnes, Ø.A., Holter, E., Johansen, B., Lie, E., Lund, T.B. (Eds.), Norwegian Petroleum Society Special Publications. Elsevier, pp. 333-361.

Oakey, G.N. and Chalmers, J.A. (2012) A new model for the Paleogene motion of Greenland relative to North America: Plate reconstructions of the Davis Strait and Nares Strait regions between Canada and Greenland. Journal of Geophysical Research: Solid Earth 117, B10401,doi:10410.11029/12011JB008942.

Ogata, K., Senger, K., Braathen, A., Tveranger, J. and Olaussen, S. (2012) The importance of natural fractures in a tight reservoir for potential CO2 storage: case study of the upper Triassic to middle Jurassic Kapp Toscana Group (Spitsbergen, Arctic Norway), Geological Society of London, Special Publications, London, UK, pp. 395-415.

Ohm, S.E., Larsen, L., Olaussen, S., Senger, K., Birchall, T., Demchuk, T., Hodson, A., Johansen, I., Titlestad, G.O. and Braathen, A. (2019) Discovery of shale gas in organic rich Jurassic successions, Adventdalen, Central Spitsbergen, Norway. Norwegian Journal of Geology in review.

Ostanin, I., Anka, Z., di Primio, R. and Bernal, A. (2013) Hydrocarbon plumbing systems above the Snøhvit gas field: Structural control and implications for thermogenic methane leakage in the Hammerfest Basin, SW Barents Sea. Marine and Petroleum Geology 43, 127-146.

Oyama, A. and Masutani, S.M. (2017) A Review of the Methane Hydrate Program in Japan. Energies 10, 1447, doi:1410.3390/en10101447.

Özel, O. (2012) Investigation of gas and gas hydrate accumulations in the Western Black Sea continental slope, Master thesis, The Graduate School of Natural and Applied Sciences. Dokuz Eylül University.

Palomino, D., Lopez-Gonzalez, N., Vázquez, J.T., Fernandez-Salas, L.M., Rueda, J.L., Sanchez-Leal, R. and Diaz-del-Rio, V. (2016) Multidisciplinary study of mud volcanoes and diapirs and their relationship to seepages and bottom currents in the Gulf of Cadiz continental slope (northeastern sector). Marine Geology 378, 196-212.

Panieri, G., Bünz, S., Fornari, D.J., Escartin, J., Serov, P., Jansson, P., Torres, M.E., Johnson, J.E., Hong, W., Sauer, S., Garcia, R. and Gracias, N. (2017) An integrated view of the methane system in the pockmarks at Vestnesa Ridge, 79°N. Marine Geology 390, 282-300.

Pape, T., Kasten, S., Zabel, M., Bahr, A., Abegg, F., Hohnberg, H.J. and Bohrmann, G. (2010) Gas hydrates in shallow deposits of the Amsterdam mud volcano, Anaximander Mountains, Northeastern Mediterranean Sea. Geo-Mar Lett 30, 187-206.

Pedersen, G.K., Andersen, L.A., Lundsteen, E.B., Petersen, H.I., Bojesen-Koefoed, J.A. and Nytoft, H.P. (2006) Depositional environments, organic maturity and petroleum potential of the Cretaceous coal-bearing Atane Formation at Qullissat, Nuussuaq Basin, West Greenland. Journal of Petroleum Geology 29, 3-25.

Pérez-Belzuz, F., Alonso, B. and Ercilla, G. (1997) History of mud diapirism and trigger mechanisms in the Western Alboran Sea. Tectonophysics 282, 399-422.

Pérez-Gussinyé, M., Ranero, C.R., Reston, T.J. and Sawyer, D. (2003) Mechanisms of extension at nonvolcanic margins: Evidence from the Galicia interior basin, west of Iberia. Journal of Geophysical Research: Solid Earth 108, 2245, doi:2210.1029/2001JB000901.

Pérez-Gussinyé, M. and Reston, T.J. (2001) Rheological evolution during extension at nonvolcanic rifted margins: Onset of serpentinization and development of detachments leading to continental breakup. Journal of Geophysical Research: Solid Earth 106, 3961-3975.

Perissoratis, C., Ioakim, C., Alexandri, S., Woodside, J., Nomikou, P., Dahlmann, A., Casas, D., Heeschen, K., Amman, H., Rousakis, G. and Lykousis, V. (2011) Thessaloniki Mud Volcano, the shallowest gas hydrate-bearing mud volcano in the Anaximander Mountains, eastern Mediterranean. Journal of Geological Research, doi:10.1155/2011/247983.

Petersen, C.J., Bünz, S., Hustoft, S., Mienert, J. and Klaeschen, D. (2010) High-resolution P-Cable 3D seismic imaging of gas chimney structures in gas hydrated sediments of an Arctic sediment drift. Marine and Petroleum Geology 27, 1981-1994.

Pinheiro, L.M., Ivanov, M.K., Sautkin, A., Akhmanov, G., Magalhaes, V.H., Volkonskaya, A., Monteiro, J.H., Somoza, L., Gardner, J., Hamouni, N. and Cunha, M.R. (2003) Mud volcanism in the Gulf of Cadiz: results from the TTR-10 cruise. Marine Geology 195, 131-151.

Pinheiro, L.M., Wilson, R.C.L., Pena dos Reis, R., Whitmarsh, R.B. and Ribeiro, A. (1996) The western Iberia margin; a geophysical and geological overview. Proceedings of the Ocean Drilling Program, Scientific Results 149, 3-23.

Platt, J.P., Whitehouse, M.J., Kelley, S.P., Carter, A. and Hollick, L. (2003) Simultaneous extensional exhumation across the Alboran Basin: Implications for the causes of late orogenic extension. Geology 31, 251-254.

Plaza-Faverola, A., Bünz, S., Johnson, J.E., Chand, S., Knies, J., Mienert, J. and Franek, P. (2015) Role of tectonic stress in seepage evolution along the gas hydrate charged Vestnesa Ridge, Fram Strait. Geophysical Research Letters 42, 733-742.

Plaza-Faverola, A., Bünz, S. and Mienert, J. (2011) Repeated fluid expulsion through sub-seabed chimneys offshore Norway in response to glacial cycles. Earth and Planetary Science Letters 305, 297-308.

Plaza-Faverola, A., Vadakkepuliyambatta, S., Hong, W.L., Mienert, J., Bünz, S., Chand, S. and Greinert, J. (2017) Bottom-simulating reflector dynamics at Arctic thermogenic gas provinces: An example from Vestnesa Ridge, offshore west Svalbard. Journal of Geophysical Research: Solid Earth 122, 4089-4105.

Plaza-Faverola, A., Westbrook, G.K., Ker, S., Exley, R.J.K., Gailler, A., Minshull, T.A. and Broto, K. (2010) Evidence from three-dimensional seismic tomography for a substantial accumulation of gas hydrate in a fluid-escape chimney in the Nyegga pockmark field, offshore Norway. Journal of Geophysical Research: Solid Earth 115, B08104, doi:08110.01029/02009JB007078.

2000 Popescu, I., De Batist, M., Lericolais, G., Nouzé, H., Poort, J., Panin, N., Versteeg, W. and Gillet, H.
2001 (2006) Multiple bottom-simulating reflections in the Black Sea: Potential proxies of past climate
2002 conditions. Marine Geology 227, 163-176.

2003 Popescu, I., Lericolais, G., Panin, N., De Batist, M. and Gillet, H. (2007) Seismic expression of gas
2004 and gas hydrates across the western Black Sea. Geo-Mar Lett 27, 173-183.

2005 Popescu, I., Lericolais, G., Panin, N., Wong, H.K. and Droz, L. (2001) Late Quaternary channel
2006 avulsions on the Danube deep-sea fan, Black Sea. Marine Geology 179, 25-37.

2007 Posewang, J. and Mienert, J. (1999) The enigma of double BSRs: indicators for changes in the
2008 hydrate stability field? Geo-Mar Lett 19, 157-163.

2009 Praeg, D., Geletti, R., Mascle, J., Unnithan, V. and Harmegnies, F. (2008) Exploration for gas
2010 hydrates in the Mediterranean Sea and a bottom simulating reflection on the Nile Fan, GNGTS,
2011 Trieste, Italy.

2012 Praeg, D., Geletti, R., Wardell, N., Unnithan, V., Mascle, J., Migeon, S. and Camerlenghi, A. (2011)
2013 The Mediterranean Sea: a natural laboratory to study gas hydrate dynamics?, 7th International
2014 Conference on Gas Hydrates, Edinburgh, UK.

2015 Praeg, D., Migeon, S., Mascle, J., Unnithan, V., Wardell, N., Geletti, R. and Ketzer, J.M. (2017)
2016 Geophysical Evidence of Gas Hydrates Associated with Widespread Gas Venting on the Central Nile
2017 Deep-Sea Fan, Offshore Egypt, 9th International Conference on Gas Hydrates, Denver, Colorado,
2018 USA.

2019 Priest, J.A., Best, A.I. and Clayton, C.R.I. (2005) A laboratory investigation into the seismic
2020 velocities of methane gas hydrate-bearing sand. Journal of Geophysical Research: Solid Earth 110,
2021 B04102, doi:04110.01029/02004JB003259.

2022 Przybylak, R., Araźny, A., Nordli, Ø., Finkelnburg, R., Kejna, M., Budzik, T., Migała, K., Sikora, S.,
2023 Puczko, D., Rymer, K. and Rachlewicz, G. (2014) Spatial distribution of air temperature on Svalbard
2024 during 1 year with campaign measurements. International Journal of Climatology 34, 3702-3719.

2025 Rangin, C., Demirbag, E., Imren, C., Crusson, A., Le Pichon, X. and Sengor, A.M.C. (2001) Marine
2026 atlas of the Sea of Marmara (Turkey): data collected on board R.V. le Suroit, September 2000.
2027 Ifremer, Plouzane, France.

2028 Reston, T.J. (2005) Polyphase faulting during the development of the west Galicia rifted margin.
2029 Earth and Planetary Science Letters 237, 561-576.

2030 Rey, D. and Gran Burato Science Team (2010) GB4240 Cruise Technical Report. University of Vigo,
2031 Vigo, Spain.

2032 Rey, D. and Gran Burato Science Team (2011) GRAN BURATO 2011 Cruise Technical Report.
2033 University of Vigo, Vigo, Spain.

2034 Ribeiro, T. (2011) Multichannel Seismic Investigation of the Gran Burato area, off W Galicia. MSc
2035 thesis, University of Aveiro.

2036 Riboulot, V., Ker, S., Sultan, N., Thomas, Y., Marsset, B., Scalabrin, C., Ruffine, L., Boulart, C. and
2037 Ion, G. (2018) Freshwater lake to salt-water sea causing widespread hydrate dissociation in the Black
2038 Sea. Nature Communications 9, 117, doi:110.1038/s41467-41017-02271-z.

2039 Riedel, M., Spence, G.D., Chapman, N.R. and Hyndman, R.D. (2002) Seismic investigations of a vent
2040 field associated with gas hydrates, offshore Vancouver Island. Journal of Geophysical Research: Solid
2041 Earth 107, 2200, doi:2210.1029/2001JB000269.

2042 Riedel, M., Wallmann, K., Berndt, C., Pape, T., Freudenthal, T., Bergenthal, M., Bünz, S. and
2043 Bohrmann, G. (2018) In Situ Temperature Measurements at the Svalbard Continental Margin:
2044 Implications for Gas Hydrate Dynamics. Geochemistry, Geophysics, Geosystems 19, 1165-1177.

2045 Rise, L., Bellec, V., Chand, S. and Bøe, R. (2015) Pockmarks in the southwestern Barents Sea and
2046 Finnmark fjords. Norwegian Journal of Geology 94, 163-282.

2047 Rise, L., Ottesen, D., Berg, K. and Lundin, E. (2005) Large-scale development of the mid-Norwegian
2048 margin during the last 3 million years. Marine and Petroleum Geology 22, 33-44.

2049 Ritzmann, O. and Jokat, W. (2003) Crustal structure of northwestern Svalbard and the adjacent
2050 Yermak Plateau: evidence for Oligocene detachment tectonics and non-volcanic breakup.
2051 Geophysical Journal International 152, 139-159.

2052 Römer, M., Sahling, H., Pape, T., Ferreira, C.D., Wenzhofer, F., Boetius, A. and Bohrmann, G.
2053 (2014) Methane fluxes and carbonate deposits at a cold seep area of the Central Nile Deep Sea Fan,
2054 Eastern Mediterranean Sea. Marine Geology 347, 27-42.

2055 Roy, S., Marin-Moreno, H. and max, M.D. (2017) Natural Gas Hydrates and fluid flow: implications
2056 from Irish offshore, 9th International Conference on Gas Hydrates, Denver, Colorado, USA.

2057 Roy, S. and Max, M. (2017) Acoustic Evidence of Fluid Flow in Ireland Offshore and Physical
2058 Property Measurements on Methane Gas Hydrate in Sediment Cores from the Irish GHSZ, AAPG
2059 International Conference, London, U.K.

2060 Roy, S. and Max, M. (2018) Assessment of Natural Gas Hydrate Petroleum System in western Irish
2061 offshore, American Geophysical Union - Fall Meeting, Washington, D.C.

2062 Roy, S., Senger, K., Hovland, M. and Noormets, R. (2012) Gas Hydrate formation potential in the
2063 fjords of Svalbard, Arctic Frontiers Conference-Energies of the High North, Tromsø, Norway.

2064 Roy, S., Senger, K., Hovland, M., Römer, M. and Braathen, A. (2019) Geological controls on shallow
2065 gas distribution and seafloor seepage in an Arctic fjord of Spitsbergen, Norway. Marine and
2066 Petroleum Geology 107, 237-254.

2067 Rubin-Blum, M., Antler, G., Turchyn, A.V., Tsadok, R., Goodman-Tchernov, B.N., Shemesh, E.,
2068 Austin, J.A., Coleman, D.F., Makovsky, Y., Sivan, O. and Tchernov, D. (2014) Hydrocarbon- related
2069 microbial processes in the deep sediments of the Eastern Mediterranean Levantine Basin. Fems
2070 Microbiology Ecology 87, 780-796.

2071 Ruffine, L., Donval, J.P., Croguennec, C., Bignon, L., Birot, D., Battani, A., Bayon, G., Caprais, J.C.,
2072 Lanteri, N., Levache, D. and Dupre, S. (2017) Gas Seepage along the Edge of the Aquitaine Shelf
2073 (France): Origin and Local Fluxes. Geofluids 2017, doi:10.1155/2017/4240818.

2074 Ruppel, C.D. and Kessler, J.D. (2017) The interaction of climate change and methane hydrates.
2075 Reviews of Geophysics 55, 126-168.

2076 Ryan, W.B.F., Pitman Iii, W.C., Major, C.O., Shimkus, K., Moskalenko, V., Jones, G.A., Dimitrov,
2077 P., Gorür, N., Sakinç, M. and Yüce, H. (1997) An abrupt drowning of the Black Sea shelf. Marine
2078 Geology 138, 119-126.

Santamarina, J.C., Dai, S., Terzariol, M., Jang, J., Waite, W.F., Winters, W.J., Nagao, J., Yoneda, J., Konno, Y., Fujii, T. and Suzuki, K. (2015) Hydro-bio-geomechanical properties of hydrate-bearing sediments from Nankai Trough. Marine and Petroleum Geology 66, 434-450.

Saritas, H. (2013) Mapping and exploration of gas and possibly gas hydrate accumulation in Western High, Sea of Marmara in light of 2D-3D high resolution seismic data, Masters thesis, Institute of Marine Sciences and Technology. Dokuz Eylul University.

Sarıtaş, H., Çifçi, G., Géli, L., Thomas, Y., Marsset, B., Henry, P., Grall, C. and Rochat, A. (2018) Gas occurrence and shallow conduit systems in the Western Sea of Marmara: a review and new acoustic evidence. Geo-Mar Lett 38, 385-402.

Sarkar, S., Berndt, C., Minshull, T.A., Westbrook, G.K., Klaeschen, D., Masson, D.G., Chabert, A. and Thatcher, K.E. (2012) Seismic evidence for shallow gas-escape features associated with a retreating gas hydrate zone offshore west Svalbard. Journal of Geophysical Research 117, B09102, doi:09110.01029/02011JB009126.

Sassen, R. and MacDonald, I.R. (1994) Evidence of structure H hydrate, Gulf of Mexico continental slope. Organic Geochemistry 22, 1029-1032.

Senger, K., Betlem, P., Liira, M., Roy, S., Midttømme, K., Wheeler, W., Beka, T., Olaussen, S. and Ohm, S. (2017) Integrated thermo-baric modelling of the gas hydrate stability zone onshore Svalbard, Arctic Norway, 9th International Conference on Gas Hydrates, Denver, USA.

Senger, K., Brugmans, P., Grundvåg, S.-A., Jochmann, M., Nøttvedt, A., Olaussen, S., Skotte, A. and Smyrak-Sikora, A. (2019) Petroleum, coal and research drilling onshore Svalbard: a historical perspective. Norwegian Journal of Geology 99, in press.

Senger, K., Bünz, S. and Mienert, J. (2010) First-Order Estimation of In-Place Gas Resources at the Nyegga Gas Hydrate Prospect, Norwegian Sea. Energies 3, 2001-2026.

Serov, P., Vadakkepuliyambatta, S., Mienert, J., Patton, H., Portnov, A., Silyakova, A., Panieri, G., Carroll, M.L., Carroll, J., Andreassen, K. and Hubbard, A. (2017) Postglacial response of Arctic Ocean gas hydrates to climatic amelioration. Proceedings of the National Academy of Sciences 114, 6215-6220.

Shannon, P.M., Moore, J.G., Jacob, A.W.B. and Makris, J. (1993) Cretaceous and Tertiary basin development west of Ireland. Geological Society, London, Petroleum Geology Conference series 4, 1057-1066.

Shillington, D.J., White, N., Minshull, T.A., Edwards, G.R.H., Jones, S., Edwards, R.A. and Scott, C.L. (2008) Cenozoic evolution of the eastern Black Sea: a test of depth-dependent stretching models. Earth and Planetary Science Letters 265, 360-378.

Singhroha, S., Chand, S. and Buenz, S. (2019) Constraints on gas hydrate distribution and morphology in Vestnesa Ridge, western Svalbard margin, using multicomponent ocean-bottom seismic data. Journal of Geophysical Research: Solid Earth 124, 4343-4364.

Sloan, E.D. and Koh, C.A. (2008) Clathrate Hydrates of Natural Gases, Third Edition. CRC Press-Taylor & Francis Group, Boca Raton, Florida.

Smith, A.J., Mienert, J., Bünz, S. and Greinert, J. (2014) Thermogenic methane injection via bubble transport into the upper Arctic Ocean from the hydrate-charged Vestnesa Ridge, Svalbard. Geochemistry, Geophysics, Geosystems 15, 1945-1959.

Smith, W.H.F. and Sandwell, D.T. (1997) Global Sea Floor Topography from Satellite Altimetry and Ship Depth Soundings. Science 277, 1956-1962.

Somoza, L., Diaz-del-Rio, V., León, R., Ivanov, M., Fernandez-Puga, M.C., Gardner, J.M., Hernandez-Molina, F.J., Pinheiro, L.M., Rodero, J., Lobato, A., Maestro, A., Vazquez, J.T., Medialdea, T. and Fernandez-Salas, L.M. (2003) Seabed morphology and hydrocarbon seepage in the Gulf of Cadiz mud volcano area: Acoustic imagery, multibeam and ultra-high resolution seismic data. Marine Geology 195, 153-176.

Somoza, L., Ercilla, G., Urgorri, V., León, R., Medialdea, T., Paredes, M., Gonzalez, F.J. and Nombela, M.A. (2014) Detection and mapping of cold-water coral mounds and living Lophelia reefs in the Galicia Bank, Atlantic NW Iberia margin. Marine Geology 349, 73-90.

Somoza, L., Medialdea, T., León, R., Ercilla, G., Vázquez, J.T., Farran, M.L., Hernandez-Molina, J., Gonzalez, J., Juan, C. and Fernandez-Puga, M.C. (2012) Structure of mud volcano systems and pockmarks in the region of the Ceuta Contourite Depositional System (Western Alboran Sea). Marine Geology 332, 4-26.

Song, Y.C., Yang, L., Zhao, J.F., Liu, W.G., Yang, M.J., Li, Y.H., Liu, Y. and Li, Q.P. (2014) The status of natural gas hydrate research in China: A review. Renewable & Sustainable Energy Reviews 31, 778-791.

Sorlien, C.C., Akhun, S.D., Seeber, L., Steckler, M.S., Shillington, D.J., Kurt, H., Cifci, G., Poyraz, D.T., Gurcay, S., Dondurur, D., Imren, C., Perincek, E., Okay, S., Kucuk, H.M. and Diebold, J.B. (2012) Uniform basin growth over the last 500 ka, North Anatolian Fault, Marmara Sea, Turkey. Tectonophysics 518, 1-16.

Spangenberg, E. and Kulenkampff, J. (2006) Influence of methane hydrate content on electrical sediment properties. Geophysical Research Letters 33, L24315, doi:24310.21029/22006GL028188.

Stadnitskaia, A., Ivanov, M.K., Blinova, V., Kreulen, R. and van Weering, T.C.E. (2006) Molecular and carbon isotopic variability of hydrocarbon gases from mud volcanoes in the Gulf of Cadiz, NE Atlantic. Marine and Petroleum Geology 23, 281-296.

Stoffers, P., Degens, E.T. and Trimonis, E.S. (1978) Stratigraphy and suggested ages of Black Sea sediments cored during Leg 42B. Initial Reports of the Deep Sea Drilling Project 42, 483-487.

Stuevold, L.M. and Eldholm, O. (1996) Cenozoic uplift of Fennoscandia inferred from a study of the mid-Norwegian margin. Global and Planetary Change 12, 359-386.

Tayber, Z., Meilijson, A., Ben-Avraham, Z. and Makovsky, Y. (2019) Methane Hydrate Stability and Potential Resource in the Levant Basin, Southeastern Mediterranean Sea. Geosciences 9, 306.

Thomas, Y., Marsset, B., Westbrook, G.K., Grail, C., Géli, L., Henry, R., Çifçi, G., Rochat, A. and Saritas, H. (2012) Contribution of high-resolution 3D seismic near-seafloor imaging to reservoir-scale studies: Application to the active North Anatolian Fault, Sea of Marmara. Near Surface Geophysics 10, 291-301.

Toyos, M.H., Medialdea, T., León, R., Somoza, L., Gonzalez, F.J. and Melendez, N. (2016) Evidence of episodic long-lived eruptions in the Yuma, Ginsburg, JesA(0)s Baraza and Tasyo mud volcanoes, Gulf of Cadiz. Geo-Mar Lett 36, 197-214.

Uchida, S., Soga, K. and Yamamoto, K. (2012) Critical state soil constitutive model for methane hydrate soil. Journal of Geophysical Research 117, B03209, doi:03210.01029/02011JB008661,.

Unnithan, V., Shannon, P.M., McGrane, K., Readman, P.W., Jacob, A.W.B., Keary, R. and Kenyon, N.H. (2001) Slope instability and sediment redistribution in the Rockall Trough: constraints from GLORIA. Geological Society, London, Special Publications 188, 439-454.

Vadakkepuliyambatta, S., Bünz, S., Mienert, J. and Chand, S. (2013) Distribution of subsurface fluid-flow systems in the SW Barents Sea. Marine and Petroleum Geology 43, 208-221.

Vadakkepuliyambatta, S., Chand, S. and Bünz, S. (2017) The history and future trends of ocean warming-induced gas hydrate dissociation in the SW Barents Sea. Geophysical Research Letters 44, 835-844.

Vadakkepuliyambatta, S., Hornbach, M.J., Bünz, S. and Phrampus, B.J. (2015) Controls on gas hydrate system evolution in a region of active fluid flow in the SW Barents Sea. Marine and Petroleum Geology 66, 861-872.

Van Rensbergen, P., Depreiter, D., Pannemans, B., Moerkerke, G., Van Rooij, D., Marsset, B., Akhmanov, G., Blinova, V., Ivanov, M., Rachidi, M., Magalhaes, V., Pinheiro, L., Cunha, M. and Henriet, J.P. (2005a) The El arraiche mud volcano field at the Moroccan Atlantic slope, Gulf of Cadiz. Marine Geology 219, 1-17.

Van Rensbergen, P., Rabaute, A., Colpaert, A., Ghislain, T.S., Mathijs, M. and Bruggeman, A. (2005b) Fluid migration and fluid seepage in the Connemara Field, Porcupine Basin interpreted from industrial 3D seismic and well data combined with high-resolution site survey data. International Journal of Earth Sciences 96, 185-197.

Vanneste, M., Guidard, S. and Mienert, J. (2005) Bottom-simulating reflections and geothermal gradients across the western Svalbard margin. Terra Nova 17, 510-516.

Vassilev, A. and Dimitrov, L. (2002) Spatial and quantity evaluation of the Black Sea gas hydrates. Russian Geology and Geophysics 43, 672-684.

Vaular, E.N., Barth, T. and Haflidason, H. (2010) The geochemical characteristics of the hydrate-bound gases from the Nyegga pockmark field, Norwegian Sea. Organic Geochemistry 41, 437-444.

Vázquez, J.T., Medialdea, T., Ercilla, G., Somoza, L., Estrada, F., Puga, M.C.F., Gallart, J., Gracia, E., Maestro, A. and Sayago, M. (2008) Cenozoic deformational structures on the Galicia Bank Region (NW Iberian continental margin). Marine Geology 249, 128-149.

Vorren, T.O. and Laberg, J.S. (1997) Trough mouth fans — palaeoclimate and ice-sheet monitors. Quaternary Science Reviews 16, 865-881.

Vorren, T.O., Laberg, J.S., Blaume, F., Dowdeswell, J.A., Kenyon, N.H., Mienert, J., Rumohr, J.A.N. and Werner, F. (1998) The Norwegian-Greenland Sea Continental Margins: Morphology and Late Quaternary Sedimentary Processes and Environment. Quaternary Science Reviews 17, 273-302.

Vorren, T.O., Richardsen, G., Knutsen, S.M. and Henriksen, E. (1991) Cenozoic erosion and sedimentation in the western Barents Sea. Marine and Petroleum Geology 8, 317-340.

Waghorn, K.A., Bünz, S., Plaza-Faverola, A. and Johnson, J.E. (2018) 3D Seismic Investigation of a Gas Hydrate and Fluid Flow System on an Active Mid-Ocean Ridge; Svyatogor Ridge, Fram Strait. Geochemistry, Geophysics, Geosystems 19, 2325-2341.

Wallmann, K., Pinero, E., Burwicz, E., Haeckel, M., Hensen, C., Dale, A. and Ruepke, L. (2012) The Global Inventory of Methane Hydrate in Marine Sediments: A Theoretical Approach. Energies 5, 2449-2498.

Wallmann, K., Riedel, M., Hong, W.L., Patton, H., Hubbard, A., Pape, T., Hsu, C.W., Schmidt, C., Johnson, J.E., Torres, M.E., Andreassen, K., Berndt, C. and Bohrmann, G. (2018) Gas hydrate dissociation off Svalbard induced by isostatic rebound rather than global warming. Nature Communications 83, doi:10.1038/s41467-017-02550-9, 9.

Weitemeyer, K.A., Constable, S.C., Key, K.W. and Behrens, J.P. (2006) First results from a marine controlled-source electromagnetic survey to detect gas hydrates offshore Oregon. Geophysical Research Letters 33, L03304, doi:03310.01029/02005GL024896.

Westbrook, G.K., Chand, S., Rossi, G., Long, C., Bünz, S., Camerlenghi, A., Carcione, J.M., Dean, S., Foucher, J.P., Flueh, E., Gei, D., Haacke, R.R., Madrussani, G., Mienert, J., Minshull, T.A., Nouzé, H., Peacock, S., Reston, T.J., Vanneste, M. and Zillmer, M. (2008) Estimation of gas hydrate concentration from multi-component seismic data at sites on the continental margins of NW Svalbard and the Storegga region of Norway. Marine and Petroleum Geology 25, 744-758.

Westbrook, G.K., Thatcher, K.E., Rohling, E.J., Piotrowski, A.M., Palike, H., Osborne, A.H., Nisbet, E.G., Minshull, T.A., Lanoiselle, M., James, R.H., Huhnerbach, V., Green, D., Fisher, R.E., Crocker, A.J., Chabert, A., Bolton, C., Beszczynska-Moller, A., Berndt, C. and Aquilina, A. (2009) Escape of methane gas from the seabed along the West Spitsbergen continental margin. Geophysical Research Letters 36, L15608, doi:15610.11029/12009GL039191.

Wilson, R.C.L., Hiscott, R.N., Willis, M.G. and Gradstein, F.M. (1989) The Lusitanian Basin of West-Central Portugal: Mesozoic and Tertiary Tectonic, Stratigraphic, and Subsidence History, in: Tankard, A.J., Balkwill, H.R. (Eds.), Extensional Tectonics and Stratigraphy of the North Atlantic Margins. American Association of Petroleum Geologists, pp. 341-361.

Winguth, C., Wong, H.K., Panin, N., Dinu, C., Georgescu, P., Ungureanu, G., Krugliakov, V.V. and Podshuveit, V. (2000) Upper Quaternary water level history and sedimentation in the northwestern Black Sea. Marine Geology 167, 127-146.

Woodside, J.M., Ivanov, M.K. and Limonov, A.F. (1997) Neotectonics and fluid flow through the seafloor sediments in the Eastern Mediterranean and Black Seas. Part I: eastern Mediterranean Sea, IOC Technical Series, pp. 1-128.

Worsley, D. (2008) The post-Caledonian development of Svalbard and the western Barents Sea. Polar Res 27, 298-317.

Yefremova, A.G. and Zhizchenko, B.P. (1974) Occurrence of crystal hydrates of gases in the sediments of modern marine basins. Akademii Nauk SSSR 214, 1179-1181.

Zander, T., Haeckel, M., Berndt, C., Chi, W.-C., Klaucke, I., Bialas, J., Klaeschen, D., Koch, S. and Atgın, O. (2017) On the origin of multiple BSRs in the Danube deep-sea fan, Black Sea. Earth and Planetary Science Letters 462, 15-25.

Zavatarelli, M. and Mellor, G.L. (1995) A numerical study of the Mediterranean Sea circulation. Journal of Physical Oceanography 25, 1384-1414.

Zillmer, M., Flueh, E.R. and Petersen, J. (2005) Seismic investigation of a bottom simulating reflector and quantification of gas hydrate in the Black Sea. Geophysical Journal International 161, 662-678.

Zitter, T.A.C., Huguen, C. and Woodside, J.M. (2005) Geology of mud volcanoes in the eastern Mediterranean from combined sidescan sonar and submersible surveys. Deep-Sea Research Part I-Oceanographic Research Papers 52, 457-475.

2243 Zonenshain, L.P. and Le Pichon, X. (1986) Deep Basins of the Black Sea and Caspian Sea as
2244 Remnants of Mesozoic Back-Arc Basins. Tectonophysics 123, 181-211.

2245

There is direct and indirect evidence for hydrate occurrence in several areas around Europe

Hydrate is particularly widespread offshore Norway and Svalbard and in the Black Sea

Hydrate occurrence often coincides with conventional thermogenic hydrocarbon provinces

The regional abundance of hydrate in Europe is poorly known